FEDERAL UNIVERSITY OF TECHNOLOGY – PARANÁ

AUGUSTO ARAUJO VUITIK

CELLULOSE BASED HYDROGELS FOR WOUND DRESSING APPLICATIONS

TOLEDO
2023

AUGUSTO ARAUJO VUITIK

CELLULOSE BASED HYDROGELS FOR WOUND DRESSING APPLICATIONS

Hidrogéis de cellulose para utilização em curativos

Dissertation presented as requirement for obtaining the title of Master in Biosciences Technologies, from the Department of Postgraduation in Biosciences Technologies of the Federal University of Technology – Toledo Campus.
Supervisor: Prof. Dr. Kelen Menezes Flores Rossi de Aguiar
Co-supervisor: Prof. Dr. Sajjad Ullah (University of Peshawar – Pakistan).

TOLEDO

2023

Ministério da Educação
Universidade Tecnológica Federal do Paraná
Campus Toledo

AUGUSTO ARAUJO VUITIK

HIDROGÉIS DE CELULOSE PARA UTILIZAÇÃO EM CURATIVOS

Trabalho de pesquisa de mestrado apresentado como requisito para obtenção do título de Mestre Em Tecnologias Em Biociências da Universidade Tecnológica Federal do Paraná (UTFPR). Área de concentração: Tecnologias Em Biociências.

Data de aprovação: 24 de Fevereiro de 2023

Dra. Kelen Menezes Flores Rossi De Aguiar, Doutorado - Universidade Tecnológica Federal do Paraná

Dra. Lidiane Patricia Goncalves, Doutorado - Suzano Papel e Celulose

Dra. Liliane Cristina Battirola, Doutorado - Universidade Federal da Integração Latino-Americana (Unila)

Dra. Priscila Vaz De Arruda, Doutorado - Universidade Tecnológica Federal do Paraná

I dedicate this work to my parents and my brothers,
whose achievements inspire me every day.

ACKNOWLEDGEMENTS

To my supervisor, Dr. Kelen Menezes Flores Rossi de Aguiar, and co-supervisor, Dr. Sajjad Ullah, for the guidance and support throughout this research project.

To Dr. Ricardo Schneider from the Group of Polymers and Nanostructures (GPAN - UTFPR), Dr. Gabrielle Peiter from the Laboratory of Microorganism's Biotechnology (LaBiM - UTFPR) for enable and perform some of the characterizations described in this work.

To Msc. Emerson Blum for the daily support and personal advice during the years of this research.

To Laboratório Multiusuário da Central Analítica da UTFPR – Campus Toledo, for the infrastructure and utilities.

To Prati, Donaduzzi (Toledo, Bazil) for kindly providing the main reagents employed in this work, and for allow the use of its laboratories at the early stage of this project.

To the members of the Coordination for Postgraduation of UTFPR, Toledo, especially those associated with the Department of Postgraduation in Biosciences Technologies.

ABSTRACT

The treatment of acute and chronic wounds is of great concern for the health systems because it directly impacts the well-being of the patients and the duration of various therapies. In this way, it is crucial to develop technologies that enable shorter and more efficient treatments, which provide more comfort to the patients. Hydrogels are low-cost biocompatible materials that can retain substantial amounts of water and contribute to healing. Silver is largely employed as a biocidal agent from traditional medicine to nowadays treatments, but its production as nanoparticles is up for debate, especially regarding the potentially toxic reagents used in synthesis. This work aims to combine a cellulosic hydrogel with the antimicrobial properties of silver towards an environmentally friendly production. For this purpose, hydrogels of sodium Carboxymethyl Cellulose (CMC) with citric acid as a crosslinker were produced by the cast drying method and then treated with silver particles obtained by chemical reduction of silver nitrate and different reduction agents. The effectiveness of the crosslinking reaction was assessed by infrared spectroscopy using the Attenuated Total Reflectance (ATR) accessory, and the incorporation of silver was assessed by X-Ray Diffraction (XRD), Laser-induced Breakdown Spectroscopy (LIBS) and UV-Vis Spectroscopy. The morphology and composition of the films were also checked by Scanning Electron Microscopy (SEM) with an Energy Dispersive Spectroscopy (EDS) accessory. Microbiological tests were performed through disk diffusion with *C. albicans*, *E. coli* and *S. aureus*. Further functional analysis of the hydrogel evaluated swelling degree and pH. Results indicated the formation of crosslinks in the cast-drying method, and the chemical evaluation pointed to metallic silver. Despite the formation of amorphous particles, they were responsible for the antimicrobial response of the material, confirming the potential for use as a wound dressing.

Keywords: biological polymers; crosslinking; citric acid; silver; glycerol; sodium borohydride.

RESUMO

O tratamento de feridas agudas e crônicas é uma grande preocupação dos sistemas de saúde, pois impacta diretamente na qualidade de vida dos pacientes e na duração de diversas terapias. Neste sentido, é crucial desenvolver tecnologias que permitam tratamentos mais curtos, eficientes e que proporcionem mais conforto aos pacientes. Hidrogéis são materiais biocompatíveis e de baixo custo, capazes de reter grandes quantidades de água e contribuir com a cicatrização. A prata é amplamente utilizada como um agente biocida, desde tratamentos tradicionais até os modernos, mas sua produção como nanopartícula é alvo de debates, especialmente sobre os reagentes potencialmente tóxicos usados na síntese. Este trabalho tem como objetivo combinar um hidrogel celulósico com as propriedades antimicrobianas da prata, visando uma produção mais ambientalmente amigável. Para este propósito, hidrogéis de Carboximetil Celulose de Sódio (CMC) com ácido cítrico como agente reticulante foram produzidos pelo método de evaporação de solvente, e depois tratados com partículas de prata, obtidas pela redução química de nitrato de prata com diferentes agentes redutores. A efetividade das ligações cruzadas foi conferida por espectroscopia do infravermelho utilizando o acessório de Reflexão Total Atenuada (ATR), e a incorporação da prata foi avaliada por Difração de Raios-X (DRX), espectroscopia de quebra induzida por laser (LIBS) e espectroscopia UV-Vis. A morfologia e composição dos filmes foi também examinada por Microscopia Eletrônica de Varredura (MEV) com um acessório de Espectroscopia de Energia Dispersiva (EDS). Testes microbiológicos foram executados por meio de disco de difusão com *C. albicans*, *E. coli* e *S. aureus*. Outras análises funcionais do hidrogel avaliaram o grau de inchamento e o pH. Os resultados indicaram a formação de ligações cruzadas no método de evaporação de solvente e as análises químicas apontaram a presença de prata metálica. Apesar da formação de partículas amorfas, elas foram responsáveis pela resposta antimicrobiana do material, confirmando seu uso potencial como um curativo.

Palavras-chaves: biopolímeros; ligação cruzada; ácido cítrico; prata; glicerol; borohidreto de sódio.

LIST OF FIGURES

LIST OF CHARTS

INDEX

1 INTRODUCTION

Wound dressing represents a significant aspect of health treatments in general. Wounds can be a burden for both patients and society and effective wound treatment is a topic of growing interest in research (BOATENG; CATANZANO, 2015). The development of modern, more effective, and cost-effective wound dressings could improve the life quality of the patients and optimize the heath treatment costs for the SUS – Brazilian Unified Health System.

An ideal wound dressing should sustain a moist environment while protecting the wound bed from external agents including bacteria, fungi, and viruses. Additional advantages are obtained if the dressing material presents antimicrobial activity and provide comfort for the patient. Modern hydrogels can fulfil a significant part of these attributes (ANDREU *et al.*, 2015). The incorporation of additives, particularly metallic ions, in a hydrogel matrix is a useful strategy to improve the healing and antibacterial properties of wound dressings.

Silver (Ag) has been widely employed in medicine and domestic utensils, from ancient settlements in South America to the Roman Empire. With the advent of modern germ theory, researchers noted the antibiotic properties of silver, and with the rising of metallic nanocomposites, silver nanoparticles (AgNPs) were extensively combined with different materials to acquire a biocidal aspect. However, there is no consensus on the exact mechanism of action against microorganisms and in the overall impact of AgNPs in the human body or the environment.

In this contest, the present study exploits a simple method for hydrogel synthesis, known as a slow cast drying method, where the crosslinking is done by heating and water evaporation. Different hydrogel concentrations, drying methods and moulding sizes were employed, considering the results available in the literature (CAPANEMA. et al., 2018a; MALI et al., 2018). The effectiveness of hydrogel synthesis was checked by Fourier Transformed Infrared (FTIR) spectroscopy which allows evaluation of the crosslinking bands' presence in the hydrogel’s network.

AgNPs were incorporated in the synthesized hydrogel by immersion in silver nitrate ($AgNO_3$) solution, followed by chemical reduction with different agents. Treated and untreated samples were submitted to lyophilization to capture SEM images of the microstructure and compositional data was collected with an energy dispersive x-ray spectroscopy (EDS) detector. Samples were also analysed by X-Ray diffraction (XRD),

laser-induced backscattering spectroscopy (LIBS) and UV-Vis spectroscopy.

Microbiological assessments were performed through the disk diffusion method, employing one fungus and two bacteria. The tests were also made with different controls to elucidate the role of each component in the biocidal properties. Additional analysis of the hydrogel's pH and the swelling behaviour helped to evaluate the functional aspects of the material.

About the text structure, this research is organized into three chapters. The *first chapter* addresses the wound healing process, the basic mechanisms of the phenomenon and some strategies to optimize the treatment. One of these strategies involves the use of hydrogels, which are the subject of chapter two. *Chapter two* highlights the basic concepts involved in hydrogel synthesis and how their properties are analysed. Major focus is placed on natural materials-based hydrogels, especially cellulose based hydrogels, which is the object of this research.

The *third chapter* discusses silver/ silver nanoparticles (Ag/ AgNPs), the use of this metal as antibiotic over time and the currently available commercial products containing Ag. Biological and environmental aspects of both Ag and AgNPs are briefly discussed, as well as the potential mechanisms for the biocidal action. Finally, different strategies for synthesis of AgNPs are presented.

Lastly, the experimental procedures are detailed, with a discussion of the results. A comparison with the available data is made, and suggestions for improvements for future analysis are put forth.

2 OBJECTIVES

The general and specific objectives of this research are presented below.

2.1 GENERAL OBJECTIVE

This research aims to develop a method to produce hydrogels by employing sodium carboxy methyl cellulose (CMC-Na) and citric acid (CA) as crosslinker, doped with silver particles for wound dressing applications.

2.2 SPECIFIC OBJECTIVES

Produce cellulose-based hydrogel through cast drying method.

Test different agents to incorporate silver particles in the hydrogel by chemical reduction.

Assess the chemical composition and morphology of the hydrogel.

Investigate the biocidal potential of the material against fungus and different bacteria.

3 HEALING PROCESS

Wounds can significantly impact health since everyone is vulnerable to injuries, either by trauma of various extents or surgery (OKUR *et al.*, 2020). Most of the time, the body can address and resolve minor scratches or injuries easily and naturally. However, in severe cases, non-healing wounds can result in limb amputation, impaired mobility or death (SAGHAZADEH *et al.*, 2018). One of the reasons for that is the delayed healing process by super antibiotic-resistant microorganisms (mainly bacteria) caused by poor primary treatment (BOATENG; CATANZANO, 2015).

Socially, wounds affect the quality of life since they reduce mobility and cause discomfort during treatment. Most patients do not adhere to the treatment properly, especially in vulnerable backgrounds. Other social aspects include increasing obesity, type II diabetes and population ageing, mainly in the Global North countries, with low birth rates (BOATENG; CATANZANO, 2015).

The economic impact of wound care affects National Health Providers. Wound complications are linked to hospital bed occupation, the necessity of surgical or medical interventions, and more nurse time dedicated to wound care (ANDREU *et al.*, 2015; BOATENG; CATANZANO, 2015)

The cost of acquisition and application of wound dressings in Brazil could be estimated through the Systems of Heath Information (Sistemas de Informação à Saúde – SIS). However, data input lacks standardization, turning unclear the cost of wound treatment in Brazil (MAI *et al.*, 2021). Without more data, this cost is estimated at billions of dollars annually worldwide (ANDREU *et al.*, 2015). The development of modern, more effective, and cost-reduced wound dressings could optimize health treatment expenses.

3.1 WOUND CHARACTERIZATION

A wound can be defined as an injury or disruption to an organ's anatomical structure and function, which can extend to other tissues and structures (BOATENG; CATANZANO, 2015).

The primary goals of all wound management are rapid wound closure and a functional and aesthetically satisfactory scar (KUJATH; MICHELSEN, 2008). A slow

and incorrect repair can cause severe damage to the surrounding tissues (BOATENG; CATANZANO, 2015).

Wound assessment has distinct aspects regarding the extension of the wounds and their origins. They can be simple or complex, depending on the number of layers of skin or other tissues affected, and can be acute or chronic, depending on the origin (ANDREU *et al.*, 2015).

Acute wounds usually are produced by trauma (from minor cuts, lacerations or abrasions to severe traumatic lacerations) and repair themselves in an organized and well-timed process, aiming to re-establish the anatomic and physiologic integrity of the area. It has been well-documented that acute wounds expect to heal within a predictable time, regardless of the nature of the injury (ANDREU *et al.*, 2015; OKUR *et al.*, 2020; SAGHAZADEH *et al.*, 2018).

Usually, wounds that do not heal in 90 days are referred to as chronic wounds because they fail over time, and complete restoration is not successful in these cases. Chronic wounds can start as skin damage and evolve to compromise tendons, bone and muscle. Ultimately, they can lead to infection, osteomyelitis, septicaemia and death (ANDREU *et al.*, 2015).

3.2 WOUND HEALING PROCESS

Wound healing is a complex process affected not only by the injury type but also by the systemic response of the organism and previous health conditions of the patient. The process involves different cell types and a biochemical combination of growth factors, chemokines, and cytokines. This process has been discussed in-depth in reviews and textbooks (BOATENG; CATANZANO, 2015; OKUR *et al.*, 2020; SAGHAZADEH *et al.*, 2018).

In most cases, the healing occurs naturally with minimal or no intervention; however, in difficult situations, the body may not reach optimal conditions for healing. That means the treatment must be tailored to improve the organism's natural response, and each phase may require a different approach.

There is no consensus on how to classify the various stages of wound healing. Recent works often consider three distinct phases, while other authors can identify up to five steps. The number of phases depends on the point of view or referential adopted for wound healing: the immunological response, the overall tissue response, or the

interactions with the dressing.

From an immunological point of view, the three phases are inflammation, proliferation, and wound modulation (ANDREU *et al.*, 2015). This summary is presented in Figure 1.

Figure 1: Summary of the wound healing process.

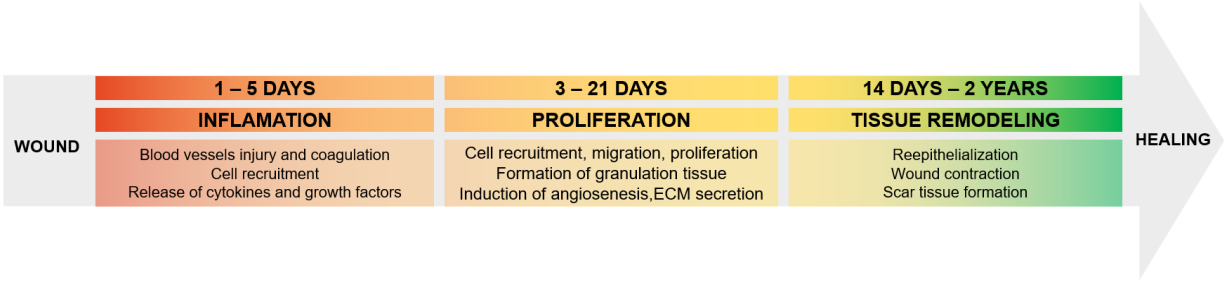

Source: Author (2023) adapted from (ANDREU *et al.*, 2015).

Adopting the standpoint of wound care may be more practical. In this case, a classification into four phases should be preferred: exudative phase, resorptive phase, proliferative phase, and regenerative phase. The resorptive and proliferative phases can be overlapped (KUJATH; MICHELSEN, 2008).

In the exudative phase, the platelets secrete clotting factors, stimulating fibrin deposition. This protein functions as a temporary scaffold for the cells in the wound bed to form a durable cloth. Platelets are also trapped inside the cloth, responsible for vasoconstriction and secreting growth factors essential to other phases of healing (KUJATH; MICHELSEN, 2008; SAGHAZADEH *et al.*, 2018).

The reabsorption phase represents an effective system of phagocytosis and defence. The initial fibrin degrades and activates the chemotaxis, a process where the cells trapped in the cloth are fermented and eliminated. This inflammation process begins right after the injury, lasts about three days, and is characterized by the swelling of the wound (KUJATH; MICHELSEN, 2008; SAGHAZADEH *et al.*, 2018).

Next, granulated tissue is formed by the growth of epidermal cells in the margins of the wound. This stage is the proliferative phase, characterized by the migration and proliferation of fibroblasts and replacing the temporary fibrin structures with a more robust collagen matrix. This process is complex, and dressings must be changed gently. The final remodelling and restructuring process can take up to a year – the regenerative phase – consisting of the recovery of the regular layers of skin and scar formation (KUJATH; MICHELSEN, 2008; SAGHAZADEH *et al.*, 2018).

The unbalance of one or more of these phases can have two consequences: the formation of a hypertrophic scar or the development of a chronic wound (OKUR *et al.*, 2020). Both scenarios are distressful for the patient, as they may require surgical intervention, solid antibiotic therapy, or longer times to improve skin nutrition or strengthen the immune system. (OKUR *et al.*, 2020). While these conditions are treated, the wound dressing must comfort the patient.

3.3 FACTORS THAT INFLUENCE THE HEALING

While most wounds tend to heal rapidly and with low interference, in some circumstances, injuries may be trapped in the process, unable to complete the healing cycle (OKUR *et al.*, 2020).

The most common disruptive factors for wound healing are bacterial infections and previous conditions such as obesity, diabetes, vascular dysfunctions, or immunosuppression (ANDREU *et al.*, 2015; OKUR *et al.*, 2020; SAGHAZADEH *et al.*, 2018). Another example is age, since elderly patients present thinner skin layers, which hinds the migration and proliferation response. Nutrition factors may also be detrimental to wound healing because low protein levels can slow the action of fibroblasts and collagen adsorption. Many drugs can also debilitate the healing process as a side effect in the circulatory system or the immune response (OKUR *et al.*, 2020).

The wound is usually populated with bacteria native to the human skin and does not cause harm to the heathy tissues in the surroundings. Some inflammation levels are normal, expected, and beneficial to the healing process. However, the delayed response of the organism leads to an unbalanced microbiota, causing an excess of inflammation, biofilm formation and critic damage to the growth factors in the wound bed. This process is called hypoxia and is common in individuals with comorbidity factors such as diabetes, obesity, or elderly age (ANDREU *et al.*, 2015; OKUR *et al.*, 2020; SAGHAZADEH *et al.*, 2018).

Severe episodes of hypoxia can put the patients in danger and require invasive surgical procedures, such as tissue amputation. These procedures, in turn, require other kinds of wound dressing, increasing the healing time and costs for the Health System.

Wound pH and temperature have been related to the status of the wound. Elevated temperature indicates inflammation, and elevated or significantly acidic pH

can indicate non-healing wounds that are usually contaminated with pathogens (SAGHAZADEH *et al.*, 2018).

In addition to the unbalance in the inflammatory phase, the exudate production may also represent a delay in the healing process. An excess or absence of exudate production and changes in the composition of the exudate may cause patient distress and consume healthcare resources. Appropriately selecting the wound dressing is vital to optimize the wound exudates and provide more comfort for the patients (ANDREU *et al.*, 2015).

The comfort aspect is essential for the treatment since pain can be very debilitating depending on the size and location of the injury. The central origin of the pain is the action of enzymes and free radicals associated with the inflammation; however, it can also be caused by repeated tissue insults during the dressing cleaning or change. The cleaning process is known as debridement and is important for removing degradation products and other elements that could disturb the healing pathway (SAGHAZADEH *et al.*, 2018).

The control of inflammation, optimization of the exudates, facilitation of the cleaning, and comfort provided for the patient are fundamental to the healing process. In the case of chronic wounds, it is important to take notice of the local or systemic disorders causing the interruption of the healing cycle (KUJATH; MICHELSEN, 2008).

3.4 WOUND DRESSINGS

Wound care dates to several millennia. The most ancient therapies were based on covering the wound with leaves and cloth and applying natural ointments to reduce pain, prevent infection, and keep the wound closed (SAGHAZADEH *et al.*, 2018).

Nowadays, wound management focuses on two purposes: a temporary dressing that covers the injured area and sustains a favourable microenvironment and materials that facilitate cell growth and wound closure (KUJATH; MICHELSEN, 2008). Protection from external physical agents is necessary to sustain a moisty environment and ventilation. It is also essential for the dressing material to inhibit pathogenic replication while supporting the growth of new heathy tissue (SAGHAZADEH *et al.*, 2018).

Selecting wound dressings materials remains challenging since the structures

must combine several physical and biological properties. These structures should be safe, non-irritant, easy to apply, pain-free, cost-effective, and highly absorbent (OKUR *et al.*, 2020).

They should not induce immunogenicity and toxicity while hindering the growth of microorganisms or eliminating them. The mechanical properties should be robust enough to allow the handling of the dressing while matching those of the native skin. The adhesion on the wound bed should be enough to fixate and protect the area but not too strong to cause damage during detachment (KUJATH; MICHELSEN, 2008). At the same time, the structure must have a long shelf life and be comfortable, conformable, and cost-effective (OKUR *et al.*, 2020).

As expected, finding a material that fulfils all the requirements for an ideal wound dressing is not easy. Therefore, more technological advances are required in temporary and permanent smart dressings for wound care (OKUR *et al.*, 2020). It is possible to combine various dressings and use surgical interference, when needed, as an alternative. For the treatment of burns, different dressing strategies are employed in the pre and post-operative phases (KUJATH; MICHELSEN, 2008).

Depending on the specific circumstances, materials used for wound dressing applications vary in terms of the origin of materials, physical forms, architecture, and properties. Simply put, there are several different types of wound dressing products in the form of gauze, thin film, foam, hydrogels, hydrocolloids, and membranes, each of which is suitable for treating a specific wound type.

Authors diverge on how distinct types of wound dressings can be categorized. Some studies consider the type and level of interaction between the material and the wounded site (OKUR *et al.*, 2020), while others focus on the composition of the materials (ANDREU *et al.*, 2015; KUJATH; MICHELSEN, 2008)

The dressings can be natural or synthetic. Examples of dressings from natural sources are collagen, fibrin, Hyaluronic Acid (HA) and polysaccharides like chitosan or cellulose. Synthetic materials include PLA (Poly Lactic Acid), PGA (Polyglycolic Acid) and other polymers approved by regulatory agencies for use as dressings (OKUR *et al.*, 2020). Natural polymers are preferable because of their biocompatibility, biodegradability, low cost, and environmentally friendly perspective (KUJATH; MICHELSEN, 2008).

Concerning the level of interaction, dressings can be inert/passive, interactive, and bioactive. Passive dressings have a minimal contribution to healing, as they serve

as a mechanical barrier against external agents. While they are strong enough to prevent mechanical shocks in the wound bed, most lack vapour permeation and need to be changed constantly when the dressing becomes moistened, either by wound exudate or external fluids. Conventional gauzes and micropore tapes can be cited as examples, and they are generally employed as secondary dressings (KUJATH; MICHELSEN, 2008).

The interactive dressings aim to improve water and gas permeation while acting as a physical barrier to bacteria. They enhance the debridement, granulation, and re-epithelization while removing toxic components from the bacteria or tissue degradation. They are indicated for heavily exudating wounds; however, they are easily adhered to the wound bed and may be difficult to remove without causing pain (SAGHAZADEH *et al.*, 2018).

Hydro active wound dressings are preferable to contour the undesirable adhesion between health tissue and the dressing material. Hydrocolloids, alginates, collagen, Hyaluronic Acid (HA) products, foams, hydrogels, and semipermeable films are examples of such dressings (OKUR *et al.*, 2020). These materials offer much less painful maintenance, and dressings can be left in place for several days if necessary (SAGHAZADEH *et al.*, 2018).

Bioactive dressings are an evolution to improve the healing process of complex wounds. They deliver active substances, which change the environment of the local wound, positively stimulating the healing pathway (KUJATH; MICHELSEN, 2008).

In real-life applications, wound dressings can have multiple layers, each performing a specific function. They can be used in combination with traditional antiseptics or antibiotics. These substances inhibit microorganisms but may also harm cell regeneration (ANDREU *et al.*, 2015).

3.5 HYDROGEL DRESSINGS

Hydrogels are hydrophilic polymer networks capable of absorbing substantial amounts of water without complete dissolution. This property enables them to absorb excess exudates or donate moisture to the wound bed. Their jelly aspect enables them to assume various forms and to be easily applied and removed when necessary. Transparency is an interesting aspect of monitoring regeneration (KUJATH;

MICHELSEN, 2008).

However, they usually need a secondary dressing to hold it close to the injured site. The porosity of the hydrogels facilitates the permeation or release of drug products, but this also represents a permeability to gas, which sometimes is undesirable and can be a drawback (ANDREU *et al.*, 2015; NARAYANASWAMY; TORCHILIN, 2019).

Several commercial wound dressings are available as hydrogels; examples are presented in Chart 1 It is noticeable that most commercial applications combine natural and synthetic polymers, all of which are made in Europe. It represents that the manufacturing process is still restricted and decreases the availability of these treatments for millions of patients.

Chart 1: Examples of hydrogel dressings that are commercially available.

Commercial name	Company - Location	Composition	Presentation
Intrasite™	Smith & Nephew Medical Limited - England	Carboxymethylcellulose Propylene glycol	Amorphous gel in a single-use applicator
Nu-gel™	Systagenix Wound Management – England	Sodium alginate Propylene glycol	
Aquaform™	Aspen Medical Europe – England	Glycerol, modified starch copolymer, methylparaben, imidazolidinyl urea	
Neoheal™	Kikgel – Poland	polyvinylpyrrolidone, polyethylene glycol, agar	Hydrogel film (3 mm thick with 90% of water)

Source: Author (2023), adapted from (BOATENG; CATANZANO, 2015).

The incorporation of metallic ions in a hydrogel matrix is a current strategy to improve these materials' healing and antibacterial properties. Examples include silver nanoparticles (Ag-NP) and zinc oxide nanoparticles because of their solid and broad-spectrum antimicrobial characteristics (BOATENG; CATANZANO, 2015; KUJATH; MICHELSEN, 2008).

The ions deactivate certain enzymes in the cell membrane of bacteria by binding to thiol groups. It compromises the nutrition of the bacteria since these proteins are responsible for energy production and transport. Usually, the metal or oxide nanoparticles are stable and only become active in the presence of moisture – the wound exudate – when the metals achieve their ionized form (BOATENG; CATANZANO, 2015).

With further advances in wound therapy, hydrogels are presented as a versatile platform for drug delivery and wound dressing (NARAYANASWAMY;

TORCHILIN, 2019). The next section will bring aspects of hydrogel synthesis and properties that could be tailored to improve the properties of hydrogels for wound healing.

4 HYDROGELS

The term hydrogel describes three-dimensional network structures obtained from a class of synthetic and/or natural polymers which absorb and retain large amounts of water (GULREZ; AL-ASSAF; PHILIPS, 2011). The hydrophilic groups presented in the hydrogel enables the water absorption, while the crosslinks in the structure prevents the total dissolution of the material. (AHMED, 2015)

One of the first references to the term “hydrogel” dates to 1960, from the work of Wichterle and Lim, published in Nature. The authors produced glycol methacrylate hydrogels after alcoholic re-estherification and polymerization in aqueous solution (WICHTERLE; LÍM, 1960) .

Hydrogels start as a polydisperse branched polymer called “sol”. This dispersion may go through treatment, increasing the number of branches, reducing the solubility, and creating the gel. This is called the “sol-gel transition”, or gelation. Different routes for the gelation process are proposed and consist in one way of classifying these polymer materials (GULREZ; AL-ASSAF; PHILIPS, 2011)

Hydrogels can be classified by the polymer source, in natural hydrogels or synthetic. Biopolymer based hydrogels may present outstanding biocompatibility, however, modern versions of synthetic hydrogels have improved features, like mechanical resistance and smart behaviour (KABIR *et al.*, 2018).

Other less usual forms of classification for hydrogels may include the polymeric composition – homopolymer or copolymer – the configuration – amorphous, semicrystalline, or crystalline – or network electrical charge (AHMED, 2015).

Hydrogel technologies can be applied in many fields, including agriculture, water treatment, drug delivery systems and tissue engineering. This section will focus on the various forms of synthesis, their advantages and disadvantages and the major applications in the biomedical sciences.

This section will focus on the different forms of hydrogel synthesis, especially those applied to natural-based hydrogels, providing a brief outlook on hydrogel properties and how to assess them.

4.1 HYDROGEL SYNTHESIS

Briefly, a hydrogel is a hydrophilic polymeric network cross-linked in some way to present an elastic structure (AHMED, 2015). The process generally includes one of the following: chemical reaction; recombination of free radicals after an exposure to ionizing radiation; or physical interaction by entanglements or electrostatic attraction (GASPERINI; MANO; REIS, 2014).

Gulrez, Al-Assaf and Philips present in Figure 2 a classification for the gelation mechanisms with examples (GULREZ; AL-ASSAF; PHILIPS, 2011).

Figure 2: Summary for the mechanisms of hydrogel synthesis.

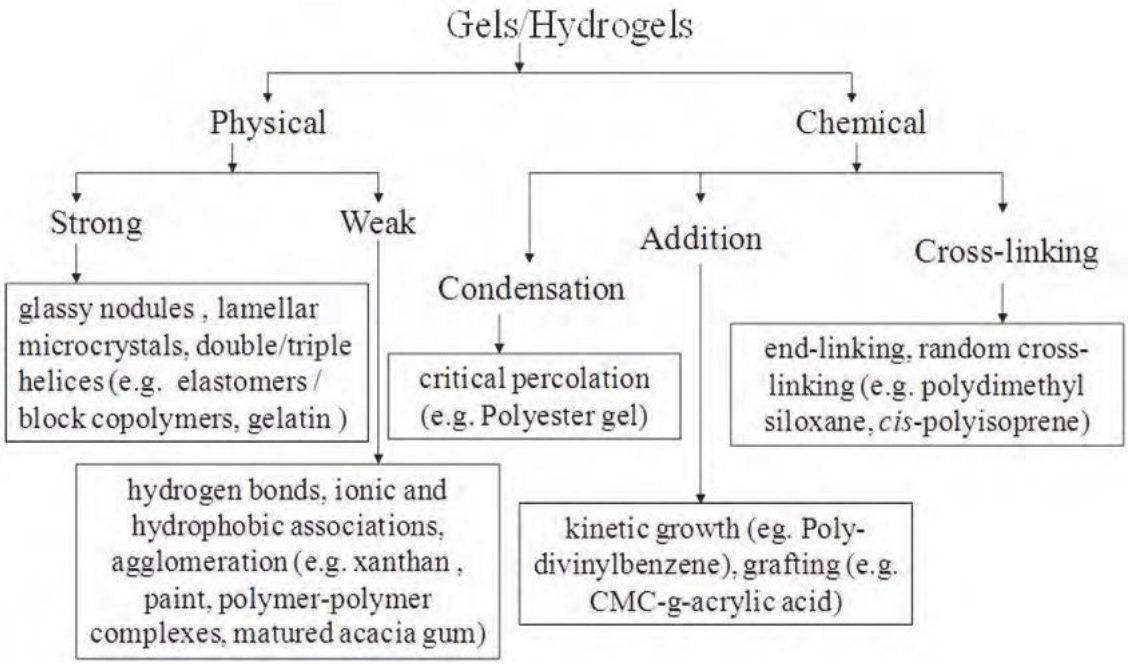

Source: (GULREZ; AL-ASSAF; PHILIPS, 2011).

Liu, et al. produced cellulose-based hydrogels by exposing solutions of sodium carboxymethyl cellulose (25% w/w) to a radiation of 14,8 kGy for approximately one hour. The hydrogels presented stability in water environment, being able to absorb up to 5 times its weight of water within 15 hours (LIU, Pengfei *et al.*, 2005).

As example of hydrogels formed by physical interactions, there are the poly(vinyl alcohol) (PVA) hydrogels. They are commonly prepared through freezing−thawing (FT) cycles, that are repeated until crystallites of desired number and size are achieved. These crystallites act as crosslinkers for the PVA hydrogel (CHEN *et al.*, 2016).

The ability of the PVA hydrogel to absorb water and its mechanical properties are dependent from the crystallite domains. Increasing the packaged phase within the hydrogel, the water absorption may be hindered, as well as the mobility of the chains (YOKOYAMA *et al.*, 1986). The improvement of these properties is usually done by blending with other polymers that can compensate the effect of the crystal domains (CROISFELT *et al.*, 2019).

The use of chemical reactions requires the mixing of the stater monomers, the initiator with the substance responsible for the crosslinking. The gelation takes place in the presence of heat, light or catalyst. After this step, may be necessary to wash the hydrogel to remove the impurities or the excess of any of the employed reagents (AHMED, 2015). Usually this is done with deionized water or a neutralizing agent – acidic or alkali solutions.

In addition to the traditional routes of polymerization, hydrogels can also be produced after grafting or surface treatment of fibres or particles, as illustrated in Figure 3.

Figure 3: Surface functionalization of cellulose nanocrystals by poly (NIPAM-co-DMAEMA).

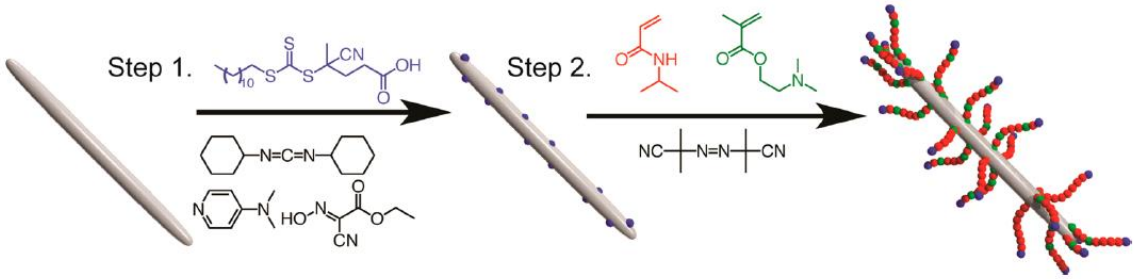

Source: (THÉRIEN-AUBIN *et al.*, 2016).

Thérien, *et al* produced cellulose hydrogels from cellulose nanocrystals (CNC) after chemical treatment. Firstly, the CNC was treated with a chain transfer agent, capable to interact with N-isopropylacrylamide (NIPAM) and N,N-dimethylaminoethyl methacrylate (DMAEMA). The resulting system presented a sol-to-gel transition temperature around 37°C due to the chosen copolymers (THÉRIEN-AUBIN *et al.*, 2016). This change results from a hydrophilic to hydrophobic behaviour.

As disadvantage, the grafting of CNC with PNIPAm requires delicate control of the reaction parameters and the remotion of the unreacted entities is time consuming. Also, the reagents are not cost effective for large scale applications.

The chemical synthesis of hydrogels may employ different agents that are

responsible for the crosslinking. They include N,N0-methylenebisacrylamide (MBA), epichlorohydrin (ECH), glutaraldehyde polyethylene glycol diacrylate (PEGDA), citric acid, and 1,3-diaminopropane, etc (FU *et al.*, 2019). The choice depends on the polymer matrix and the reaction parameters. Recent works try to take hand of the polymer functionalization to employ environment friendly or biocompatible crosslink agents (PRIYADARSHI; KUMAR; RHIM, 2020).

4.2 NATURAL BASED HYDROGELS

Despite its mechanical properties, hydrogels made from synthetic polymers present several disadvantages, like the difficult in biocompatibility, potentially toxic methods of production and low rate of biodegradability (CROISFELT *et al.*, 2019). Even when the synthetic substances are recognised as safe by the regulator agencies, the cost of the raw materials may be high – as observed for PNIPAm – or the applications may be limited – the case for PVA.

Natural based hydrogels, from polysaccharides or peptides are receiving large attention not only for the biocompatibility, but also for the low cost and abundant raw materials.

Examples of natural based hydrogels include, but are not limited to, calcium alginate, starch, collagen, chitosan, and cellulose derivatives. Some of these hydrogels are reviewed by del Valle, *et al.* in terms of chemical structure, hydrogel synthesis and applications (DEL VALLE; DIAZ; PUIGGALI, 2017). Other natural and synthetic sources are briefly discussed by (CROISFELT *et al.*, 2019).

However, most of the works focus on chitosan or cellulose, especially for biomedical applications. Both polysaccharides present relatively low cost and are abundant. They also present similar structures and properties, with chemical sites that are prone to substitution. Chitosan presents an inherent antimicrobial ability, but also possess low water solubility, hindering the formation of hydrogels. The solubility may be increased by substitution of pendant groups; however, this procedure reduces the antimicrobial properties of chitosan.

The presence of hydroxyls in cellulose creates strong inter and intramolecular interactions, leading to poor solubility and processability of pure cellulose under common organic solvents (OPREA; VOICU, 2020). In this case the processing of hydrogels can be made through chemical dissolution with polar solvents like dimethyl

sulfoxide (DMSO) or N-methyl morpholine oxide (NMMO). Since 2000 there are registers of the use of ionic liquids – imidazolium, pyridinium, among other cations – paired with strong basic anions (SHEN *et al.*, 2015).

The use of polar solvents leads to physical and reversible interactions between the molecules of hydrogel. The formation of more stable networks can be done by chemical crosslinking, which is possible when employing cellulose derivatives (KABIR *et al.*, 2018; SHEN *et al.*, 2015). The use of derivatives also allows the use of water as solvent, leading to more straightforward and accessible processes.

4.3 CELLULOSE AND CARBOXYMETHYL DERIVATIVE

Cellulose is the most abundant polymer that can be obtained from renewable sources. The material consists of a linear syndiotactic homopolymer composed of D-anhydro glucopyranose units linked by $\beta - (1 \rightarrow 4)$ glycosidic bonds (DUFRESNE, 2018) The basic structure, cellobiose, presents six hydroxyl groups and nine oxygens, resulting in six donation groups and nine receivers which translates to four major polymorphisms.

Figure 4: Basic structure of the cellulose (cellobiose), with the numbered hydroxyl groups and the glycosidic bond.

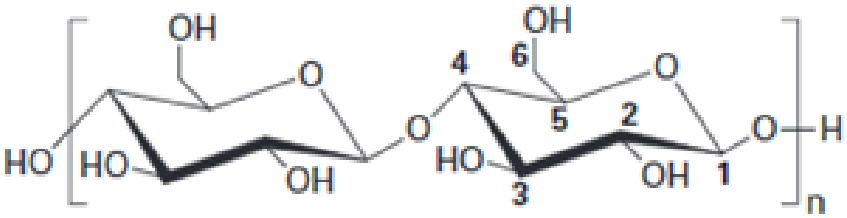

Source: (DUFRESNE, 2018)

An alternative to enhance the processability of cellulose is to perform different substitutions, tailoring the surface energy and the water repulsion (SAITO *et al.*, 2007). The hydroxyl of the primary alcohol on carbon 6 is considered the most reactive group, while the secondary alcohol on carbon 3, is the least reactive. Some authors roughly assume that one third of the hydroxyl groups is available at the surface for substitution (DUFRESNE, 2018).

The key for obtaining cellulose derivatives is to remove the order in the system, which is sustained by the hydrogen bonds. This is performed by activation with strong caustic, followed by reaction with various hydrophilic and/or hydrophobic substituents.

The reaction introduces point defects in the molecular structure and prevents crystallite order that was present in the native cellulose. This phenomenon improves the solubility of the material in a variety of solvents (QIU *et al.*, 2009).

Kabir *et al.* provide a detail on the etherification of cellulose. Cellulose ether derivatives include methylcellulose (MC), ethyl cellulose (EC), hydroxyethyl methylcellulose (HEMC), hydroxypropyl cellulose (HPC) and sodium carboxymethyl cellulose (CMCNa) (KABIR *et al.*, 2018).

Figure 5: Ether groups commonly employed in cellulose substitution.

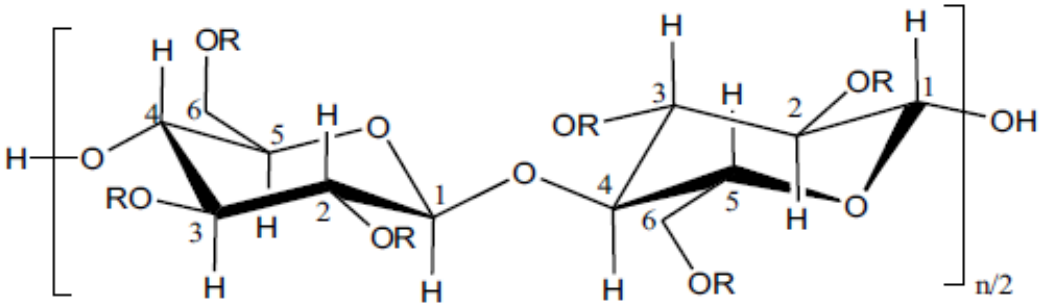

Cellulose ethers	R groups
Methylcellulose	H, CH_3
Ethylcellulose	H, CH_2CH_3
Hydroxyethyl methylcellulose	H, CH_3, $[CH_2CH_2O]_nH$
Hydroxypropyl cellulose	H, $[CH_2CH(CH_3)O]H$
Carboxymethyl cellolose	H, CH_2COONa

Source: (KABIR *et al.*, 2018).

The first step to obtain carboxymethyl cellulose (CMC) is soaking the raw cellulose in an aqueous solution of sodium hydroxide, extracting the alkali cellulose afterwards. Then, the alkali cellulose reacts with monochloroacetic acid or sodium monochloroacetate in alcoholic medium. This last step is called esterification phase (KANIKIREDDY *et al.*, 2020; QIU *et al.*, 2009).

Regardless of the substitution process, it is important to assess the degree of substitution of cellulose. The remaining hydroxyl groups and other pendant structures will dictate the hydrophilic behaviour of the material and the final properties of the hydrogel. The degree of substitution (DS) represents the fraction of sites substituted per anhydro glucose ring (KANIKIREDDY *et al.*, 2020).

Capanema *et. al* published several works investigating CMC based hydrogels

with different DS: 0.77 and 1.22 (CAPANEMA et al., 2018a). It has been reported that a higher degree of substitution decreases the rigidity of the final hydrogel, since the COO^- groups induces the repulsion between adjacent chains, hindering the crosslinks.

The repulsion also causes the expansion of the polymer networks, increasing the water absorption, while the presence of the sodium carboxylate group causes a growth of the osmotic pressure. Thus, the swelling degree of the hydrogel is directly proportional to the degree of substitution from the cellulose derivative CMC (KABIR *et al.*, 2018).

Most studies report that the cellulose-based hydrogels reach the limit of water absorption between 50 and 90 minutes at room temperature. However, some authors monitored the absorption at regular intervals up to 24 hours. The standard procedure is to compare the mass of hydrogel before (W_0) and after (W) a water bath of one hour at room temperature.

4.4 CITRIC ACID AS CROSSLINKER AGENT

For the crosslinker agent, the use of PNIPAm is the standard, despite of its intricate processing, requiring several freeze-pump-thaw cycles (THÉRIEN-AUBIN *et al.*, 2016). Kumar, H. *et al.* take hand of epichlorohydrin (EPH) in alkali conditions to achieve the crosslinking (KUMAR *et al.*, 2019). Recent works present valuable results from CMC hydrogels crosslinked with citric acid (CA), with simple casting-drying crosslinking techniques (SHEN *et al.*, 2015).

Citric acid (2-hydroxy-1, 2, 3-propanetricarboxylic acid, CA) is an acidulant, preservative, emulsifier, flavouring, sequestrant and buffering agent widely used across many industries (CIRIMINNA *et al.*, 2017; WANG, Baoshi *et al.*, 2017). CA is an organic acid that can be produced by chemical or biological synthesis and occurs naturally in several fruits and vegetables.

The vast amount of applications of citric acid can be justified by the low cost, the environmentally friendly production, and its biodegradability. The major uses of this substance take place on the food industry, as preservative or flavouring agent and in pharmaceutical applications, as crosslinker agent for controlled drug release (MORES *et al.*, 2021).

In the year of 2016, it was estimated that the food industry responded for 62,53% of the marked, when the pharmaceutical industry required other 17,08%. An

estimative for the 2021 market predicted a growth around 6% for each of the two segments mentioned above (MORES *et al.*, 2021). By 2018, the share of citric acid consumption was 70% for food and beverage industry and 20% for pharmaceutical and cosmetic applications (SWEIS; CRESSEY, 2018).

Through the 19th century the acid was directly extracted from concentrated lemon juice by adding lime to precipitate calcium citrate, and then recovering the acid using diluted sulfuric acid (CIRIMINNA *et al.*, 2017). This chemical process achieved its peak by 1915 – 1916, when it started to decline due to the high demand and cost. A bioprocess alternative for citric acid was proposed in 1919 in Belgium, by fermentation of *Cytromices* mold (*Penicillium*), however, the process was time consuming and could lead to contamination (SWEIS; CRESSEY, 2018).

The synthesis route employed nowadays is an optimization of the fermentation proposed by the American food chemist James Currie in 1917, from his experiments with strains of *Aspergillus niger* that were capable of produce citric acid with high yields from low-cost start materials (SWEIS; CRESSEY, 2018). The fermentation process is estimated to be up to five times cheaper than the conventional extraction from lemon juice (CIRIMINNA *et al.*, 2017)

Despite of the general consumer associate the citric acid with natural ingredients, the substance is in fact manufactured by fermentation process. The ingredient produced by this route has the status of “generally considered as safe” (GRAS) by the United States Food and Drug Administration (US FDA). However, this classification was adopted in 1958 and supported by the lack of significant harm associated with prior use. From this date, no study was conducted by the FDA to assess the safety of citric acid (SWEIS; CRESSEY, 2018).

A recent report conducted by Sweis and Cressey. evaluated four case studies of patients with different comorbidities, trying to elucidate a relationship between inflammatory reactions and the ingestion of manufactured citric acid – fermented from *A. niger*. The group compared the organism response of the patients before and after the ingestions of natural citric acid and of products containing significant amounts of the manufactured ingredient (SWEIS; CRESSEY, 2018)

However, there was a lack of consistent evidence, and the results were assumed to be linked with individual response to certain by-products of the *A. niger* metabolism. Thus, the authors recommend in dept blind studies of the ingestion of natural and manufactured versions of CA, along with the control of impurities and

related substances from the *A. niger* fermentation.

Since the study and control of related substances is a major activity in the production and quality control of pharmaceutical ingredients, the citric acid can be considered safe once the suppliers follow the international recommendations for the limits of these substances and the overall of Good Manufacture Practices (GMP). As for the converter – i.e., the pharmaceutical industry – it is responsible for the evaluation of the material as received.

4.5 CROSSLINKING PARAMETERS FOR CITRIC ACID AND CMC

Several processes are described on the literature for obtaining cellulose-based hydrogels employing citric acid as crosslinker agent. The methods are simple, consisting of three steps: solution of CMC on water, stirring at room temperature; a pre-drying stage; and a crosslinking stage. The samples are usually poured into petri dishes for the drying and curing steps, assuming circular shapes.

Mali, *et al.* performed pre-formulation test batches of CMC-TG (tamarind gum) hydrogels varying the curing time and temperature. The optimal parameters were a polymer concentration of 2% w/v, curing at 150°C for 5 minutes, after a pre-dry stage at 30°C for 24 hours. As for the CA concentration, reasonable results were found for the samples with 10 to 20% w/v of crosslinker agent (MALI *et al.*, 2018).

Despite also employing 2% w/w CMC solutions, other studies carried by Sannino, et. al. and Capanema *et al.* set longer times and gentle temperatures for the crosslinking stage: 80°C for 24 hours, after the same drying conditions: 30°C for 24 hours (CAPANEMA et al., 2018b; SANNINO et al., 2009).

After the crosslinking step, Saputra, *et.al.* (2015) also washed the samples by soaking on 96% ethanol for 14 hours. In this work, 3% w/v CMC solutions were crosslinked with 5 to 15% of CA, following a pre-dry stage under vacuum, at 30°C for 24 hours. The crosslinking was done at 80°C for 13 hours (SAPUTRA *et al.*, 2015).

As for the degree of substitution on CMC, the value is generally 0,7; however, values up to 1,2 are also reported.

From the method initially proposed by Capanema, *et al.* was established a concentration of CMC of 2% (w/v) and 15% (wlw) of CA. As for the drying and curing stages, is proposed a first step at 40°C for 4 hours and a subsequent heat at 80°C for another 4 hours. A temperature above 60° is needed to obtain the anhydro form of CA,

while temperatures above 120° may lead to undesirable degradation (Ghorpade et al., 2019; Sannino et al., 2009).

Xie and Liu investigated the use of citric acid as crosslinker agent to improve the thermal stability of corn starch. A mixture of 40% w/w citric acid to corn starch was dried at 50°C for 12 hours and subsequently casted at different setups of time and temperature, varying between 120 – 150°C and 3 – 9 hours (XIE; LIU, 2004).

From the degree of substitution of starch obtained for the different samples, the authors could suggest the mechanism of crosslinking for citric acid. It was proposed that the crosslinking reaction would take place after the solution was exposed to enough heat to dehydrate the acid and form an anhydride. After this step, the acid anhydride would be able to link two starch chains (XIE; LIU, 2004). A similar behaviour was proposed by (Sannino et al., 2009). The crosslinking reaction is shown in Figure 6:

Figure 6: Cycle of cellulose crosslinking with citric acid activated by temperature.

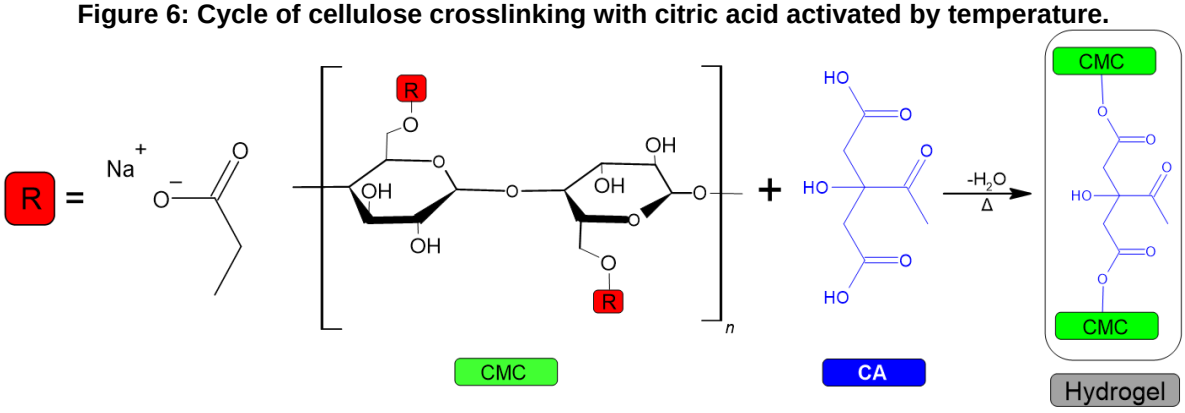

Source: Author (2023).

The efficiency of the reaction can be validated by checking the FTIR of the hydrogel's samples against the neat cellulose and neat citric acid. The crosslinking between these reagents is indicated by an ester bond with a peak around 1760 cm^{-1}; however, the exact position of this band relies on the pH of the media. The sodium atoms coupled with the COO- groups are prone to substitution with H+ ions under acid conditions, changing the FTIR spectrum (CAPANEMA, et al., 2018a; MALEŠ et al., 2020).

5 SILVER NANOPARTICLES (AgNPs)

Silver has been used in human history for centuries in food preservation and healthcare applications. However, the chemical mechanisms that allow these applications are not always precise.

In the last decade, the development of metal nanoparticles and silver's known antimicrobial properties made room for incorporating this metal in many nanocomposites, especially in the healthcare segment. However, apart from the challenge of synthesising and incorporating silver nanoparticles (AgNPs) into the matrix, it is also difficult to elucidate how small particles would interact with the human body and the environment after use.

The following section aims to bring a background of the applications of silver in medicine, trying to elucidate the mechanisms of action against microorganisms and the interaction with wounded skin. It also summarises the strategies for synthesising silver nanoparticles and recent studies on the environmental impact.

5.1 USE OF SILVER IN MEDICINE

The manipulation of silver dates back to 3000 BC, being used as currency and cutlery. Egyptians, Greeks, Romans, and Phoenicians noticed that water and milk stored in silver vessels would last longer. The Andean civilisations in South America were also known for have used silver nitrate to treat wounds. However, all these practices were associated with folklore rather than medical science (MARX; BARILLO, 2014).

The advent of the Germ Theory right before the 19th century established a relationship between microbial inhibition and silver, but the mechanisms behind this were unclear. By early 1900, diluted solutions of silver nitrate were recommended in most of the United States to prevent ophthalmic infections in newborns. Near 1965, silver nitrate was already successfully employed for treating burns, and by 1968 silver sulfadiazine was synthesised, which to the present day remains one of the primary treatments for burns (BARILLO; MARX, 2014).

In Brazil, silver sulfadiazine is considered the gold-standard treatment for burns, being one of the few topical delivery medicines available in the Brazilian Unified Health System – SUS, primarily because of its low cost. However, some studies

indicate that silver sulfadiazine may delay the healing process of the wound since its antimicrobial properties suppress the healing properties. Due to the rapid absorption of the silver sulfadiazine, this treatment requires constant changes of the dressings and renewing of the cream, which usually leads to pain and stress (NOGUEIRA *et al.*, 2022).

Recent studies focus on improving the healing properties of silver dressings while reducing the number of changes and improving the comfort of patients and healthcare professionals.

Modern treatments incorporate silver in wound dressings to improve the antibacterial properties while providing an environment prone to cicatrisation. Most of the dressings consist of the association of an absorbent layer and an antimicrobial material. The result is a more comfortable treatment for the patient, with a slow release of antimicrobial agents.

Commercial treatments employed in Brazil are reported in Chart 2.

Chart 2: Commercial alternatives of wound treatments employed by the Brazilian Unified Health System – SUS.

Trade name	Register	Manufacturer (country)	Layers (Inside to outside)
Acticoat	80804050022	Smith and Nephew, Inc. (USA)	PE+ NC Ag/ PES/ PE + NC Ag
Mepilex Ag	10224000043	Mölnlycke Health Care (Sweden)	Soft silicone with silver sulphate
Aquacel Ag	80523020005	ConvaTec Limited (UK)	Two layers of CMC-Na fibres, impregnated with 1.2% Ag^{+}, EDTA and BECL

Source: (ANVISA, 2022)

The Acticoat® dressing was released in the late 1990s and consists of a polyester layer between two layers of polyethene impregnated with silver nanocrystals. A case study in Brazil reported that 98% of the burns treated with Acticoat® were recovered entirely in less than 21 days (NOGUEIRA *et al.*, 2022).

The Mepilex® Ag presents a technology that provides a gentle adhesion in the surroundings without affecting the wound bed. This property reduces the pain during changes and prevents the skin's abrasion, which makes this dressing favourable for paediatric patients. The Aquacel® Ag consists of an absorbent layer of CMC-Na with 1.2% dispersed silver (NOGUEIRA *et al.*, 2022).

5.2 SILVER IN BIOCHEMISTRY

The biochemical aspects of silver are discussed in this section focusing first on the impacts of silver and silver nanoparticles in the human body. Following, the effect of silver and silver nanoparticles in different microorganisms, as well as the proposed biocidal mechanisms are presented.

5.2.1 Human body

Silver is found in nature in the form of ore (Ag_2S) and chlorate (AgCl) and presents three oxidation states – Ag^+, Ag^{2+} and Ag^{3+} – but only the first is stable enough for antimicrobial applications. It can be obtained as the silver metal ionises in water or biological fluids (MARX; BARILLO, 2014).

Silver may occur in the human body due to natural exposure by inhalation, ingestion, or direct contact. One person is estimated to ingest between 27 and 88 µg of silver per day, with most of this quantity excreted by the gastrointestinal tract. Silver ions may precipitate as silver sulphide when in contact with sweat or moisture in the skin. In this case, they are eliminated from the body through the liver, kidneys, or hair and nail growth (BARILLO; MARX, 2014).

Conventional silver can be found in the blood or urine of humans but does not accumulate in the body. It does not present a carcinogenic potential and does not appear to be mutagenic. Despite higher levels of silver being found in the blood and urine of burned patients when treated with silver sulfadiazine, this does not appear to have clinical significance. The levels tend to normalise after the end of treatment (MARX; BARILLO, 2014).

Model studies performed with rats have shown that the levels of silver in the liver and kidneys decrease by 40% in the first two weeks after the treatment. Another study with human patients demonstrates that the silver accumulated in the wounds treated with silver sulfadiazine is eliminated in the following 28 days. A similar effect was observed in samples of blood and urine of patients treated with dressings containing silver nanoparticles (MARX; BARILLO, 2014).

Another concern about using silver as an antibiotic is the possibility of adverse effects. While natural allergy is rare, temporary or permanent skin colour changes are expected (SILVA *et al.*, 2017).

Temporary skin discolouration occurs when silver interacts with tissue that is already devitalised. This side effect is expected for wound dressings containing silver; any colour changes are usually normalised once the treatment is resumed (MARX; BARILLO, 2014).

On the other hand, permanent skin discolouration is associated with the oral ingestion of large amounts of colloidal silver, which accumulates in lower layers of the skin and appears as grey, brown, or black spots in the portions most exposed to the sunlight. Such adverse effect is one of the reasons why the FDA has controlled colloidal silver products since 1999 (MARX; BARILLO, 2014).

While conventional silver may not present significant clinical implications, its nanosized counterpart is debatable. Studies with artificial skin detected the release of AgNP into sweat. In vitro studies associated nanoparticles with the death of human model cells, such as mesenchymal and hepatoma cells (PARK *et al.*, 2010).

Understanding the interaction between AgNPs and human cells is just as hard as evaluating the biocidal mechanisms of the metal. It is not clear if the cytotoxicity of AgNP is due to their size or because of chemical transformations. Wang et al. combined tomography and synchrotron light sources to elucidate the phenomenon and concluded that a chemical conversion of AgNP into ions, oxides and sulphides plays a significant role in cell toxicity (WANG, Liming *et al.*, 2015).

5.2.2 Microorganisms

While there is an agreement that the silver ions are responsible for hiding the microorganism's proliferation and that the diffusion of the ions through the cell membrane is a mandatory step, there is no consensus on the silver's mechanism of action against microorganisms (MARX; BARILLO, 2014) s. Some theories suggest that the inhibition occurs simply by the breakage of the cell membrane. Other approaches rely on interactions that may occur inside the cell: with enzymes, amino acids, or DNA (MARX; BARILLO, 2014; SAHA; KIM, 2022). These mechanisms are summarised in Figure 7.

Figure 7: Proposed mechanisms for the biocidal action of silver.

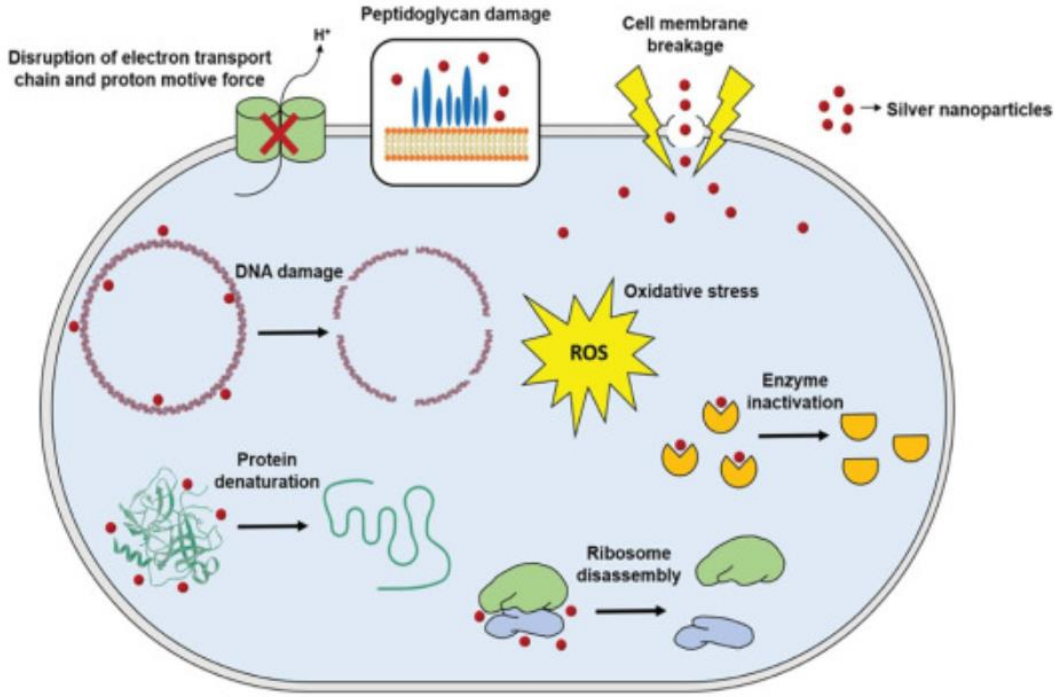

Source: reproduced with permission of (SAHA; KIM, 2022).

Since layers of cationic and anionic species constitute bacterial cell membranes, the silver ions can bind to them due to electrostatic forces. Silver may interrupt the exchange of substances between the cell and the external medium, reduce bacterial movement or even cause a rupture in the membrane.

Once inside the microorganism, silver ions can deactivate enzymes responsible for the digestion of nutrients and gas exchange. However, bacteria can overcome this simply by producing more enzymes. Silver ions are also prone to interact with the bacterial DNA dispersed in the cytoplasm, leading to mutation either by bonding with the nitrogen atom in the guanine base or causing the dimerization of thymine. The interaction with amino acids may form unstable silver complexes and free radicals that cause the precipitation of proteins. This last kind of interaction is also one of the antifungal mechanisms (MARX; BARILLO, 2014).

There is no consensus for the minimum inhibitory concentration (MIC), i.e., the minimum concentration above which there is no microbial proliferation because the antimicrobial property of silver is a combination of different mechanisms. The MIC for silver is reported to be between 8 and 80 mg/ mL (MARX; BARILLO, 2014).

An essential consideration in using any substance against bacteria is the possibility of increasing bacterial resistance over time. The association of this effect

with the use of silver is highly uncommon, with less than twenty reported cases between 1975 and 2007. Some were intentionally created in the laboratory, while others were from veterinary or human sources or the environment (MARX; BARILLO, 2014).

Studies that induced resistance in the laboratory exposed different generations of bacteria to increasing levels of silver compounds, starting way below the minimum inhibitory concentration (MIC). However, effective resistance to silver is difficult to achieve, suggesting that bacteria must combine different mechanisms to overcome silver.

When the levels of silver are high enough, various mutations occur in the bacterial colony simultaneously, each against a different type of silver attack. As a result, despite the modifications, there is no dominant effect, and the strain remains vulnerable to silver. This concentration is known as mutant prevention concentration (MPC), above which the growth of any resistant mutant is prevented (BARILLO; MARX, 2014).

5.3 SILVER IN THE ENVIRONMENT

The toxicity of silver, especially in the form of nanoparticles, is a significant concern. Most studies rely on the Ag-NP release from composite materials into the environment. However, few studies are dedicated to understanding how these particles behave once released in natural environments (SYAFIUDDIN *et al.*, 2017).

It has already been demonstrated that Ag-NP can damage algae and small animals – vertebrates and invertebrates – both in fresh and seawater. Another adverse effect is observed in the soil microbiota, where silver can affect symbiotic agents responsible for nitrogen fixation or digestion of organic matter (SILVA *et al.*, 2017). The mechanisms of action behind these effects are still an unsolved matter.

Some possible changes that may occur with Ag-NP in the environment are changes in the aggregation or oxidation states, precipitation of the secondary phase and sorption of organic or inorganic species. Most of these changes are affected by sterical, electrostatic or other stabiliser agents employed during synthesis because they prevent particle aggregation and often interfere with the particle's solubility (LEVARD *et al.*, 2012).

While insoluble under anaerobic conditions, the Ag-NP can be degraded in an

oxidative environment because a soluble layer of silver oxide is formed on their surface, releasing Ag^+ ions and exposing more metallic silver to oxidation (CHINNAPONGSE; MACCUSPIE; HACKLEY, 2011).

A study by (Levard et al., 2012) reviewed the possible modifications of Ag-NP in a synthetic environment that simulates the thermodynamical characteristics of fresh and seawater and wastewater treatment plants. The authors draw diagrams combing the activity of hydrogen ions (pH) with the activity of electrons (Eh) for a system containing Ag^+, Cl^- and HS^-

The seawater typically presents high ratios of Cl/ Ag, while these ratios are low for freshwater. Aqueous AgCl or $AgCl_2^-$ are the predominant species in the sea, while AgCl precipitates in freshwater. In anaerobic conditions observed in wastewater treatment plants, precipitation of Ag_2S is expected (LEVARD *et al.*, 2012).

In vivo studies of the impact of Ag-NP were performed with zebrafish (*Danio rerio*), often employed as a model for aquatic vertebrates, and with rice (*Oryza sativa*) as a model for plants (GAO *et al.*, 2021; OTTONI *et al.*, 2020).

Ottoni et al. observed that the dosage of Ag-NP affected the germination of seeds and the plant growth in groups of 90 seeds treated with different concentrations of Ag-NP for 15 days. While dosages up to 0.001 mM did not affect seed germination, when the concentration increased to 0.1 mM, only 28 germinated. This number dropped to 17 when the concentration was 0.5 mM. Plant growth was also impacted. While a control group presented a shoot length of 12 cm, plants in contact with 0.001 mM were reduced to 8 cm, and with 0.5 mM, there was only 1.12 cm of the shoot (OTTONI *et al.*, 2020). The authors observed that chlorophyll content on leaves decreases with the addition of AgNP and theorised that the accumulation of silver causes this.

As for the zebrafish, Ottoni et al. measured the oxygen consumption and the ammonia excretion when the fish were in contact with different concentrations of AgNP for 24 hours. The oxygen consumption dropped three times when the fish were exposed to concentrations between 0.025 and 0.05 mM of AgNP, and the ammonia excretion decreased for the AgNP exposure levels from 0.025 to 0.2 mM. Although the different levels of AgNP did not induce mortality, the deficiency in the metabolism of proteins and the low oxygen consumption are signs of concern (OTTONI *et al.*, 2020).

It is clear that AgNP varies in the way it affects different organisms, but even when one evaluates a specific organism, there are disagreements in the literature. This

paradox shows the importance of standardising the biological evaluation of AgNP to provide consistent data to the community (SILVA *et al.*, 2017).

5.4 SYNTHESIS OF SILVER NANOPARTICLES

Silver nanoparticles can be synthesised using physical, chemical, biological, or hybrid methods. Chemical routes are bottom-up, employing salts and reduction agents in simple and easy methods; however, most of the reagents, solvents or their residues may be considered toxic. Physical methods are top-down strategies that present high costs despite producing high-purity nanoparticles. Recent alternatives include biological synthesis, which is also bottom-up but employs microorganisms that can process silver ions and release the nanoparticles. The advantages of this technique include the low cost and environmentally friendly aspect; however, the common need for additional purification steps is often a negative point (SILVA *et al.*, 2017).

5.4.1 Physical methods

An early-developed physical method for the synthesis of nanoparticles is the evaporation-condensation strategy. In this technique, a piece of source metal is placed in a tube furnace at atmospheric pressure with a carrier gas. With an increase in temperature, the metal is vaporised. Despite achieving nanoparticles with high purity, the method requires specialised infrastructure to be carried out. Achieving the right temperature while protecting the surroundings from heat damage is a challenge that consumes time and energy (ABOU EL-NOUR *et al.*, 2010).

Other authors have achieved similar results with ceramic heaters, enabling the concentration of energy reaching high temperatures fast and without presenting a risk to the surroundings. This alternative provided large amounts of high-purity silver nanoparticles, representing a reasonable approach for scale-up the synthesis (JUNG *et al.*, 2006).

5.4.2 Chemical method

The chemical synthesis of AgNP does not present some drawbacks in physical

synthesis. The chemical process is cheaper and faster and can be done with various reagents. This method employs a source of silver – a silver slat like $AgNO_3$ – a reduction agent that effectively forms metallic silver and sometimes a capping agent, which is responsible for regulating the size and shape of the nanoparticles (SYAFIUDDIN *et al.*, 2017).

Some of the most typical reduction agents employed in chemical synthesis are sodium citrate, sodium borohydride, ascorbic acid, N, N-dimethylformamide and some polyethene glycol copolymers (BEYENE *et al.*, 2017).

Organic acids can act as weak reduction agents. Their mechanism is based on the dissociation of carboxylic groups, releasing electrons and proton (H^+). These released electrons will reduce the Ag^+ ions to form zero-valent Ag ions (Ag^0) (KHATOON; VELIDANDI; NAGESWARA RAO, 2023).

Sodium borohydride ($NaBH_4$) promotes a rapid and stable formation of metallic nanoparticles. The reducing activity increases with the medium's acidity since the decomposition of the sodium borohydride is faster at a pH below 9.24. The decomposition and further reaction of the species in water are described below (LUTY-BŁOCHO *et al.*, 2021):

Equation 1: Dissociation of the sodium borohydride in an aqueous medium.

$$NaBH_4 \leftrightarrow Na^+ + BH_4{}^-$$

$$BH_4{}^- + H_2O \leftrightarrow B(OH)_4{}^- + 4H_2$$

Source: (LUTY-BŁOCHO *et al.*, 2021).

While the reduction proceeds, the $BH_4{}^-$ Ions attach to the surface of the nanoparticles, providing a temporary stabilisation. The particles tend to agglomerate as hydrogen is released (RG POLTE et al., 2012).

Despite sodium borohydride being a hazard, only a small amount of the reagent is required to process the reduction. In addition, its toxicity can be neutralised to more environmentally friendly entities, like boric acid (LIU, Tianhao *et al.*, 2020).

Glycerol in alkaline media can act as an effective, greener, and lower cost reduction agent (PARVEEN; TREMILIOSI-FILHO, 2016; RAHMAN *et al.*, 2021).The incorporation of silver with glycerol as a reduction agent was proposed to improve the antibacterial properties of the cellulose-TiO_2 composite (RAHMAN *et al.*, 2021).

Hydrogel samples were exposed to an $AgNO_3$ solution of 10^{-3} mol/L for 5

hours. After this period, the pieces were dipped in an alkaline glycerol solution for 2 minutes. This solution had a glycerol concentration of 0.1 mol.L^{-1} and was prepared using NaOH at 0.2 mol.L^{-1} as solvent.

The Ag nanoparticles were formed by the diffusion of hydrated silver ions through the hydrogel, their coordination with the cellulose hydroxyl groups and their subsequent reaction with a reduction agent. (BARUD *et al.*, 2008).

Two mechanisms may explain the role of glycerol. In one of them, the metallic cations interact with hydroxide anions of the alkaline media, forming oxide particles (Ag_2O). The OH^- also turn the glycerol into aldehyde, which is responsible for reducing the silver ions on the surface of the oxide particles (LIU, Tianhao *et al.*, 2020; SARKAR; KAPOOR; MUKHERJEE, 2010).

Another proposed mechanism is that the hydroxide ions in the alkaline media turn the alcohols into alkoxides, and these alkoxides can reduce the metallic ions directly (LIU, Tianhao *et al.*, 2020; PARVEEN; TREMILIOSI-FILHO, 2016).

5.4.3 Biological method

Recently there has been a growing concern about the starting materials employed in the chemical synthesis of nanoparticles, the environmental impact of residues and the hazards to health of possible residual solvents. In the so-called green chemistry, there is an effort to establish new reduction agents that are more environmentally friendly.

One alternative is to use plant extracts with a complex matrix composed of alcohol, aldehydes, phenols, and flavonoids, which can work simultaneously as reduction agents and stabilisers (BEYENE *et al.*, 2017). Extracts of leaves, seeds, roots, or fruits can synthesise AgNP.

Some examples include leaf extracts of cherry (*Prunus yedoensis*), extracts of coffee (*Coffea arabica*) seeds and the root of ginger (*Zingiber officinale*). For the fruits, there are grapes (*Vitis vinifera*) and pepper (*Piper longum*) (SYAFIUDDIN *et al.*, 2017).

Dand et a. produced spherical-shaped silver nanoparticles using a hydroalcoholic *Coffea arabica* extract. They mixed the extract with different concentrations of $AgNO_3$ solution and incubated it at room temperature for 2 hours. It was possible to produce particles with an average diameter of 25 nm and antimicrobial activity against *E. coli* and *S. aureus* (DHAND *et al.*, 2016).

More recently, fungus and bacteria were also employed to synthesise silver nanoparticles. This route was proposed when studying the bacteria *Pseudomonas stutzeri*, commonly found in silver mines. It was observed that when placed in a highly concentrated aqueous solution of silver ions, the bacteria accumulate Ag-NP in the periplasmic space; however, the exact biochemical mechanism is still unknown (THAKKAR; MHATRE; PARIKH, 2010). Other studies performed with bacteria *Morganella sp.* found a gene probably responsible for encoding a periplasmic silver-binding protein (PARIKH *et al.*, 2008).

The fungus can be employed in the Ag-NP synthesis because they are often tolerant to the bioaccumulation of silver and are accessible to scale-up through fermentation processes. Some examples include *Verticillium sp*. and *Aspergillus fumigatus* (THAKKAR; MHATRE; PARIKH, 2010).

5.5 CHARACTERISATION

Different processing parameters, such as concentration of silver, different reagents, exposure time, pressure, and pH, can tune the final aspect and the properties of the nanoparticles. Additionally, it is accepted that size, shape and surface charge directly interfere with the biocidal properties of AgNP, so it is expected that the analysis performed in AgNP for biological applications include but are not limited to the following analysis (SILVA *et al.*, 2017).

Chart 3: Essential physical-chemical analysis to be performed on Ag-NP.

Analysis	Goal
Fourier-transformed infrared spectroscopy (FTIR)	Molecular composition of the structure
X-ray diffraction (XRD)	Confirm the synthesis. Assess the crystalline structure
Absorbance spectroscopy (UV-Vis)	Confirm the synthesis. Estimate the size and shape of AgNP
Dynamic light scattering (DLS)	Size, shape, charge, polydispersity index
Transmission electron microscopy (TEM)	Estimate lattice index. Assess morphology

Source: (SILVA *et al.*, 2017).

6 EXPERIMENTAL SECTION

The experimental section of this work can be summarised in four significant steps. The first one is focused on hydrogel synthesis through cast drying. While the second deals with the incorporation of silver nanoparticles. The other two phases are the characterisation: a chemical/ morphological characterisation and a functional evaluation of the hydrogel. A brief scheme of the procedures is illustrated in Figure 8.

The analysis performed for the chemical and morphological characterisation of the hydrogel are in the dark grey boxes, while the functional assessments are in white boxes. The dashed charts summarise the parameters employed during the hydrogel synthesis and for the silver incorporation.

Figure 8: Scheme of the experimental procedures for synthesising and modifying the cellulose hydrogel, chemical characterisation, and morphological assessment.

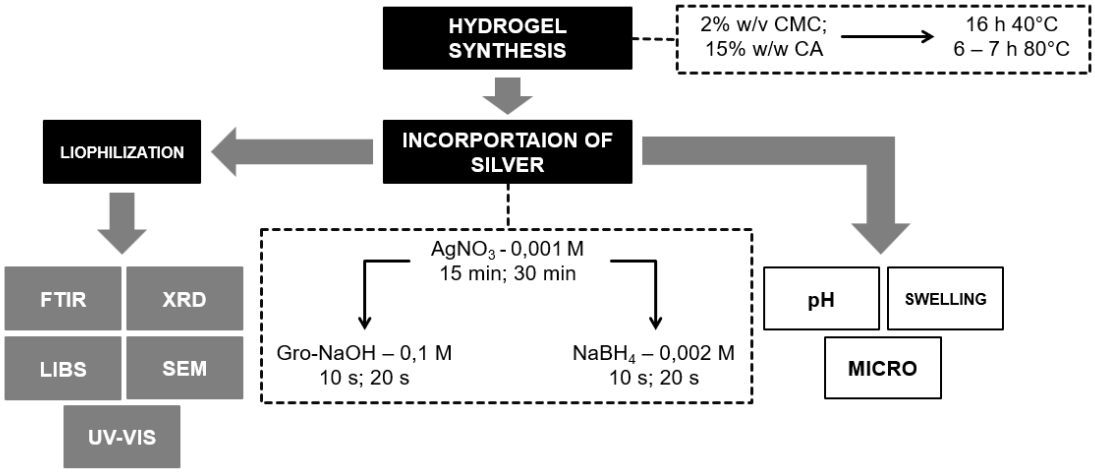

Source: Author (2023).

6.1 REAGENTS

The reagents: sodium carboxymethyl cellulose (CMC) with a degree of substitution from 0.75 to 0.80, anhydrous citric acid and glycerol were kindly provided by Prati-Donaduzzi (Brazil). Sodium hydroxide (NaOH), sodium borohydride ($NaBH_4$) and silver nitrate ($AgNO_3$) were used as received. All the solutions were done with purified water (Milli-Q®). Polystyrene Petri dishes with a diameter of 90 mm per 15 mm in height served as moulds for the hydrogels.

6.2 EQUIPMENT

- Magnetic stirrer model MS-H280 Pro from DLAB Scientific
- Drying oven model SDD 150L, with working temperature up to 250 ± 1°C.
- Spectroscope Frontier from Perkin Elmer.
- X-ray Diffractor Miniflex 600 from Rigaku Corporation.
- J200 Tandem LIBS spectrometer from Applied Spectra.
- Genesys 50 UV-Vis spectrometer from Thermo Scientific
- Electronic microscope model Vega Tescan 3.
- Ultra freezer Coldlab.
- Lyophilizator model L101 from Liotop.
- Sputter coater model SC7620 from Quorum.

All the mentioned equipment are available at UTFPR – Toledo, with the Group of Polymers and Nonostructures (GPAN) or with the Laboratório Central Analítica (LABCA).

6.3 HYDROGEL SYNTHESIS

Several works produce cellulose-derivative hydrogels through the cast drying method (CAPANEMA, et al., 2018a; DEMITRI et al., 2008; MALI et al., 2018).

Generally, they produce a solution of the hydrogel matrix and the reticulant agent, pouring the mixture into polystyrene Petri dishes and finally submitting them to two cycles of drying. Parameters such as solutions' composition, drying time and temperature may vary; however, the concentration lies between 1 – 3% w/v for the matrix and around 10 – 20% (w/w) for the crosslinker.

Trial tests were performed to evaluate the best procedure for this work. The established parameters were: 2% w/v of carboxymethyl cellulose, 15% w/w of citric acid, a drying stage at 40°C for 16 hours, followed by curing at 80°C for 7 hours.

For the mixing, all the reagents were added slowly, and the mixing speed varied between 300 and 450 RPM to avoid air bubbles. The citric acid was added first to the solution. The hydrogel solution was always freshly prepared after drying. The hydrogel mass poured in each 90 mm plate was approximately 35 grams.

Figure 9: Summary of the hydrogel synthesis through the cast drying method.

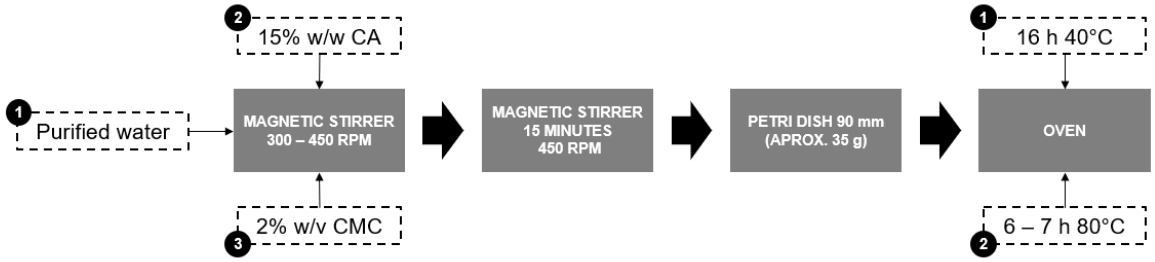

Source: Author (2023).

6.4 INCORPORATION OF SILVER

The incorporation of silver was proposed as a strategy to improve the antibacterial properties of the hydrogel and required two basic steps, adapted from Rahman et al., 2021: an absorption phase and a reduction phase.

In the first step, silver ions were absorbed by the plain hydrogel in contact with an $AgNO_3$ solution (0.001 $mol.L^{-1}$) and protected from light. Afterwards, the hydrogels were exposed to two reduction agents – alkali glycerol solution (Gro-NaOH) or sodium borohydride solution ($NaBH_4$).

The alkali glycerol solution had a concentration of 0.1 $mol.L^{-1}$ and was prepared using NaOH at 0.2 $mol.L^{-1}$ as solvent. The borohydride solution was 0.002 $mol.L^{-1}$.

The volume of solution per sample area was approximately 1.2 $mL.cm^{-2}$ for the silver nitrate and around 2 $mL.cm^{-2}$ for the reduction agents. The surface area of each sample considered both sides of the hydrogel – front and back.

Different contact times were employed to evaluate the effect of each step in the formation of AgNPs. The absorption was carried out for 15 or 30 minutes, followed by 10 or 20 seconds of reduction with each reducing agent separately (see Figure 10).

The samples were then identified by absorption and reduction time, followed by the letters G or B, corresponding to glycerol and borohydride. For instance, sample 15-10B was immersed in silver nitrate for 15 minutes and dipped in borohydride for 10 seconds.

Figure 10: Protocol for incorporating silver nanoparticles in the hydrogel, employing silver nitrate solution and two reduction agents.

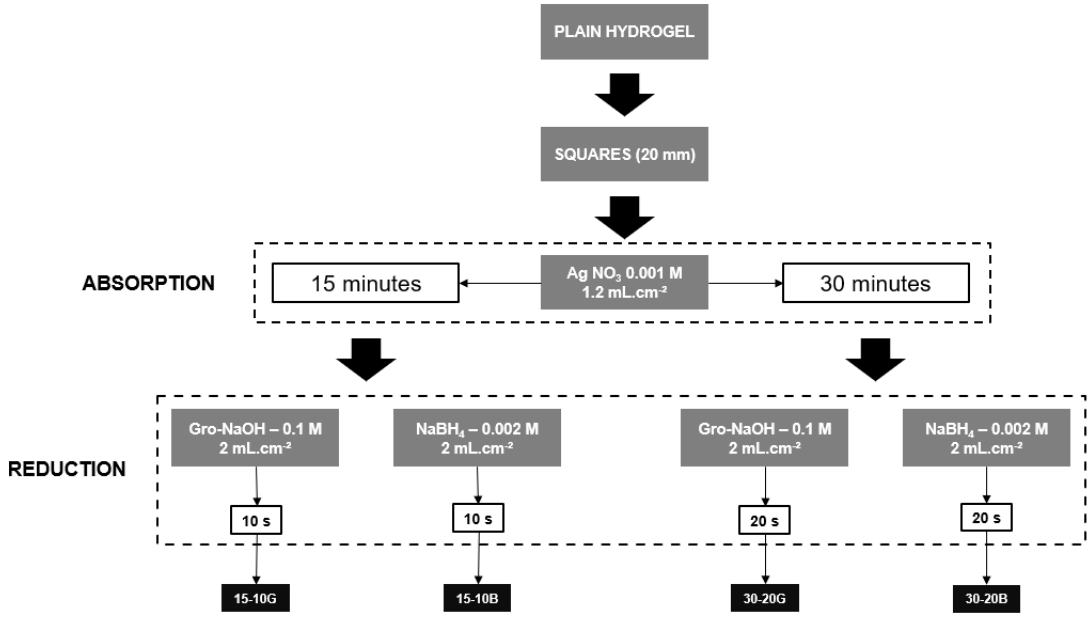

Source: Author (2023).

For the chemical and morphological analysis, the samples were frozen and lyophilised since water could disturb the results or damage the equipment. The remaining functional analysis did not require this step.

6.5 CHEMICAL AND MORPHOLOGICAL CHARACTERISATION

This section details the procedures for the evaluation of the dressings in terms of composition and its microscopic morphology.

6.5.1 Infrared spectroscopy

Fourier Transformed Infrared (FTIR) evaluated the chemical bonds of the hydrogels. This procedure helps determine the presence of crosslinks and other interactions in the hydrogel's network. FTIR spectra were acquired in range of 4000–700 cm^{-1}, with 16 scans and a resolution of 4 cm^{-1} using ATR mode.

6.5.2 Laser-induced breakdown spectroscopy (LIBS)

Freeze-dried samples of the hydrogel containing silver nanoparticles were submitted to LIBS. The measurements were performed under an air atmosphere with a 266 nm laser, using a laser power operating at 50% and a gate delay of 0.5 μs.

Under an optical microscope, a pale-yellow region of each sample was selected. In this region, a 5 per 5 matrix was drawn, covering an area of approximately 16 mm². The grid is represented in Figure 11; each spot was bombarded five times with the laser.

Figure 11 Coordinates where the sample was bombarded with laser for the backscattered diffraction.

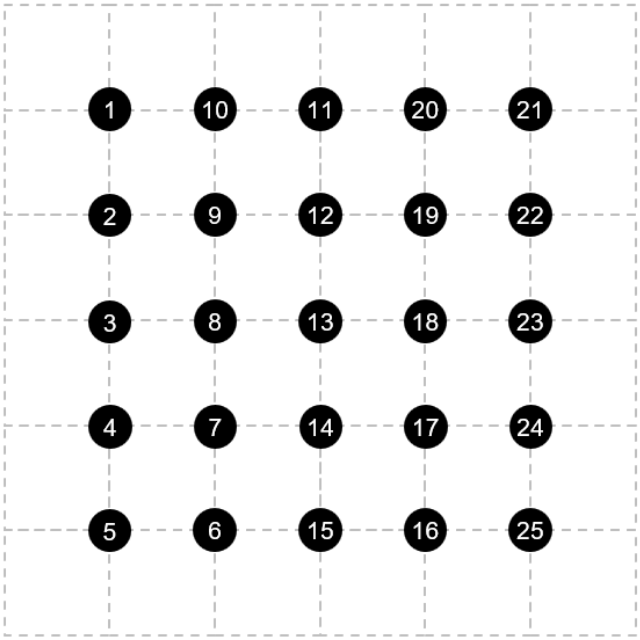

Source: Author (2023).

6.5.3 X-ray diffraction (XRD)

Dried samples of the hydrogel containing silver nanoparticles were submitted to X-ray diffraction. Only the samples 30-20B and 30-20G were evaluated since it was believed that they would present more silver and, therefore, a clearer signal.

The dried hydrogels were placed in a sample holder made of aluminium and submitted to an X-ray source of copper. The scanning was performed between 35 and 50° for the two-theta, with a speed of 5° per minute.

6.5.4 UV-Vis

UV-Vis spectra of the dried samples were acquired in a Genesys 50 (Thermo Scientific, USA) spectrophotometer in the range of 190-1100 nm and wavelength resolution of 1 nm. The films were positioned out of the sample holder. No cuvette was used.

6.5.5 Scanning electron microscopy (SEM)

Fragments of the hydrogels were placed in the sample holder with conductive carbon tape following two configurations: one with the film parallel to the sample holder to evaluate the surface of the hydrogel, and the other perpendicular to the holder, to show the cross-section of a fracture.

The holders with the hydrogel fragments were then placed in a sputter coater, where a thin layer of the gold-palladium alloy was applied to ensure electrical conductivity. The coating was performed under a pressure of 3 mbar, with 20 mA of current for 150 seconds. Finally, the coated films were analysed in the electron microscope.

A brief description of the sample preparation is described in Figure 12.

Figure 12: Sample preparation before the SEM analysis.

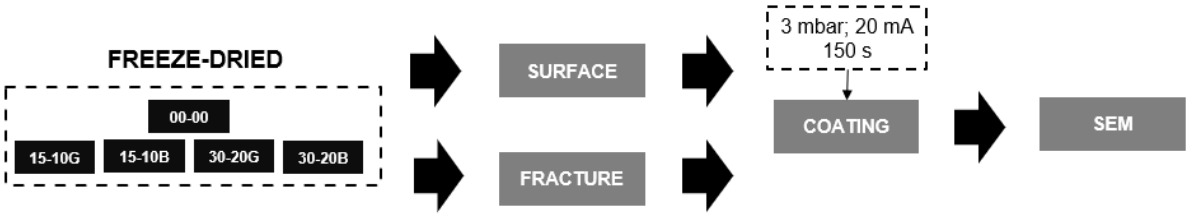

Source: Author (2023).

For the chemical composition analysis, an EDS sensor was also employed, mapping the entire field, and collecting spectra for selected regions of the sample. The acquisition time for such spectra was approximately 5 minutes. Some pieces were also painted with silver ink for comparison.

6.6 FUNCTIONAL CHARACTERISATION

This section details the evaluation of the practical use of the dressings by *an in vitro* approach: pH variations, swelling degree and microbiological assessment.

6.6.1 pH

Since measuring the pH directly from the hydrogel would require special electrodes, one alternative was to assess the pH indirectly. This analysis was performed in three ways: in the hydrogel solution after drying and curing, in the hydrogel films after a steady extraction, and after successive washes with alkali solvents. Different samples were employed for each test.

First, the pH of the hydrogel solution was measured in each preparation step: before and after citric acid mixing and before adding CMC. Three samples of the manufactured hydrogel were left overnight in distilled water without temperature control and agitation. The hydrogel was removed after this period, and the extract's pH was checked.

For the last test, the hydrogel samples were washed successively with distilled water and sodium hydroxide solution at 0.002 M. They were left in contact with distilled water for 10 seconds, followed by 10 seconds in sodium hydroxide and a final wash with running distilled water. The process was repeated seven times, always employing a new solution. The resulting pH for each solution was recorded after contact with the hydrogel.

Figure 13: Different pH measurements performed with the hydrogel solution (right) and hydrogel films (left).

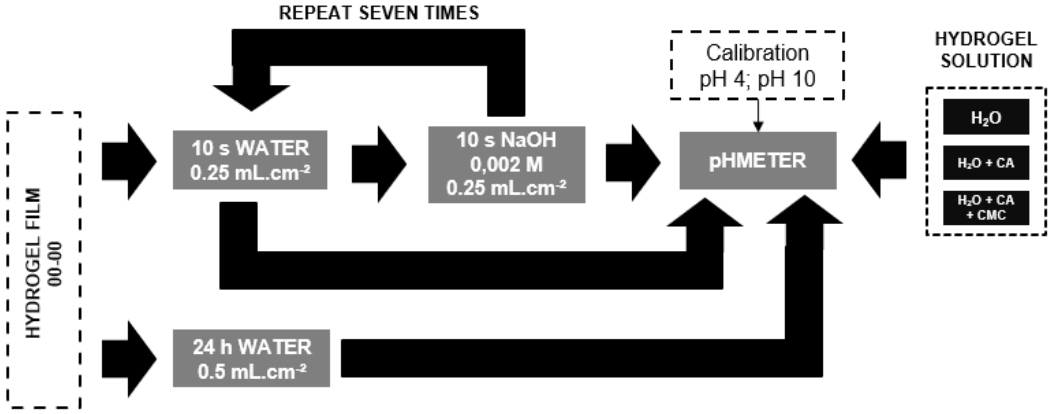

Source: Author (2023).

6.6.2 Swelling degree

The water absorption of the hydrogels was assessed by a gravimetric method. Samples of each treatment were placed in Petri dishes with purified water and weighed after defined time points.

Three samples for each condition were evaluated, cut as squares of 20 mm, and the amount of water was approximately 3 $mL.cm^{-2}$. The excess water from the hydrogels surface was gently dried with filter paper before each weighing.

The time points were less spaced in the first measurements since it is known that the hydrogels absorb more water in the first hours in contact with the liquid, as illustrated in Figure 14.

Figure 14: Time points for monitoring the mass of water absorbed by the hydrogel.

Source: Author (2023).

Weight variation was calculated by Equation 2, employing hydrogel mass before (W_0) and after (W) water bath.

Equation 2: Swelling degree of the hydrogel considering a water uptake from an initial mass (Wo) to a final mass (W).

$$SD(\%) = \frac{W - W_0}{W_0} \times 100$$

Source: Author (2023).

6.6.3 Microbiological assessment

The microbial assessment was performed through the diffusion disk method. In this technique, the material is placed against a culture media containing a microorganism following an incubation period. After this time, materials with biocidal potential present an inhibition halo, whose diameter is compared among samples and microorganisms.

Besides the sample preparation employed in this work – slow cast drying, absorption of $AgNO_3$ followed by reduction with different agents, as shown in Figures

9 and 10, other treatments were proposed exclusively for the biological tests to properly isolate the components of the hydrogel and the reagents involved in the incorporation of silver.

As for the hydrogel composition, besides the hydrogel film containing CMC and citric acid, two other substrates were evaluated: a hydrogel film of CMC, without citric acid, and conventional filter paper. The different preparations are presented in Figure 15.

Figure 15: Additional treatments to incorporate silver in different substrates to provide a better understanding of the microbiological assessments.

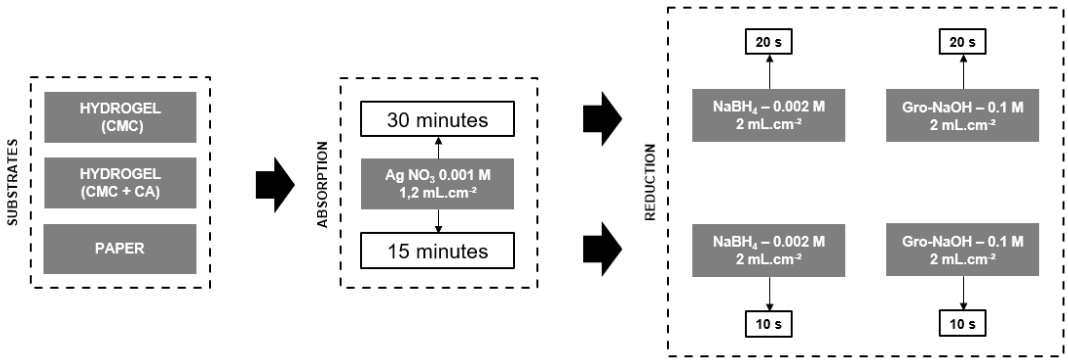

Source: Author (2023).

The different treatments executed for the microbiological assessment are also described in Chart 4, along with the sample designation. The same procedures were followed for the three selected substrates: pure CMC hydrogel, CMC+CA hydrogel, and filter paper.

Chart 4: Sample designation according to the contact time with the solution containing silver and the different reduction agents.

Contact time with $AgNO_3$ (minutes)	Contact time with reduction agent (seconds)		Sample designation
	Gro-NaOH	$NaBH_4$	
–	–	–	00-00
15	10	–	15-10G
15	–	10	15-10B
15	20	–	15-20G
15	–	20	15-20B
30	10	–	30-10G
30	–	10	30-10B
30	20	–	30-20G
30	–	20	30-20B

Source: Author (2023).

This work focused on microorganisms commonly found in human skin and frequently associated with episodes of infection. One fungus, *Candida albicans* and two bacteria: *Escherichia coli* and Staphylococcus *aureus*, were chosen as models. The tests were done in triplicate, and information about the microorganisms, their culture media and incubation parameters are presented in Chart 5.

Chart 5: Incubation conditions for the different microorganisms.

Microorganism	ATCC	Concentration	Culture Media	Incubation
E. coli	25922	10 µL (10^8 UFC.mL^{-1})	Muller–Hinton	37°C; 18 h
S. aureus	6538	10 µL (10^8 UFC.mL^{-1})	Muller–Hinton	37°C; 24 h
C. albicans	90028	10 µL (10^8 UFC.mL^{-1})	Sabouraud	37°C; 48 h

Source: Author (2023).

After incubation, the inhibition halo was measured four times for each sample, and the average was taken. These measurements were done with Image J open-source software.

7 RESULTS

7.1 HYDROGEL SYNTHESIS

After several trial tests, the CMC and citric acid concentrations were fixed at 2% w/v and 15% w/w. For better homogeneity, the acid was added first to the solution and when the powders were sprinkled at small increments with slow agitation speed – from 350 to 420 rotations per minute (RPM).

When the CMC was added first, lumps were formed due to the rapid hydration of this cellulose derivative. Vigorous agitation was required to remove these lumps, leading to the incorporation of air bubbles. On the other hand, the early addition of citric acid provides a lower pH for the system, preventing the increase of the solution's viscosity by the time the CMC was mixed. The different aspect of the solution when the order of the reagents was changed is shown in Figure 16:

Figure 16: Differences in the aspect of the solutions when the cellulose was added first (left) and when citric acid was added first (right).

Source: Author (2023).

The CMC was presented as a fine white, yellowish powder, while delicate white crystals formed the CA. A clear citric acid solution became hazy when the first portions of CMC were added. The hydrogel solution was agitated for another 15 minutes and approximately 35 grams of this solution were poured into the Petri dishes.

The moulds were placed in an oven for 16 hours at 40 °C for drying, following a curing stage at 80 °C until the hydrogels achieved 15 to 20% water content (w/w). This last stage took approximately 5 hours.

The percentage of water was calculated considering that the fraction of solids in the hydrogel is constant – approximately 14.75% of the initial solution or 5.16 grams of each 35 grams plate. The weight loss was associated with water evaporation, but the dehydration of the citric acid during crosslinking was not considered.

The water loss of ten samples was monitored at the start and finish of the drying stage and hourly during the crosslinking phase. Only the results of the last step are presented in Figure 17 since the water loss was too low in the drying stage. Each point is a mean of ten samples.

Figure 17: Variation in the water content during the crosslinking phase of the synthesis in the stationary oven at 80 °C. The amount of solution and the surface area was the same in each sample. Curing was processed after a drying stage at 40 °C for 12 hours.

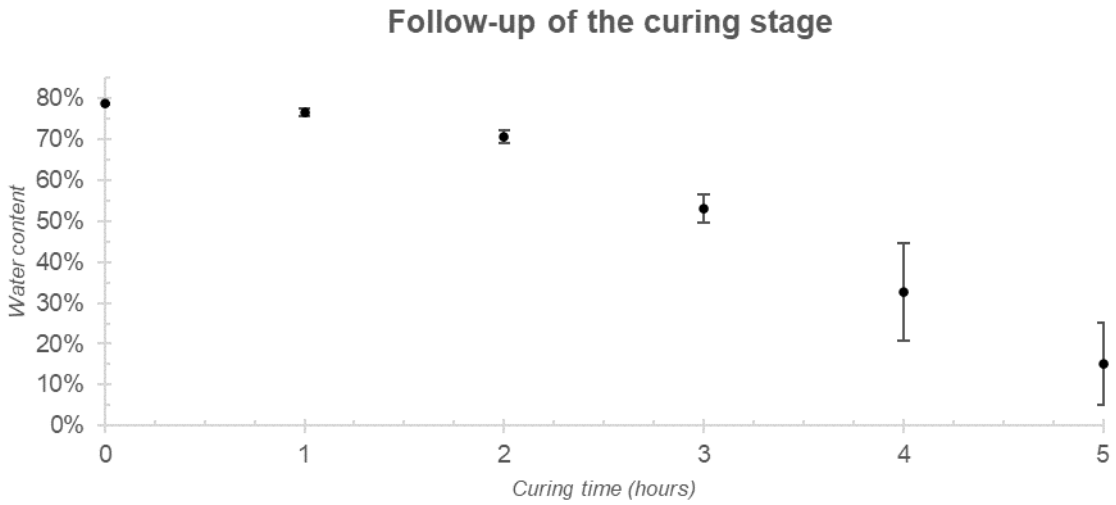

Source: Author (2023).

The final aspect of the hydrogel is soft film of approximately 4 millimetres thick, with a small number of bubbles occasionally dispersed. The presence of bubbles was minimized eliminating the dissolved air by heating the water over the boiling point and letting it cool down protected from the air.

Figure 18: Example of the final aspect of the hydrogel after completing the drying and curing stages.

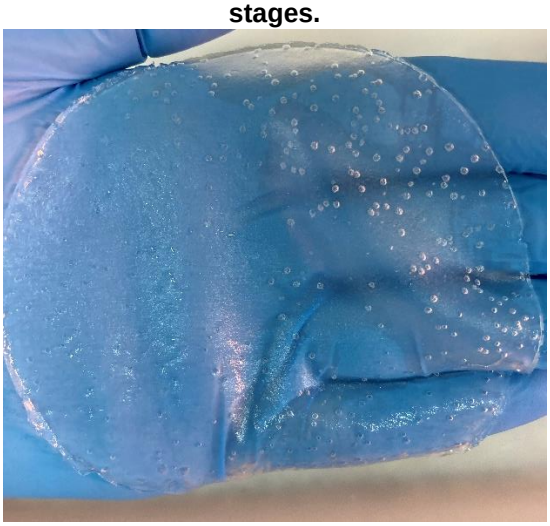

Source: Author (2023).

7.2 INCORPORATION OF SILVER

The times of exposure of the hydrogel to the different solutions are shorter than the reported in the literature (RAHMAN *et al.*, 2021). In the first trial tests, the samples acquire a vivid brown colour, or completely dissolved, as indicated in Figures 19 and 20.

Figure 19: Samples of the hydrogel at the start of the immersion in $AgNO_3$ solution (top) and after 5 hours (bottom). These samples were not protected from light.

Source: Author (2023).

Figure 20: CMC hydrogel impregnated with $AgNO_3$ in alkaline glycerol solution over time. Each plate has a diameter of 60 mm.

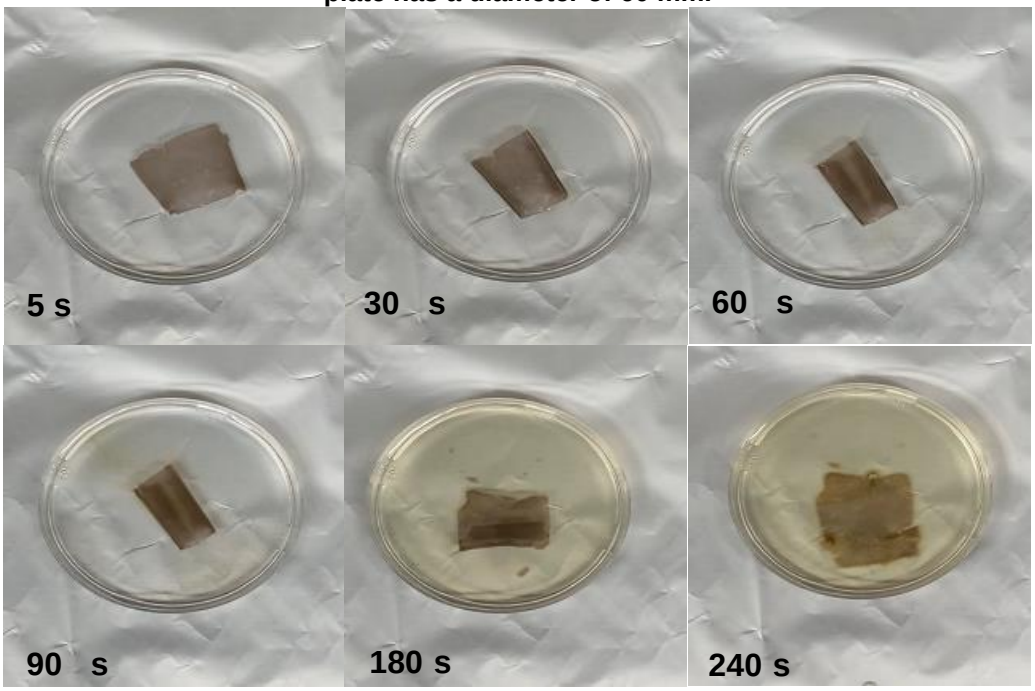

Source: Author (2023).

When the samples were protected from light, a pale-yellow tone was observed, being slightly intense for the films reduced with sodium borohydride. While the colour change may not be clear in the films, it is visible in the reducing agent solutions after the treatment in Figure 21.

The solution of borohydride presented an intense gold colour with releasing of hydrogen bubbles typical of the borohydride dissolution. For the alkali glycerol, a change in the tone was also observed, but much less pronounced.

Figure 21: Evidence of reaction observed by the change in colour of the reducing solutions of alkali glycerol (left) and sodium borohydride (right).

Source: Author (2023).

7.3 CHEMICAL CHARACTERISATION – FTIR

The FTIR spectra of pristine citric acid and CMC were obtained from the US National Institute of Standards and Technology as raw data. They were normalised and compared with the plain hydrogel samples' infrared spectra before the silver incorporation.

7.3.1 Hydrogel formation

This sequence presents the molecular structure, the infrared spectrum, and a list of the corresponding vibration types for each starting material.

For the CMC matrix, characteristic peaks are the OH stretching in 3400 cm^{-1} and the symmetric COO stretching in 1600 cm^{-1}. The relevant bonds are assigned by letters from *a* to *e* in the spectrum illustrated in Figure 22 as well in in the molecular structure depicted in Figure 23 The *b* designation corresponds to the CH bonds and is absent in the molecule illustration for better clarity. A description of each vibration mode is listed in Chart 6.

Figure 22: FTIR spectrum for original CMC.

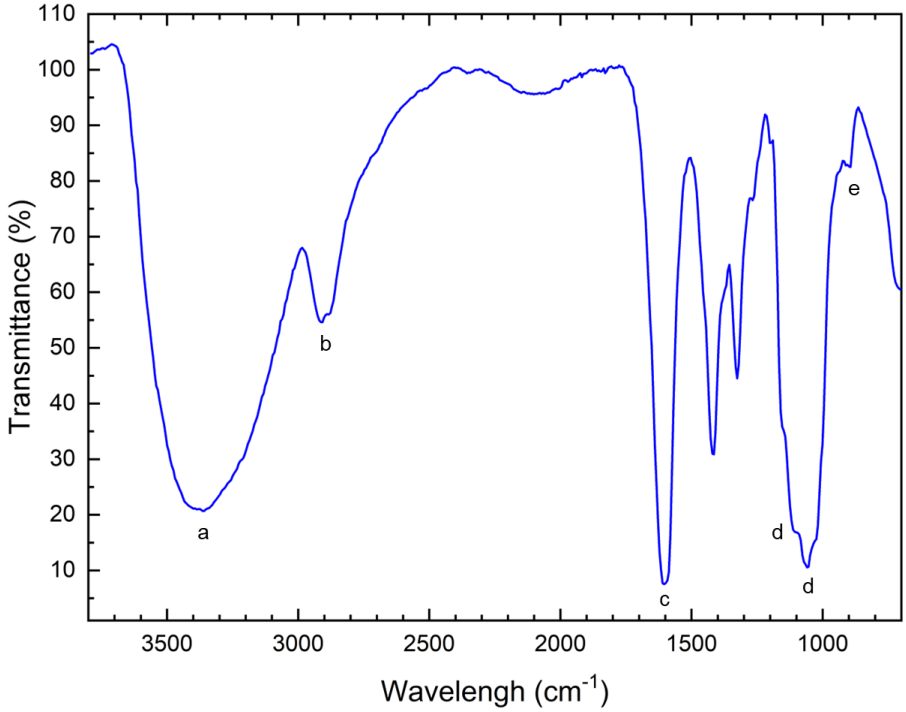

Source: Author, adapted from (NATIONAL INSTITUTE OF STANDARDS AND TECHNOLOGY, 2021a) (2023).

Figure 23: Chemical structure of the sodium carboxymethyl cellulose. The major bonds are indicated by the letter from a to e. The CH bonds (b) were not assigned in the molecular structure for better clarity.

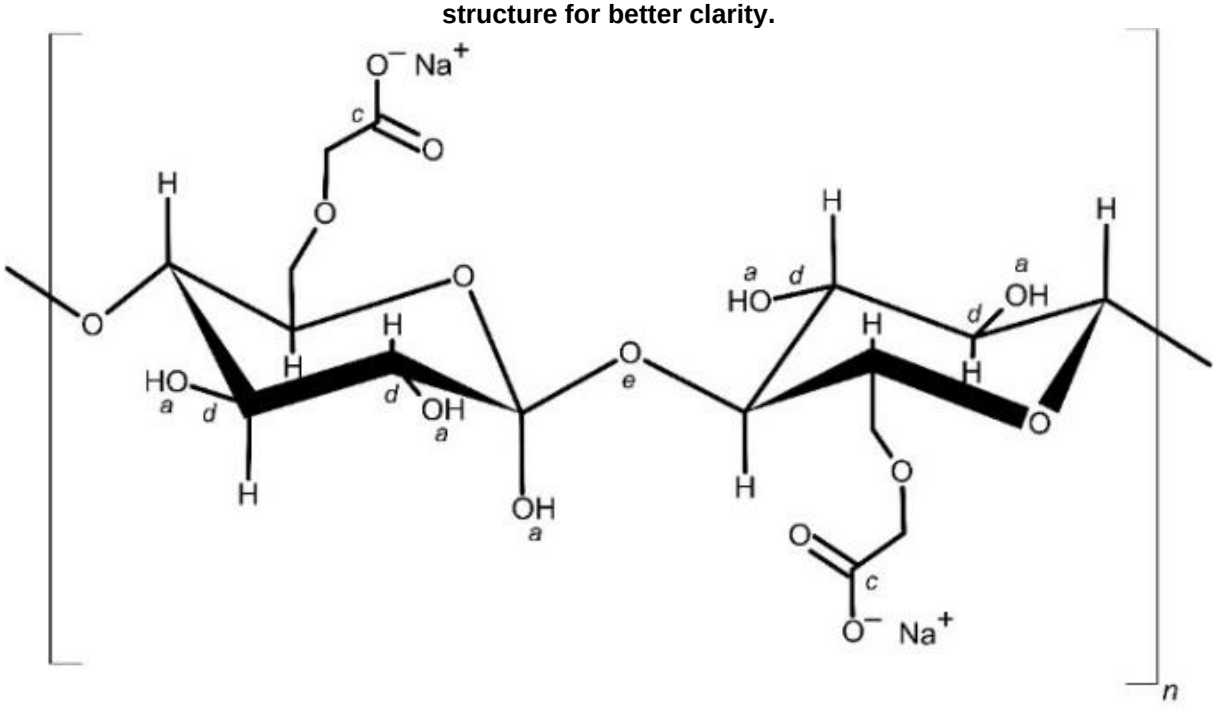

Source: Author (using Chemsketch software) (2023).

Chart 6: List of the infrared vibration types associated with each bond in the molecular structure of CMC. (*) The CH bonds (b) were not assigned in the molecular structure for better clarity.

CARBOXYMETHYL CELLULOSE		
Assigned bond	**Peak (cm^{-1})**	**Vibration type**
a	3400	Stretching OH
b*	2900	Stretching CH
c	1600	Stretching COO^- (asymmetric)
	1420; 1316	Stretching COO^- (symmetric)
d	1112; 1060	C-O alcohol
e	899	β-1,4

Source: (DE LIMA; DE SOUZA; ROSA, 2020).

Similar as done for cellulose, the characteristic peaks for citric acid are listed from *a* to *d* in the spectrum (Figure 24) and in the molecular structure of the acid (Figure 25). The vibration modes are listed in Chart 7.

The main peaks are near 1700 cm^{-1} (1750 and 1710 cm^{-1}). They correspond to the stretching of the double bond on the aliphatic carboxylic acid.

Figure 24: FTIR spectra for the citric acid.

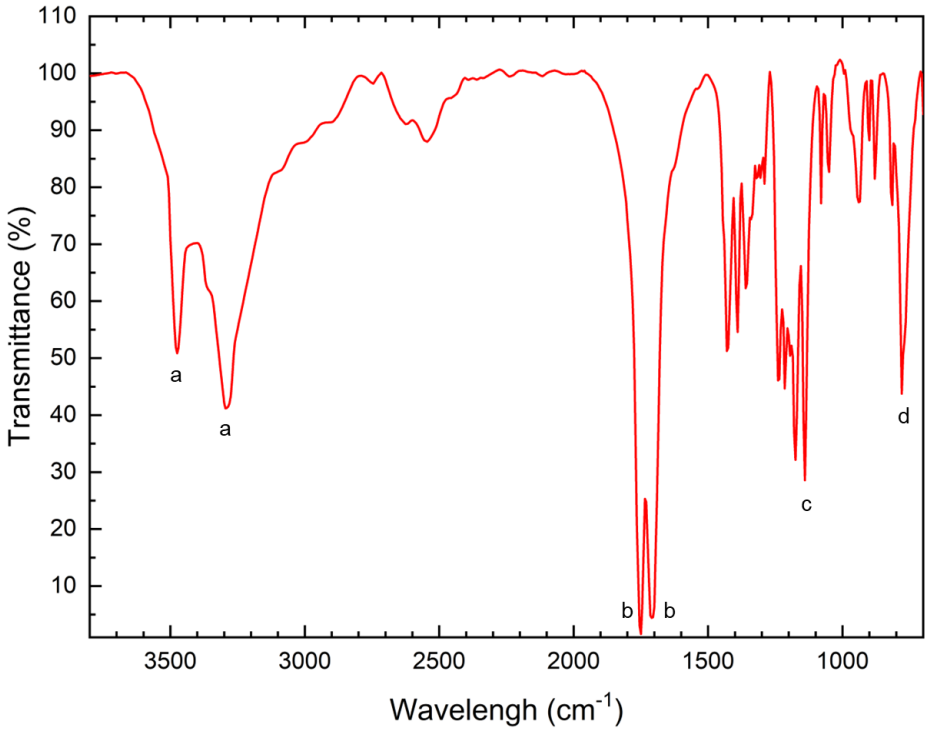

Source: Author, adapted from (NATIONAL INSTITUTE OF STANDARDS AND TECHNOLOGY, 2021b) (2023).

Figure 25: Chemical structure of the citric acid. The meaningful bonds are indicated by the letter from a to d.

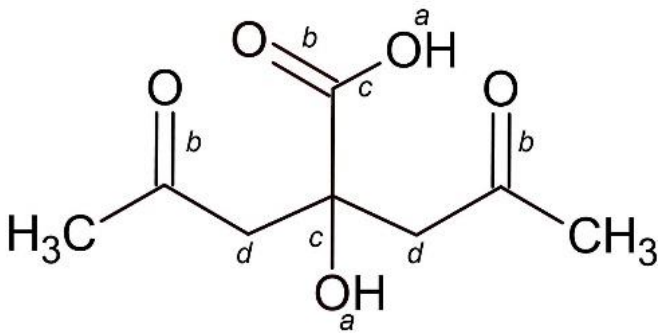

Source: Author (using Chemsketch software) (2023).

Chart 7: List of the infrared vibration types associated with each bond in the molecular structure of citric acid.

CITRIC ACID		
Assigned bond	**Peak (cm^{-1})**	**Vibration type**
a	3475; 3290	Stretching OH
b	1750; 1710	Stretching C=O
c	1175	Stretching C-O
d	780	Rocking CH_2

Source: (COJOCARU *et al.*, 2022).

Combining the CMC with the citric acid under heat would lead to the gradual dehydration of the acid, creating ester bonds between the cellulosic chains, as illustrated in Figure 26. According to Saputra and Ruth, this crosslinking may occur up to three times in each cellulosic unit (SAPUTRA; RUTH, 2019).

Figure 26: Structure of the crosslinked hydrogel. As an example, one ester bond between two cellulosic units is highlighted in red.

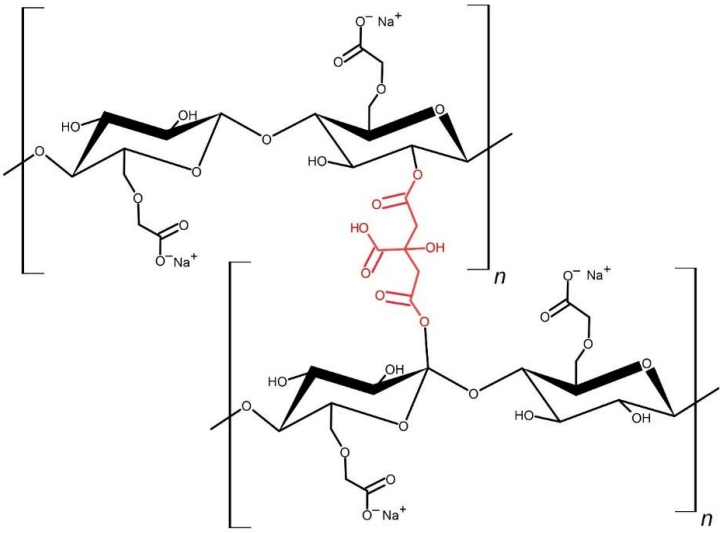

Source: Author (adapted from (SAPUTRA; RUTH, 2019) using Chemsketch) (2023).

As reported by Ghorpade et al. and Sannino et al the crosslinking reaction would be indicated by a shift in the citric acid band from 1710 cm^{-1} to higher frequencies near 1760 cm^{-1} (Ghorpade et al., 2019; Sannino et al., 2009).

However, Maleš et al. also reported that the COO^- symmetric stretching on CMC, initially at 1600 cm^{-1}, would move to higher frequencies under acidic conditions due to the protonation of the group. As a result, the CMC peak would overlap the ester bands of the hydrogel, and the resulting band would be shown in lower frequencies than expected (MALEŠ *et al.*, 2020).

This is also reported by Capanema et al. who argue that the coexistence of CMC and citric acid bands results from the replacement of Na^+ and H^+ in low pH. (CAPANEMA et al., 2018a).

The effect is shown in Figure 27, with an apparent absence of the COO^- peak at 1600 cm^{-1}, overlapped in lower frequency and the slight shift of the two C=O peaks in the same direction. Hence, there is ester bond crosslinking in the hydrogel, with an apparent excess of citric acid. A detail of the bands between 1900 and 1500 cm^{-1} is presented in Figure 28.

Figure 27: FTIR spectra for the plain hydrogel (top), the citric acid (centre) and the original CMC (bottom).

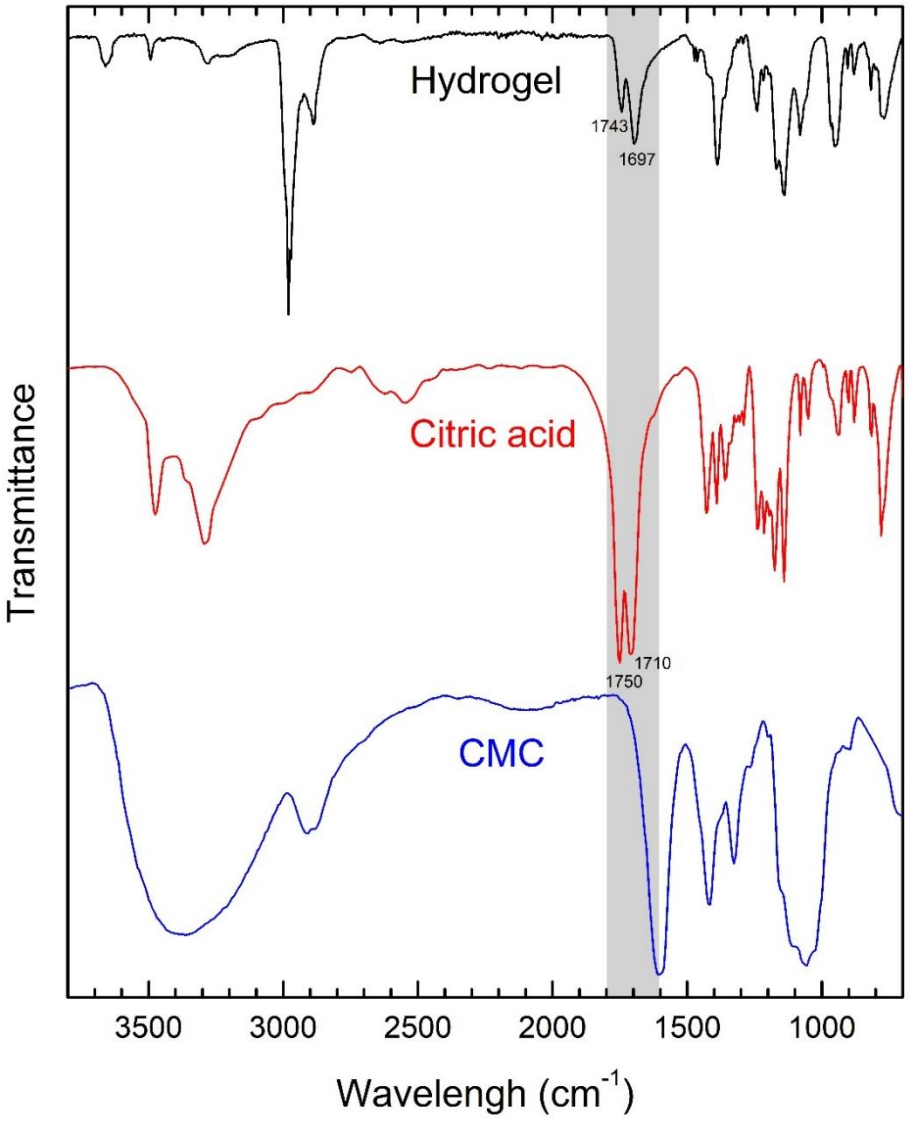

Source: Author (2023).

Figure 28: Detailed FTIR spectra for the plain hydrogel (top), the citric acid (centre) and the original CMC (bottom).

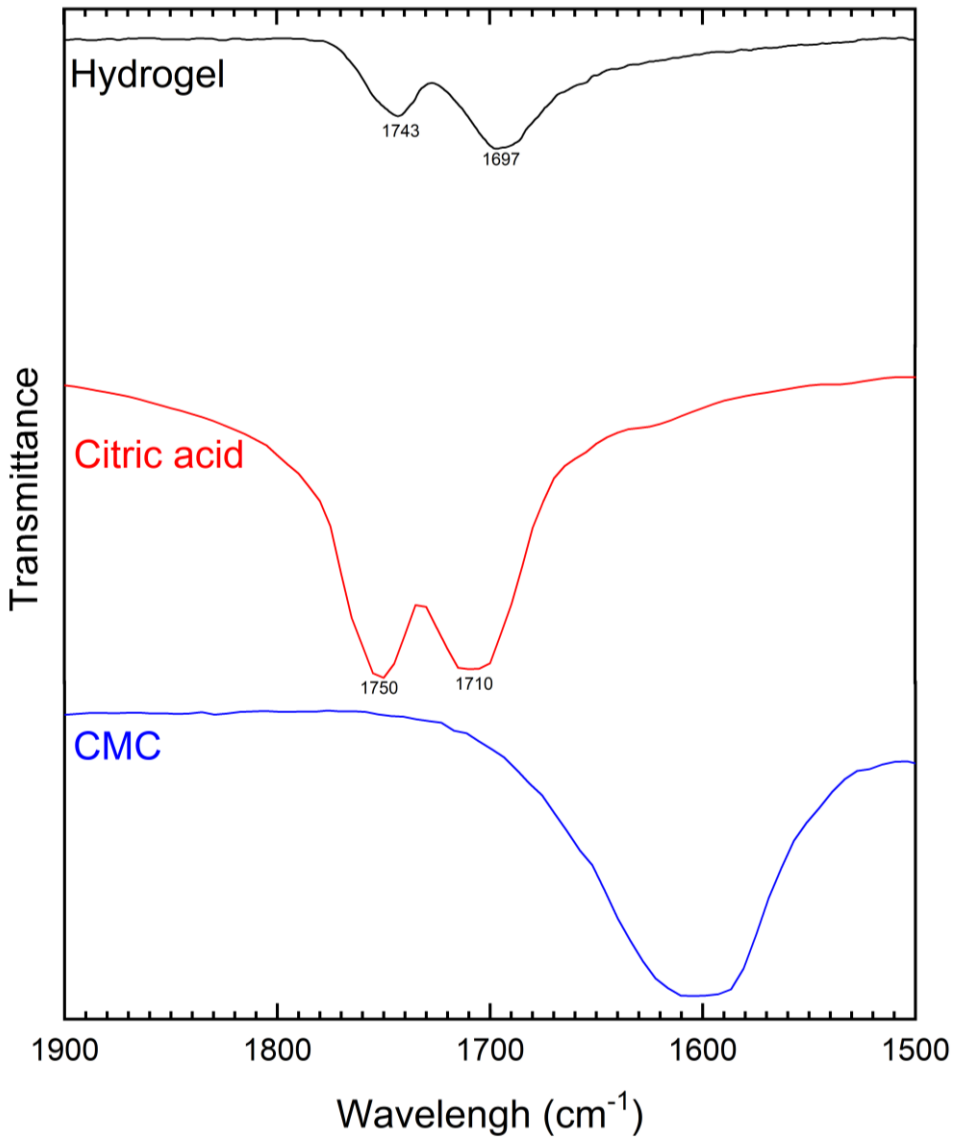

Source: Author (2023).

7.3.2 Effect of silver nanoparticles

Later, the chemical bonds of the plain hydrogel were also compared with the hydrogels submitted to Ag^{+} reduction with different agents – borohydride and alkaline glycerol (Figure 29).

After the silver treatment, the bands were broadened around 1700 cm^{-1}, regardless of the employed reduction agent. The band near 1350 cm^{-1}, associated with stretching the N=O group, may also indicate the silver nitrate's influence on the molecular structure.

Figure 29: FTIR spectra for the plain hydrogel (top); treated with sodium borohydride (centre) and alkaline glycerol (bottom).

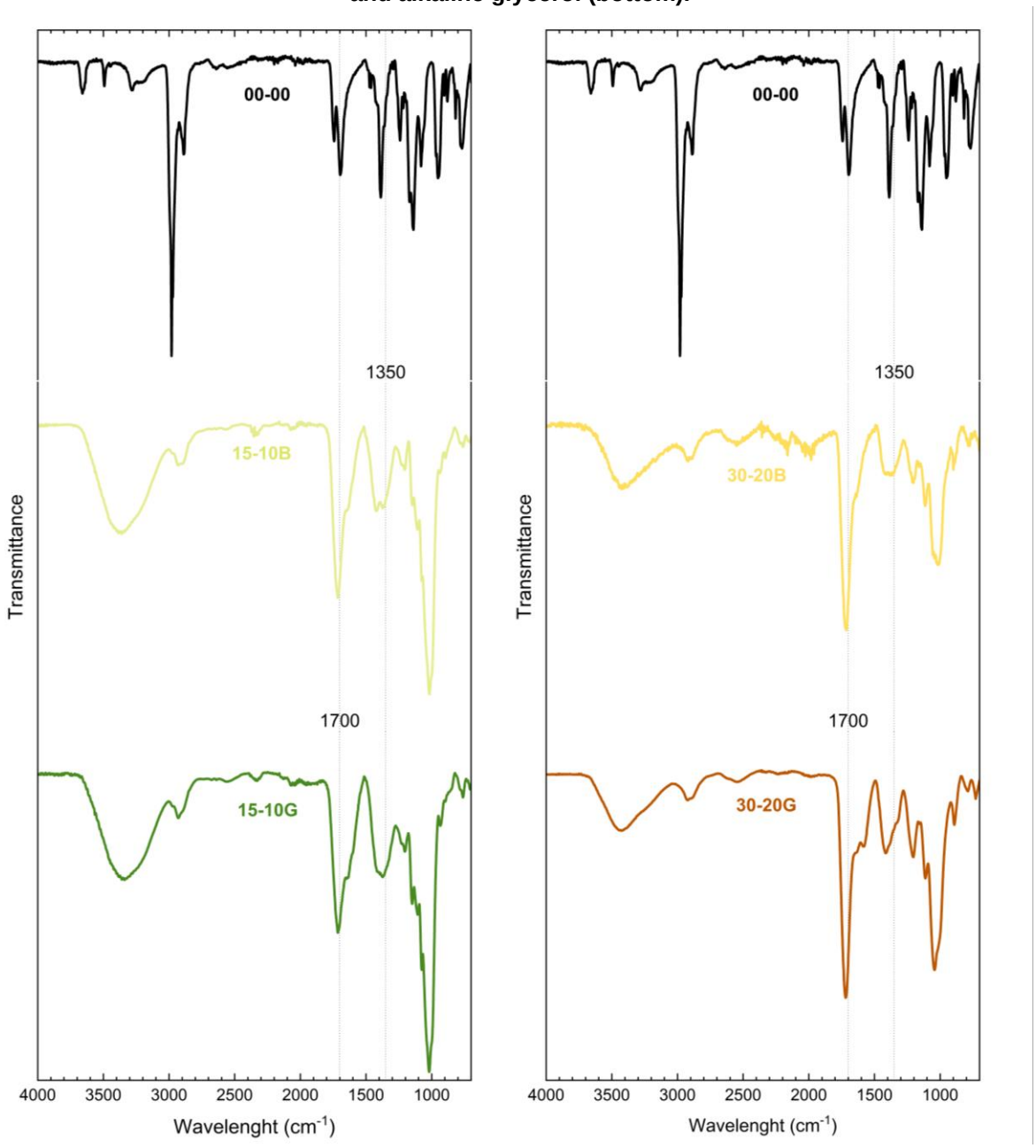

Source: Author (2023).

Due to the similarity between the spectra, the molecular structure changes may occur at the first step of the AgNP synthesis: the incorporation of silver ions rather than in the reduction phase. In the first step, the silver ions would coordinate with the available COO^- groups of the hydrogel – those not involved in the crosslinking.

This complexation with silver would cause the COO^- band displacement back to 1600 cm^{-1} and the broadening of the 1700 cm^{-1} region, since the silver atoms are heavy and hold the molecular vibration. Figure 30 gives a detailed look at these bands, where there is a change from 1697 cm^{-1} to 1650 cm^{-1} after the silver addition.

Figure 30: Detailed FTIR spectra for the plain hydrogel (top); treated with sodium borohydride (centre) and alkaline glycerol (bottom).

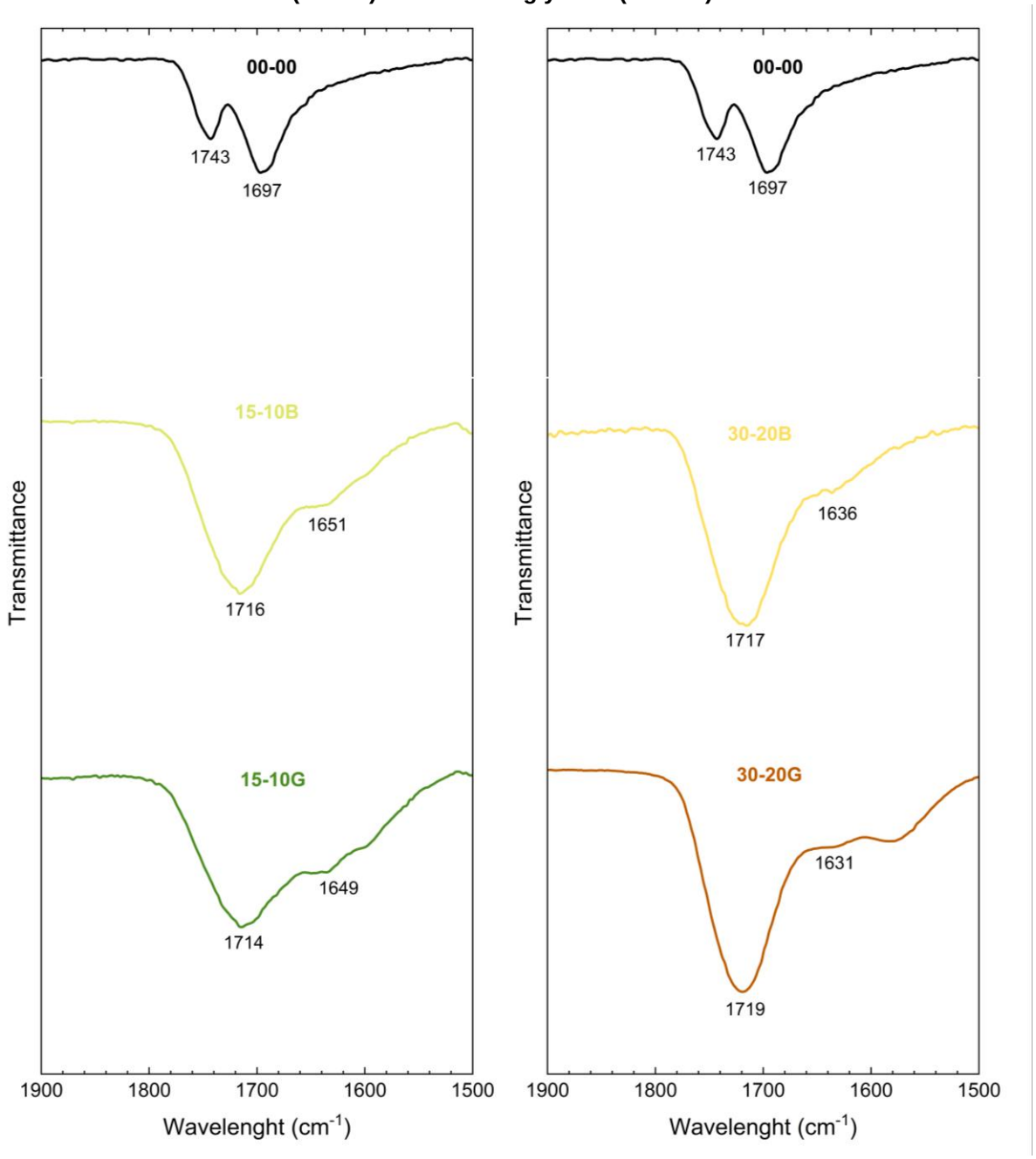

Source: Author (2023).

7.4 CHEMICAL CHARACTERISATION – LIBS

The laser-induced breakdown spectroscopy (LIBS) is a destructive analysis capable of detecting species in the order of parts per million (ppm). Briefly, the sample is bombarded by a laser pulse, which creates a localised plasma and increases the atomic – or molecular – energy. As the atoms return to their original state, they emit radiation at specific wavelengths, revealing the chemical identity of the sample

(KRAJCAROVÁ *et al.*, 2017).

Silver is characterised in LIBS by two high-intensity peaks at the wavelengths of 328 nm and 338 nm, as illustrated in Figure 31.

Figure 31: Laser-induced breakdown spectre of silver sample with high purity. The two characteristic peaks of high intensity are 328 nm and 338 nm.

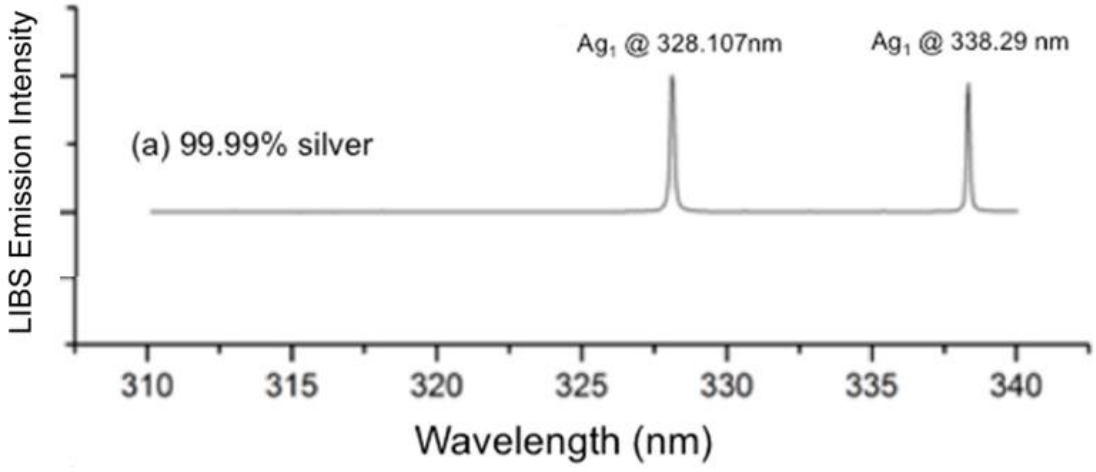

Source: Adapted from (HARMON *et al.*, 2019).

The intensity of these wavelengths was recorded for each of the 25 shots in every sample. The intensity of these wavelengths throughout the surface can estimate the overall spatial distribution of silver.

As shown in Figure 32, more prolonged exposure to $AgNO_3$ solutions promotes a more evenly distributed silver on the surface. Only the samples treated with alkaline glycerol are presented as an example.

Figure 32: Estimative for the silver distribution on the surface of the samples by the intensity of the characteristic Ag peaks (328 nm and 338 nm).

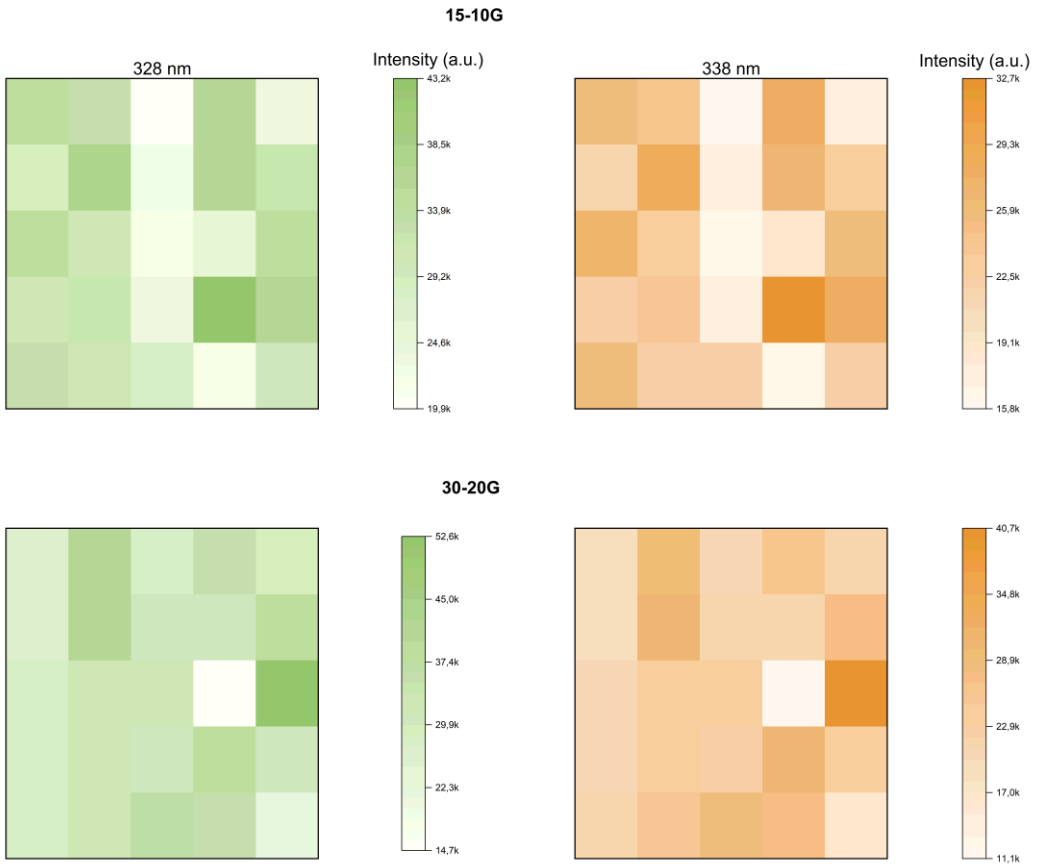

Source: Author (2023).

To better visualise the effects of each treatment, Figure 33 presents the average intensity for these two wavelengths.

Figure 33: Average intensity of the characteristic wavelengths of silver for each treatment.

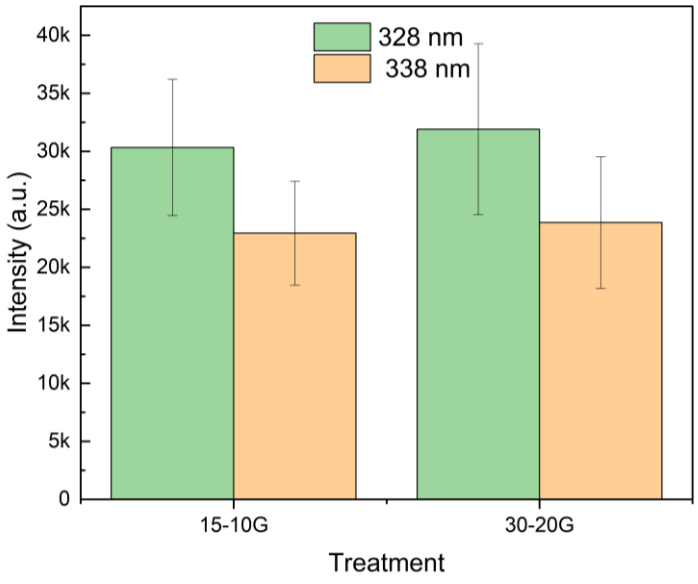

Source: Author (2023).

For all treatments, the characteristic peaks of silver are present. However, a complete quantitative analysis is impossible because no calibration curve was performed for the LIBS before the test. Another limitation of the quantitative analysis relies on the principle of the LIBS technique. Since the laser atomises the sample and measures the radiation emitted by the atom, the detector does not differentiate reduced metallic silver from the silver nitrate solution.

7.5 CHEMICAL CHARACTERISATION – DRX

Dried samples were analised by X-ray diffraction (DRX) to check for characteristic silver peaks. Despite the noise in the spectra in Figure 34, it was possible to determine two signals. The higher intensity at 38° indicates the silver plane (111), while the protuberances at 44° may indicate the plane (200), also from silver. However, since the diffraction features of Ag_2O and Ag overlap, the existence of the former cannot be excluded. A peak near 32° may be from silver oxide (111), due to the similarity with data found in literature and reproduced in Figure 35.

Figure 34: Diffractogram of the hydrogel after treatment with silver (30-20G).

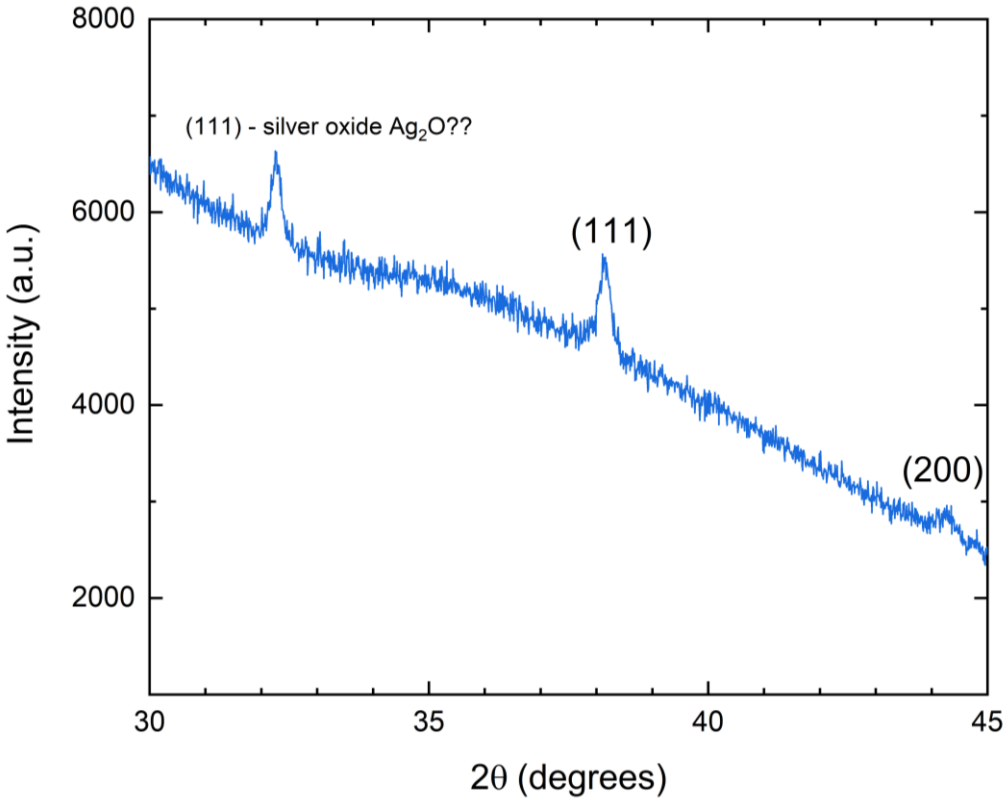

Source: Author (2023).

Figure 35: Diffractogram for the silver oxide (Ag_2O).

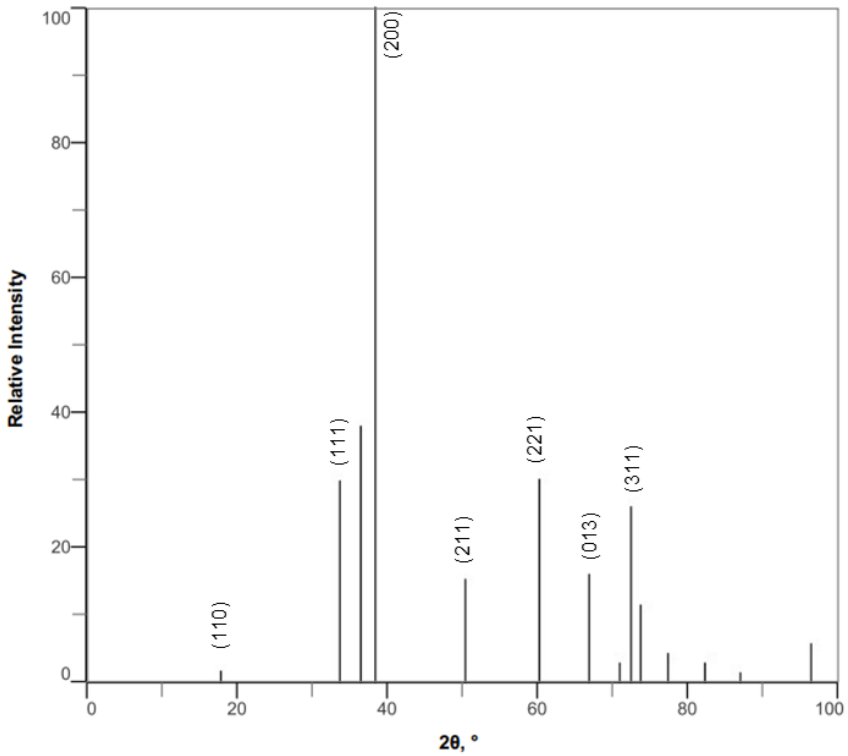

Source: (RIGAKU CORPORATION, 2019)

Similar results with low intensity and too much noise were obtained from the samples of all treatments. Figure 34 shows only the 30-20G treatment as an illustration.

There are a few reasons behind the excess of noise in the data. The small thickness of the samples combined with the lyophilisation step made it very difficult to achieve good contact between the film and the sample holder. This kind of data also suggests uneven metal distribution through the cellulosic matrix, or even that only a small amount of silver was reduced. Attempts to reduce the noise by increasing the quantity of sample – i.e., combining layers of the hydrogel – proved insufficient.

7.6 CHEMICAL CHARACTERISATION – UV-VIS

The presence of silver nanoparticles can also be detected by spectrophotometry in the range of UV-visible. When in contact with light at a specific angle, the metallic nanoparticles present surface plasmon resonance (SPR), where electrons in the surface are excited and propagate.

Since the SPR is related to the surface of the material and light propagation, it depends on the aspect ratio of the particles and the refractive index of the surrounding media (ZHOU; SHI, 2019).

An absorption peak near 417 nm characterises silver. However, the band is red-shifted towards longer wavelengths for particles with larger diameter or immersed in materials with higher reflective index. On the other hand, for smaller particles in low reflective index media, the shift occurs in the opposite direction – the blue shift.

Figure 36 compares the absorbance spectra for samples without reduction and further processed with different agents in the 200 – 1000 nm range. Only minor baseline variations are visible in the region around 400 nm. For better visualisation, the detail of the data is illustrated in Figure 37.

Figure 36: Absorbance of the hydrogel samples without reduction (15-00); (30-00); reduced by alkaline glycerol (15-10G); (30-20G) and by sodium borohydride (15-10B); (30-20B).

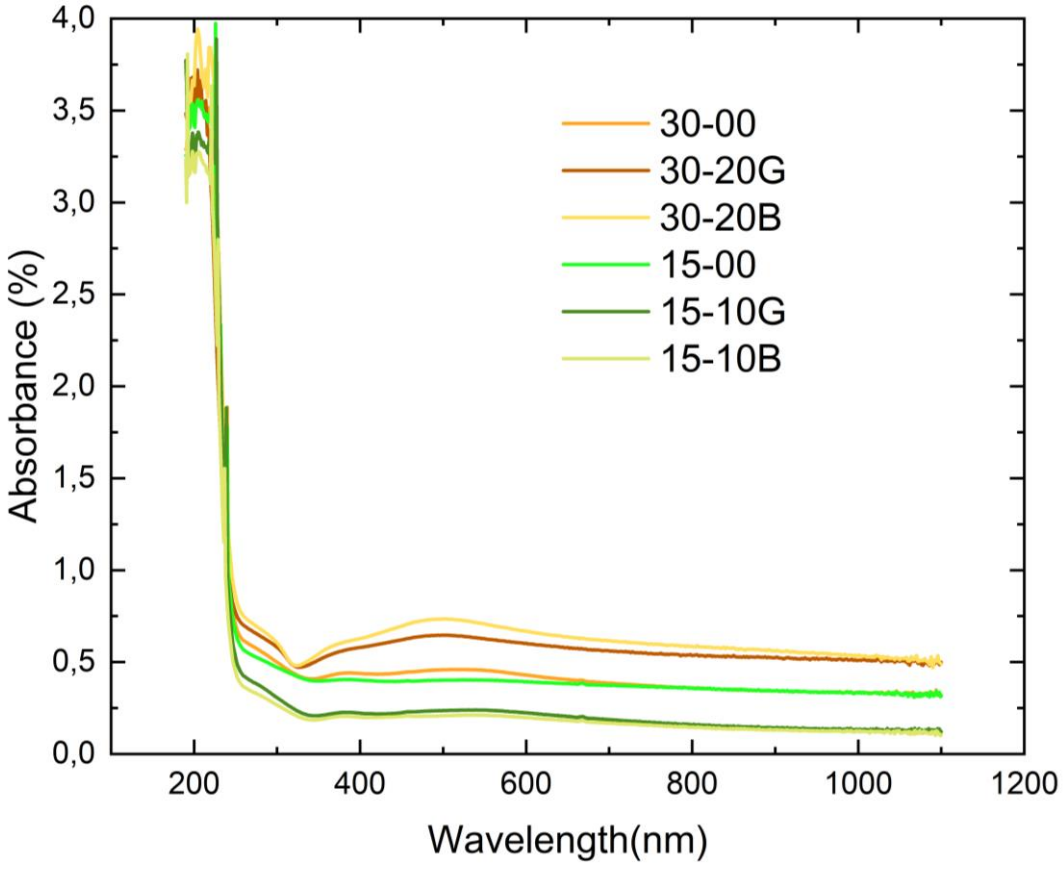

Source: Author (2023).

Figure 37: Detail the UV-vis spectra.

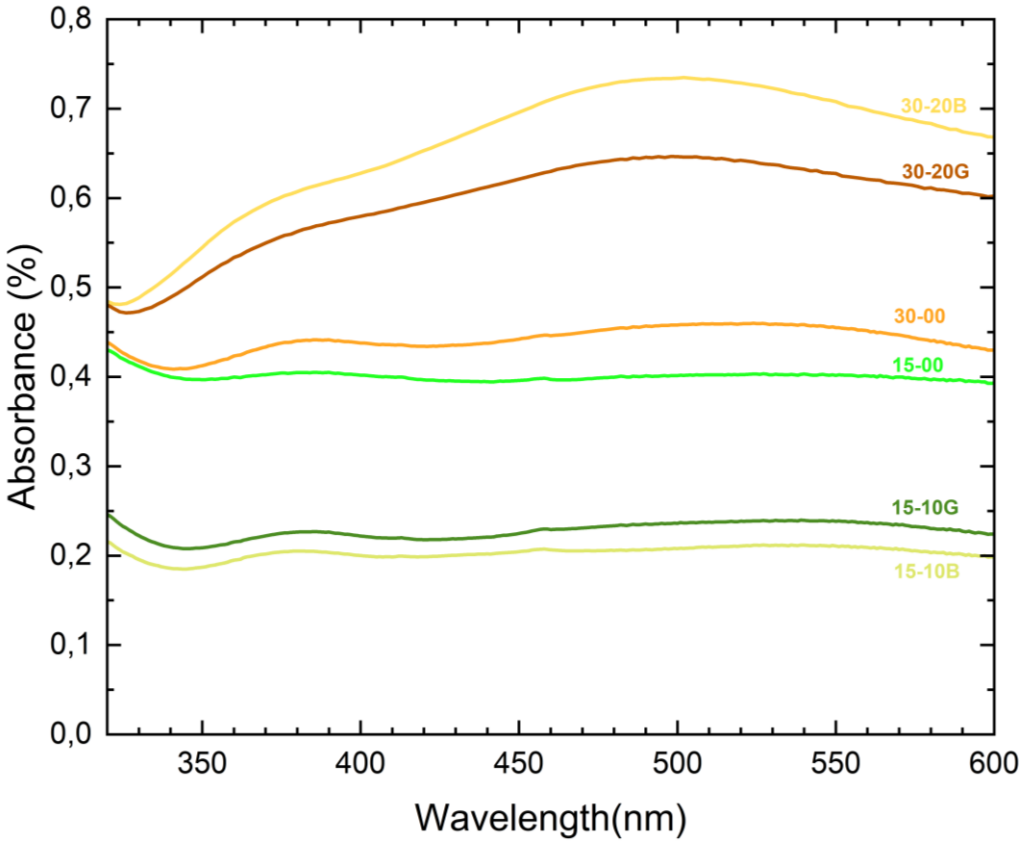

Source: Author (2023).

Apart from the different intensities among the treatments, Figure 37 illustrates bands that appear blue-shifted to 370 – 390 nm instead of visible near 417 nm. A small shoulder near 410 nm is also visible.

Two similar blue-shifted bands were observed by (MANKAD; KUMAR; JHA, 2013) in silver nanoparticles produced with different volumes of silver nitrate and sodium borohydride in the concentration of 0.01 M. The authors relate the two bands with SPR occurring in different directions: transversal (350 – 380 nm) and longitudinal (390 – 430 nm). This behaviour is characteristic of rod-shaped metallic nanoparticles.

Samples treated with more extended immersion and reduction times (30-20G and 30-20B) also present a shoulder near 380 nm, but other prominent peaks are seen near 470 nm. This result indicates that the process with sodium borohydride may lead to particles with smaller diameters. A similar result was obtained by (VIGNESHWARAN *et al.*, 2006) when synthesising AgNPs with a fungus culture.

Regarding the differences on the intensities, they are a result of the different scattering on the films, since the thickness of the samples was not standardized.

7.7 SCANNING ELECTRON MICROSCOPY

7.7.1 Sample morphology

The samples with chemical treatment presented a more fibrous appearance after the lyophilisation, like paper tissue, and tore down in the fracture. The pure CMC/CA hydrogel samples were white, smooth on the surface, and hard enough to present a fragile fracture.

Figure 38: SEM images of the fractures for the neat hydrogel (left) and hydrogel treated with silver nitrate (right). The magnification of the photos is approximately 400x.

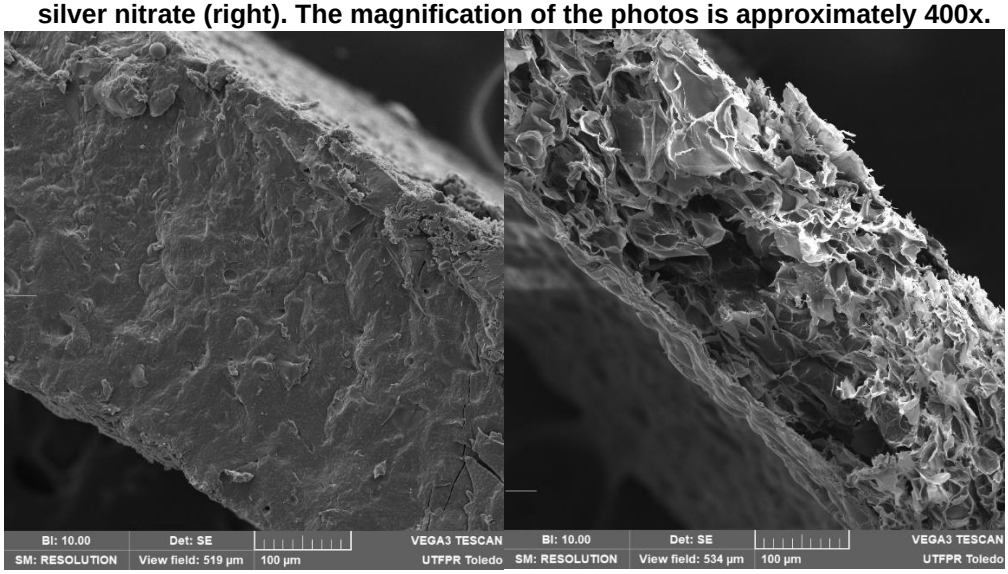

Source: Author (2023).

A comparison of the fracture in the different samples is shown in Figure 38. The selection without silver treatment presented a compacted surface with slight irregularities. Round small spots can be seen, but it is unclear if they represent the original porosity of the hydrogel or if they are the sites from where the water was removed. The fibrous aspect of the hydrogel treated with silver nitrate may indicate that the reaction was too aggressive and that portions of the hydrogel were either destroyed or separated in the presence of the solvents.

The synthesis of silver nanoparticles relies on the reaction between the silver nitrate and the free hydroxyl groups of cellulose with the posterior reduction of silver ions in the presence of glycerol. This reduction takes place either by the conversion of alcohols into alkoxides, which are the reduction agents, or by the formation of intermediate silver oxide particles.

In theory, this reaction would affect only the number of hydroxyl groups available for hydrogen bonds – the ones responsible for the secondary stability in the microstructure. The groups involved in the crosslinked segments and, therefore, responsible for the strength of the network would be less affected.

The differences can be seen in the surface of the materials in Figure 39. The plain hydrogel presented a smooth surface with a low level of rugosity, while the material treated with silver is seen as a fibrous network. This morphology is consequence of the chemical treatment combined with the lyophilization step.

Figure 39: SEM images of the surfaces for the neat hydrogel with a magnification of 284x (left) and hydrogel treated with silver nitrate, magnified by 389x (right).

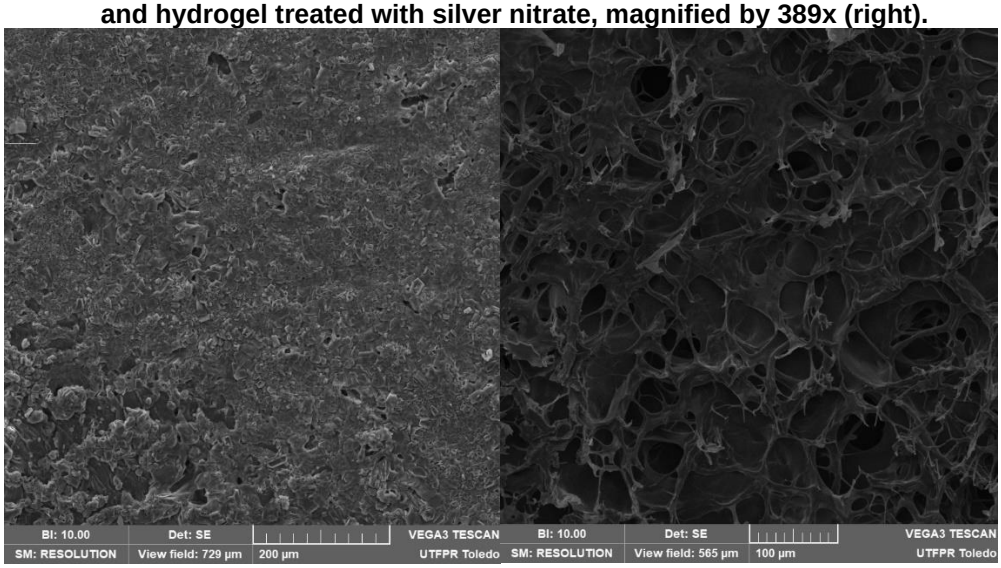

Source: Author (2023).

7.7.2 Sample composition

Energy Dispersive X-ray (EDX) microanalysis is a very known technique of semiquantitative elemental analysis associated to electron microscopy based on the generation of characteristic X-rays that reveals the presence of chemical elements mostly on the surface of samples. Thus, energy-dispersive X-ray spectroscopy (EDS) enables to map the elemental composition of a sample.

Figure 40 shows the result of the treatment 15-20G, mapping the presence of carbon, oxygen and sodium – elements known to be present in the composition of the matrix, as well as the silver.

As a control measure, a spot on the left side of the sample was covered with silver ink, making it visible in the filtered EDS image for silver in bright green. Small

spots of the same colour are sparkled in the sample, as visible in the merged EDS, indicating the formation of silver particles across the analysed field. These spots are not apparent in the individual image for silver due to the lower resolution of the picture.

Figure 40: Morphology of sample 15-20G (top left), combining EDS results (bottom left). The different elements detected in the field are illustrated individually on the right, with silver (Ag) in bright green, sodium (Na) in orange, carbon (C) in red and oxygen (O) in blue.

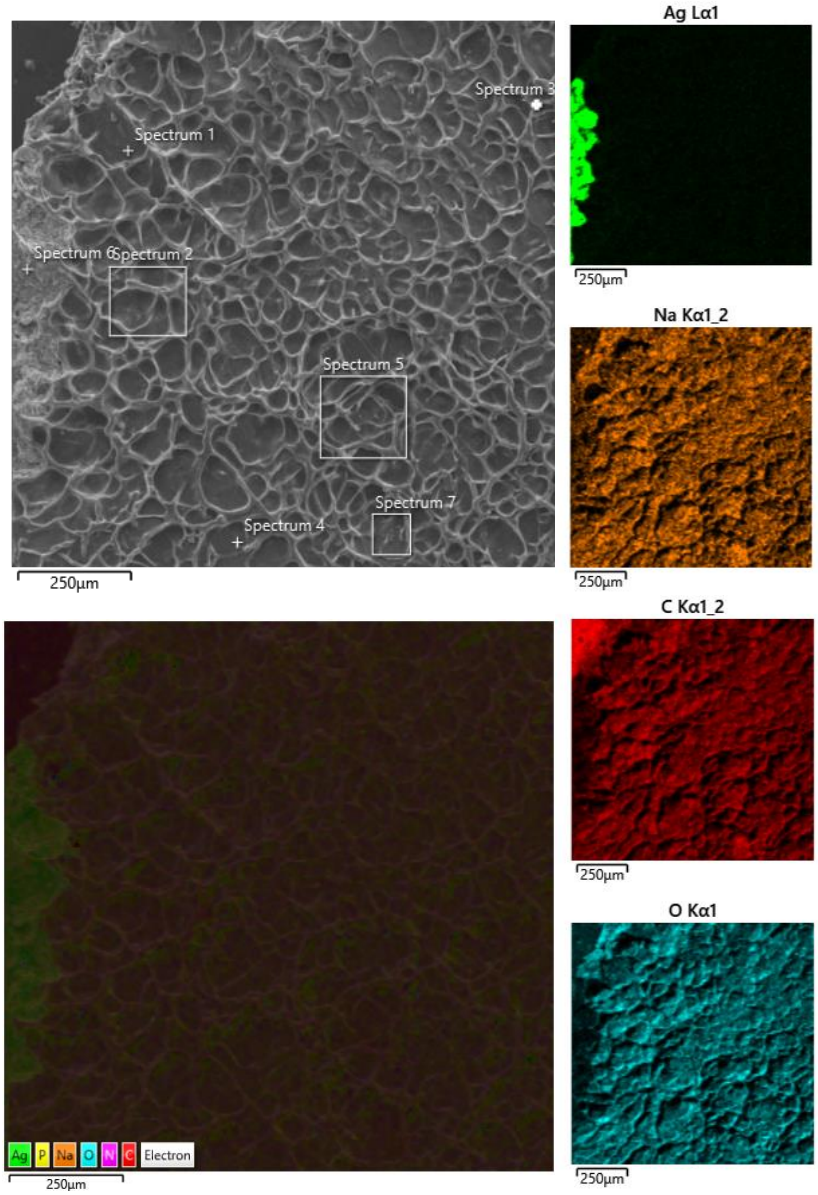

Source: Author (2023).

The presence of silver in the different regions is evidenced by the EDS spectra presented in the following figures. As expected, a sharp peak for silver is visible in Figure 41 since the spectre is assigned to the region painted with silver ink. A smaller silver peak is visible in Figure 42, indicating the formation of the metallic particles in that sample region.

Figure 41: EDS spectra of region 6, corresponding to the control with silver ink in the 15-20G sample.

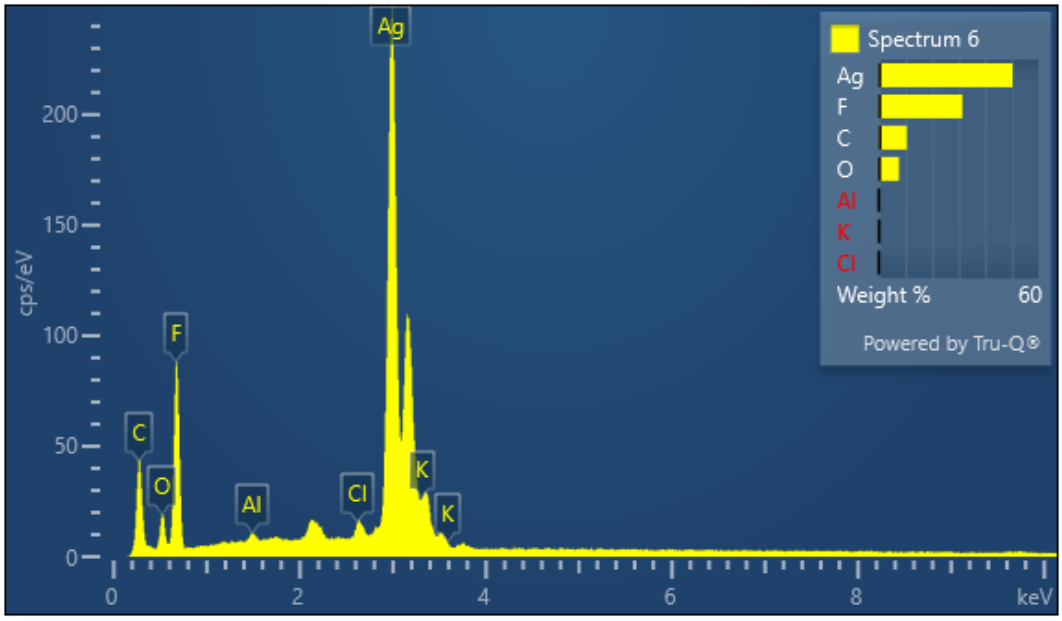

Source: Author (2023).

Figure 42: EDS spectra of region 5, in the bottom-right quadrant of the field in the 15-20G sample.

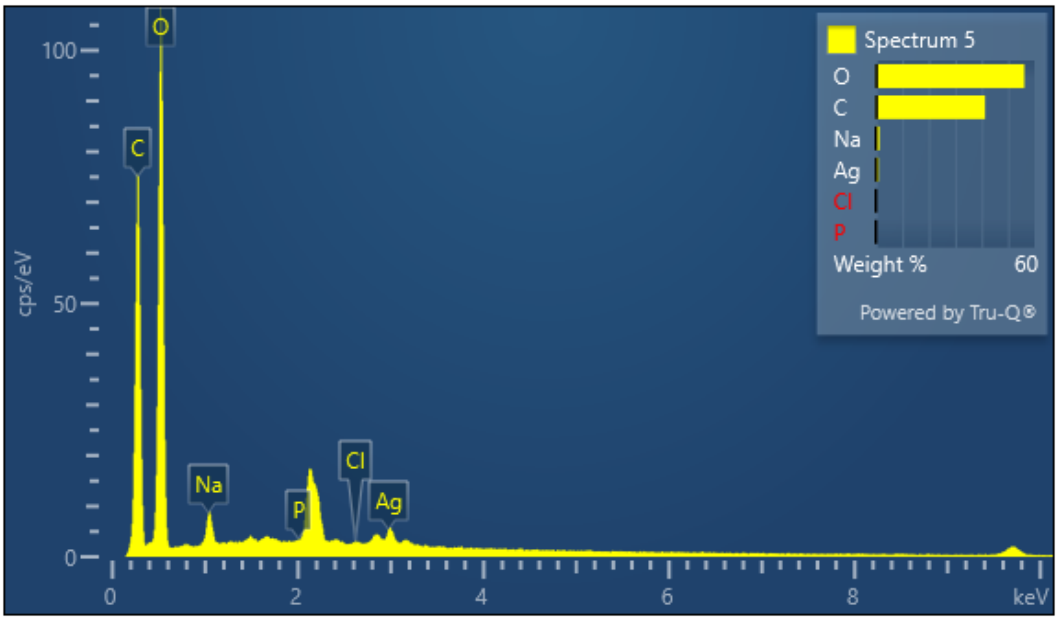

Source: Author (2023).

Figure 43 shows a side-by-side comparison of the 30-20G sample, where it is possible to note silver dispersed on the surface due to the doubled immersion time. These observations are also confirmed by the EDS spectra presented in Figure 44. The silver intensity is slightly higher than the observed for the 15-10 sample; however, the silver does not seem to be organised on a specific structure – such as particles or whiskers.

Figure 43: Morphology of sample 30-20G (left) and the silver dispersed on the structure (right).

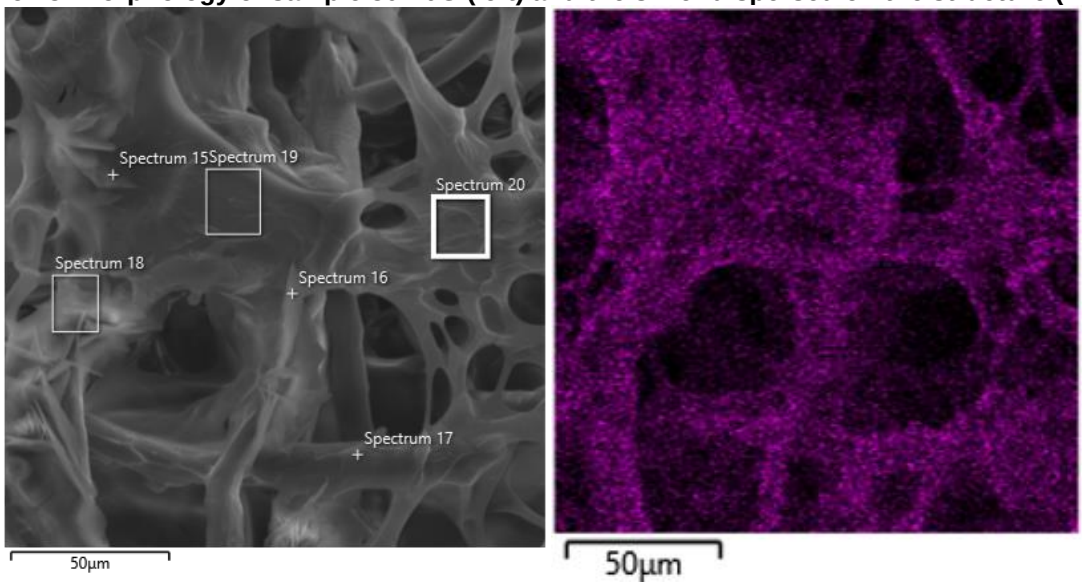

Source: Author (2023).

Figure 44: EDS spectra of region 19, in the top-left quadrant of the field in the 30-20G sample.

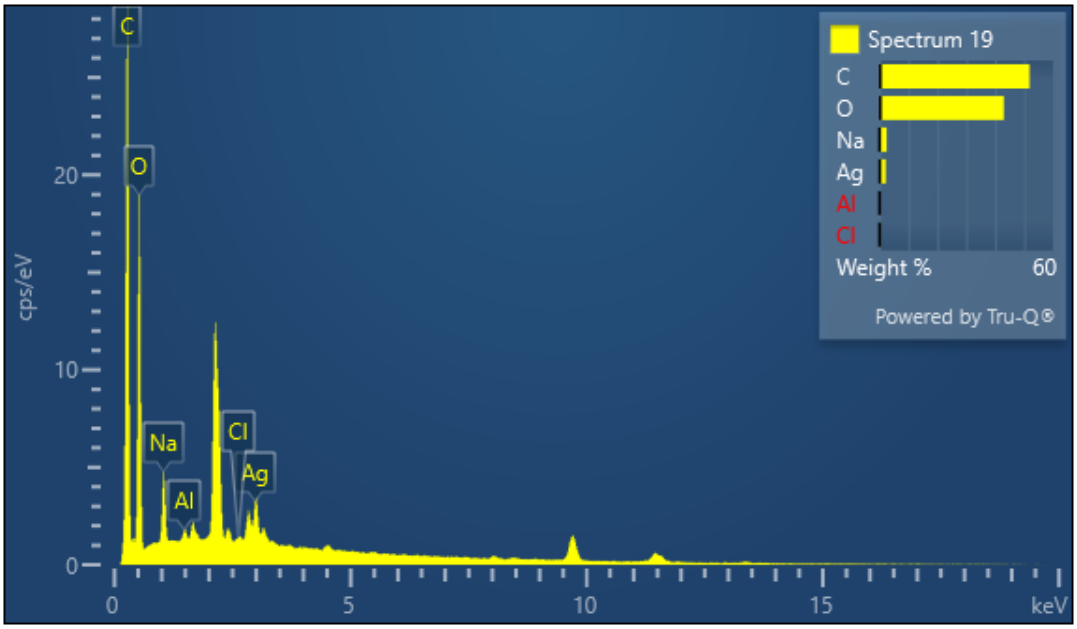

Source: Author (2023).

These results show silver in the hydrogel after the reduction treatment. However, the morphology of the silver particles inside the CMC could not be visualized or found using SEM because of the resolution of the microscope. More accurate technique, such as Transmission Electron Microscopy, could be suitable for this achievement. However, the images showed previously confirm the presence of silver distributed all over the material.

7.8 ANTIMICROBIAL TESTS

In the antimicrobial tests, this property is associated with the inhibition halo – an area free from microbial proliferation – around a piece of the material that is being tested. The larger the diameter, the best would be the biocidal action. However, larger halos can also be a signal of poor compatibility between the antimicrobial agent and matrix – in our case, the silver particles and the hydrogel – and can also result from a better compatibility between the antimicrobial agent and the culture media where the microbe is inoculated (JORGENSEN; FERRARO, 2009).

As seen in Figure 45 there is an inhibition halo in the samples without silver treatment, except for the fungus. Considering the components of the hydrogel, it is reasonable to assume that this inhibition on the plain samples is due to a leaching of excess citric acid. Citric acid reduces the pH of the culture media, which is detrimental to most bacteria, but not for the fungus *Candida albicans,* which is known to overcome shifts in the pH, explaining the growth of this microorganism.

Figure 45: Inhibition zone diameter of the CMC + CA hydrogel without silver (00-00) for each microorganism.

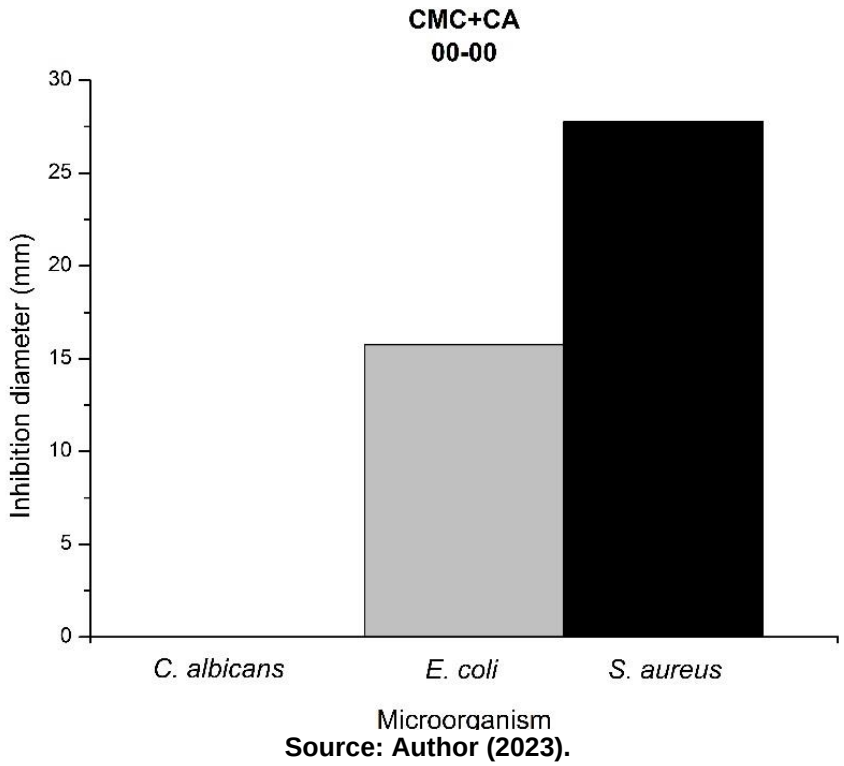

Source: Author (2023).

Figure 46: Inhibition zones obtained for the different microorganisms in contact with the CMC + CA hydrogel (00-00).

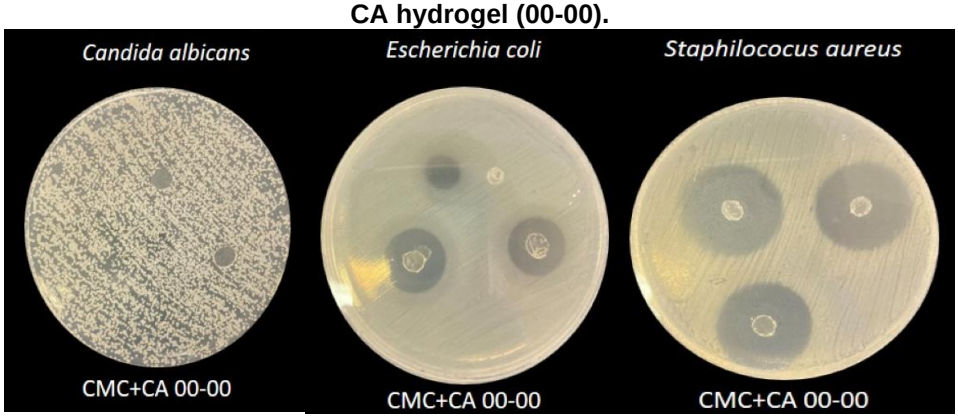

Source: Author (2023).

The process for silver incorporation was then performed with different substrates – filter paper and CMC hydrogel without citric acid, aiming to elucidate how the substrates and reagents involved in silver incorporation would interfere in the biocidal properties. These different conditions are illustrated in Figure 47.

Figure 47: Inhibition zone diameter for the microorganisms in different substrates with different treatments. Error bars correspond to the standard deviation. Images of the plates are available in the Appendix.

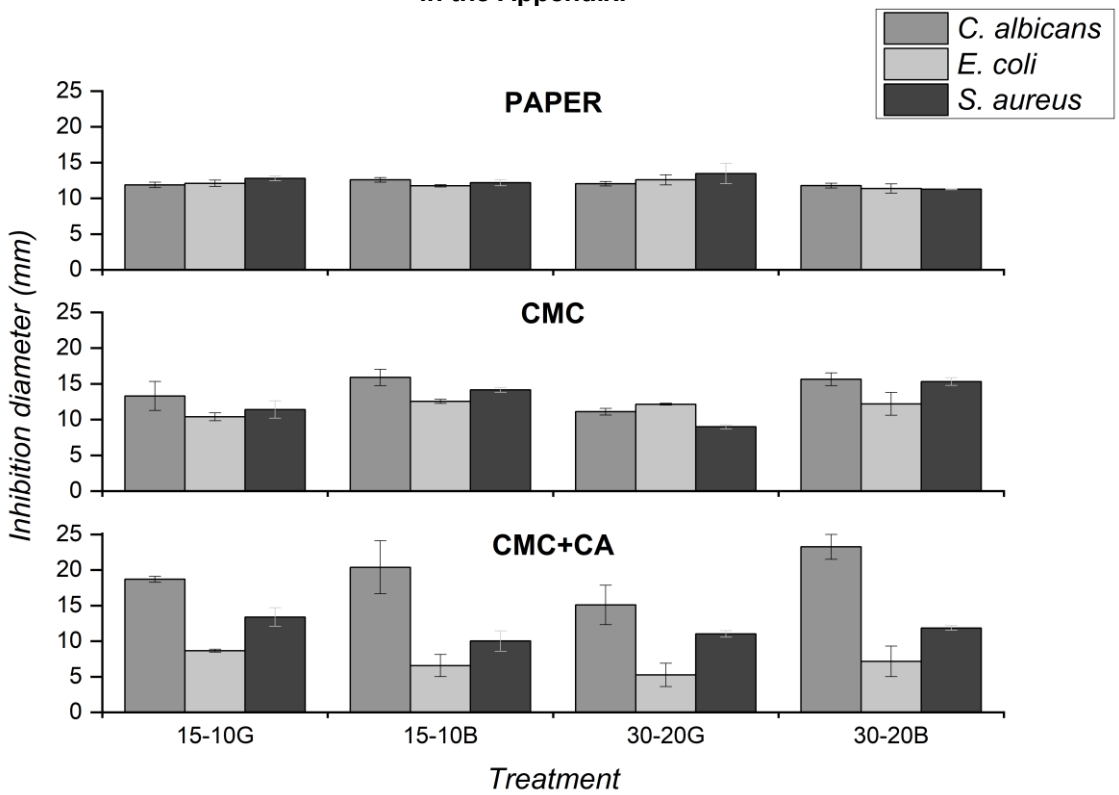

Source: Author (2023).

7.8.1 Effect of the substrate

Each substrate interacts in their own way with the silver particles, affecting how silver diffuses through the culture media. Dense networks hinder silver diffusion, while the particles move more freely in swelled hydrogels.

The inhibition was relatively constant for the paper, regardless of the treatment and the type of reducing agent employed. Paper filter are industrially manufactured and keep the properties, such as pore and thickness, constant. So, silver would spread to the culture medium in the same manner, acting nearly equal in the microorganisms. The formation of metallic silver in the paper was evident due to the change in colour – from white to intense yellow.

There was less inhibition when comparing the results for the paper with the inhibition presented by the CMC+CA hydrogel (00-00). The lower inhibition zones are evidence that silver particles could not diffuse from the paper through the culture media.

The presence of citric acid interferes with the networks' stability and the silver particles' formation. Without the crosslinker, the swelling ratio of the substrate increases. On the other hand, the absence of crosslinks also means that more hydroxyl groups from the cellulose were available to coordinate with the silver nitrate and anchor the silver particles after the reduction step. Overall, while more silver particles were formed on the CMC hydrogel, the swelled structure allowed their rapid diffusion. Most of them were probably washed out on the last step of the incorporation process.

The addition of citric acid in the hydrogel led to the opposite effect: fewer hydroxyl groups were available to react with the silver nitrate, and fewer particles were formed. Additionally, most silver particles were trapped and preserved in the crosslinked structure.

The higher mobility of the particles helps explain the higher inhibition of the CMC hydrogel compared to paper. Comparing the CMC with the CMC+CA results, there was a fall in the inhibition diameter.

7.8.2 Effect of the reducing agent

The best results were achieved using sodium borohydride as a reduction agent when comparing the different parameters for silver incorporation, especially for the

hydrogels after 30 minutes of immersion and 20 seconds of reduction. While glycerol is known to produce traces of silver oxide (Ag_2O) along with metallic particles, sodium borohydride leaves only metallic silver, enhancing microbial inhibition.

The biocidal properties of the hydrogels result from a combination of the action of silver particles and the excess of citric acid. Despite some levels of toxicity being associated with sodium borohydride, it is improbable that traces of this substance would contribute to larger inhibition halos, since the $NaBH_4$ reacts rapidly with the silver nitrate and is highly unstable in aqueous solution.

7.8.3 Response of the microorganisms

As stated before and illustrated in Figure 45, *Candida albicans* was able to proliferate in the plain hydrogel, since it can overcome the pH shifts caused by the excess of citric acid. The same effect was not observed in the samples treated with silver, which is a strong indicator that silver is indeed present and acting against the fungus.

Comparing the inhibition halo of the plain hydrogel with that of Ag-containing samples in contact with the bacteria, there was an overall reduction in the inhibition halos in the presence of silver. This may be explained by the higher diffusion rates of citric acid in the culture media.

Whitin the same substrate, the sensitivity was relatively constant for the bacteria, with the gram-negative *E. coli* presenting smaller halos than the *S. aureus* – gram-positive.

Gram-positive bacteria are prone to the adhesion of silver ions. Despite the thicker membrane, they also present a higher number of peptidoglycans, which are negatively charged and allow the bonding of silver ions. More silver availability on the membrane would facilitate the various antibacterial mechanisms of silver (DOMÍNGUEZ *et al.*, 2020).

7.9 SWELLING DEGREE

Hydrogels are, by definition, structures that are capable of absorbing large amounts of water without losing their integrity. Understanding this property dictates how the hydrogel can be further processed or analysed.

It was expected for the hydrogel to increase in size and weight as it absorbs water at a high pace in the first few minutes, decreasing the rate until it achieves a steady state after a couple of hours.

The weight variation is illustrated in Figure 48; from what can be seen, there is a sharp increase in mass in the first measurement after just 15 minutes of contact with water. Following this first uptake, the weight began to fall, reaching a stationary phase after about seven hours of contact. It is important to note that, despite the weight loss, the hydrogel films remained mechanically stable.

Figure 48: Weight variation curve for the CMC+CA hydrogel immersed in water at room temperature for up to ten hours. The results are the average of a triplicate.

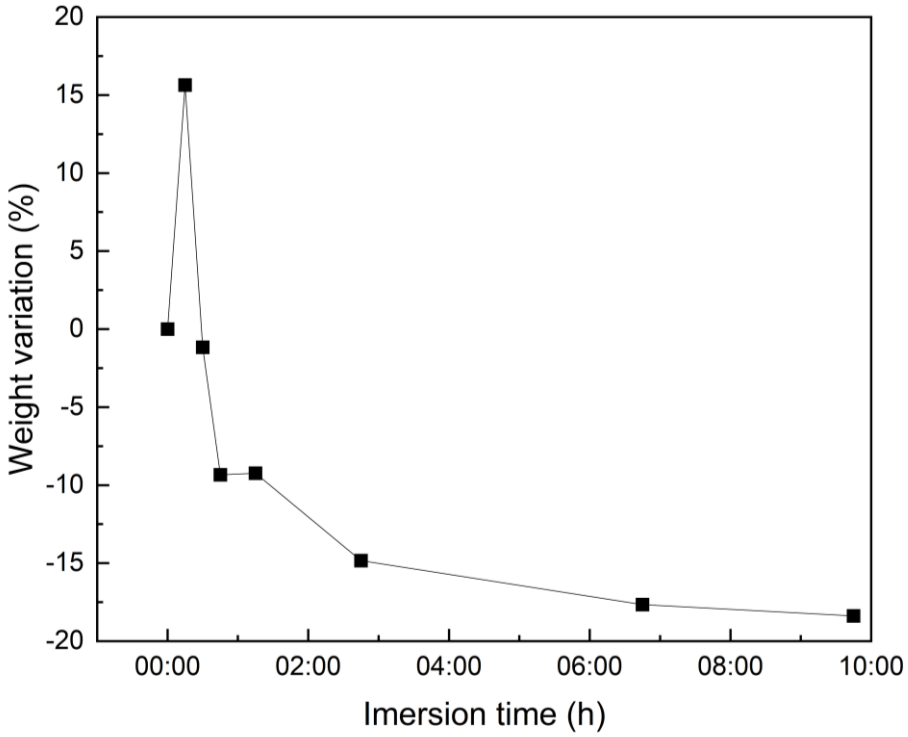

Source: Author (2023).

The rapid saturation of the hydrogel is explained by the high number of crosslinks, which prevent the chain movement to accommodate more molecules of water in the structure.

A similar study performed by Mali, K. K et al. (2018) with CMC hydrogels thermally crosslinked with tamarin gum and citric acid reported that the peak in swelling degree was reached by the first 30 minutes of immersion in phosphate buffer pH 7.4 (MALI *et al.*, 2018). However, no weight loss was reported in the mentioned work.

The low swelling capacity, around 15%, is also explained by the acidic

conditions of the media. Initially, the deprotonated carboxyl groups would repel each other, opening space for water uptake. At low pH, the protonated groups are attracted, hindering the water uptake (NASUTION *et al.*, 2022).

The weight loss observed in Figure 48 is probably due to the diffusion of citric acid in the aqueous media since an apparent excess of citric acid is also observed in the FTIR results. The system became stable as the water became saturated with the dissociated ions, removing the gradient of concentration, which was the driving force for diffusion.

7.10 pH MEASUREMENTS

During the preparation of the hydrogel solution, the pH of the distilled water was slightly acidic (6.65). After adding citric acid, the pH dropped to 1.68, and when the cellulose derivative was dissolved, there was a slight increase in the pH to 1.92. After the samples of hydrogel were left overnight in distilled water, the pH of the water raised to 2.50 on average.

The successive washes with sodium hydroxide and water promoted a variation in the pH but not enough to reach neutrality, as seen in Figure 49. After the first wash, the pH of both solutions dropped drastically. In the following iterations, the values were raised at different rates until the pH of the alkali solution reached approximately 6. The water pH, however, remained low and near 2.5. After two more repetitions, the alkali solution returned to its original pH, near 12, and the water presented only a slight increase.

Figure 49: Indirect measurements of pH. The columns indicate the pH of solutions after being used to wash a hydrogel sample. Fresh solutions were employed at room temperature and without agitation at each step. Each wash corresponds to a 10-second bath.

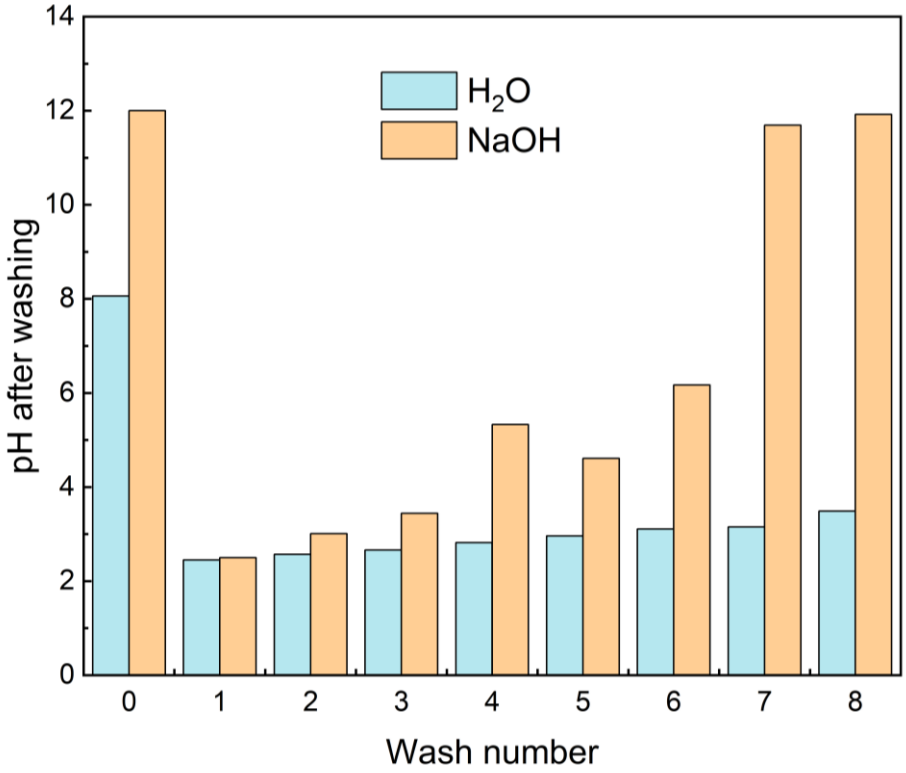

Source: Author (2023).

The resulting pH in water after the successive washes is quite similar to the one observed after simply immersing the hydrogel in water overnight – approximately 2.5. These findings follow the apparent excess of citric acid observed in the FTIR experiments and the noticeable weight loss during the swelling studies.

The sharp increase in the pH after wash number 6 with sodium hydroxide indicates that after that point, the citric acid could not diffuse from the hydrogel to the aqueous media; otherwise, it would react with the base, and the solution would present a lower pH value.

The point of apparent diffusive equilibrium reported in Figure 49, reached after approximately two minutes of testing, differs from the nearly seven hours required for the hydrogel to achieve weight loss equilibrium observed when it was immersed in water.

One explanation for this difference is that using an alkaline solution enabled the deprotonation of the carboxyl groups, increasing the water uptake and enabling the citric acid to leach faster than observed with just plain water (NASUTION *et al.*, 2022).

8 FINAL CONSIDERATIONS

This research focused on producing a hydrogel substrate made of cellulose and suitable for wound dressing applications, with additional biocidal properties provided by silver particles. The cast drying method employing CMC and citric acid proved to be a simple technique to produce hydrogel films on the bench scale, with the overall process taking approximately 24 hours, from preparing the solution to peeling the hydrogels.

The effectiveness of the synthesis process for the hydrogel was primarily confirmed by Fourier Transformed Infrared (FTIR) spectroscopy and the swelling tests. Other evidence was found in the process of silver incorporation, when preparing comparative films for the microbiological tests and in further investigating the pH.

From the FTIR, the crosslinking by esterification was evident because of the peaks in the region of 1700 cm^{-1}. The presence of crosslinks sustained the hydrogel immersed in water for longer than 24 hours, as observed during the pH measurements. The swelling degree tests indicated that the hydrogel films became saturated with water after 15 to 30 minutes of exposure, and, despite the apparent leaching, the films sustained their original aspect. During trial tests for the incorporation of silver, the hydrogels lost their stability when in contact with strong alkali solutions (NaOH 20 mM) for longer than two minutes. Another evidence of the effectiveness of citric acid as a crosslinker agent is the weaker stability observed in films prepared from simple CMC solutions for the microbiological tests. Pure CMC films turned into gels after 15 minutes of contact with silver nitrate solution (1 mM).

Different agents were employed to incorporate silver particles in the hydrogel through chemical reduction: glycerol alkaline solution and sodium borohydride. Metallic silver was formed with both agents, but the characteristic change in colour, associated with the silver reduction was promptly observed when the sodium borohydride was employed. The X-Ray diffractogram, LIBS measurements and SEM imaging associated with EDS indicated the presence of silver in the different samples.

Peaks related to the different atomic planes of silver were visible in the X-Ray diffraction, even among the noise due to the limited sample. The LIBS results confirmed that the silver solution could diffuse homogeneously throughout the surface. The EDS imaging detected regions with dispersed silver in the samples treated with both reduction agents. Silver also influenced the FTIR, since the groups where the

metallic ion was expected to coordinate presented a shift to lower wavenumbers after silver incorporation – a signal that the metal hindered the molecular vibration.

As for the morphology, as observed in the SEM results, the process of silver incorporation created a more fibrous network in the hydrogel. At the same time, the plain samples presented a more packed and homogeneous structure. The EDS detected silver particles for both agents but did not show a specific size or shape. Silver was observed as small amorphous particles sprinkled across the hydrogel matrix.

The microbiological tests were performed with different substrates, which helped to elucidate the contribution of the various components of the hydrogel in the biocidal properties. The other substrates employed – paper and CMC gel – presented different diffusion rates, which impacted the inhibition halos' diameter. However, the comparison showed that silver significantly contributes to the action against microorganisms, especially the fungus *C. albicans*. As for the bacteria, a higher inhibition was observed for the gram-positive *S. aureus*. One theory is that the silver ions bonded with the negatively charged groups in the bacterial membrane, increasing the availability of silver for their multiple biocidal mechanisms.

With the evidence presented, carboxymethyl cellulose hydrogels made with citric acid through the cast-drying method could act as an alternative substrate for wound dressings. The silver incorporation efficiently provided a biocidal agent, and the hydrogels presented enough morphological stability for the proposed end use.

From the functional perspective, the influence of this material in wound regeneration is yet to be clarified. More studies are necessary to check the material's cytotoxicity and to determine the profile of silver release. Other studies can evaluate the properties of this hydrogel as a component in a multilayer structure, similar to the commercial alternatives for wound dressings.

REFERENCES

ABOU EL-NOUR, K. M. M. *et al.* Synthesis and applications of silver nanoparticles. **Arabian Journal of Chemistry**, v. 3, n. 3, p. 135–140, July. 2010.

AHMED, E. M. Hydrogel: Preparation, characterization, and applications: A review. **Journal of Advanced Research**, v. 6, n. 2, p. 105–121, 2015.

ANDREU, V. *et al.* Smart dressings based on nanostructured fibers containing natural origin antimicrobial, anti-inflammatory, and regenerative compounds. **Materials**, v. 8, n. 8, p. 5154–5193, 2015.

ANVISA. *Consultas ANVISA - Agência Nacional de Vigilância Sanitária*. Available at: <https://consultas.anvisa.gov.br>. Accessed: 12 Dec. 2022.

BARILLO, D. J.; MARX, D. E. Silver in medicine: A brief history BC 335 to present. **Burns**, v. 40, n. S1, p. S3–S8, 1 dec. 2014.

BARUD, H. S. *et al.* Self-supported silver nanoparticles containing bacterial cellulose membranes. **Materials Science and Engineering C**, v. 28, n. 4, p. 515–518, 1 May 2008.

BEYENE, H. D. *et al.* Synthesis paradigm and applications of silver nanoparticles (AgNPs), a review. **Sustainable Materials and Technologies**, v. 13, p. 18–23, 1 sept. 2017.

BOATENG, J.; CATANZANO, O. Advanced therapeutic dressings for effective wound healing - a review. **Journal of Pharmaceutical Sciences**, v. 104, n. 11, p. 3653–3680, 1 Nov. 2015.

CAPANEMA, N. S. V. *et al.* Physicochemical properties and antimicrobial activity of biocompatible carboxymethylcellulose-silver nanoparticle hybrids for wound dressing and epidermal repair. **Journal of Applied Polymer Science**, v. 135, n. 6, 10 Feb. 2018a.

CAPANEMA, N. S. V. *et al.* Eco-friendly and biocompatible cross-linked carboxymethylcellulose hydrogels as adsorbents for the removal of organic dye pollutants for environmental applications. **Environmental Technology**, v. 39, n. 22, p. 2856–2872, 2018b.

CHEN, Y. N.*et al.* Poly(vinyl alcohol)-tannic acid hydrogels with excellent mechanical properties and shape memory behaviors. **ACS Applied Materials and Interfaces**, v. 8, n. 40, p. 27199–27206, 12 Oct. 2016.

CHINNAPONGSE, S. L.; MACCUSPIE, R. I.; HACKLEY, V. A. Persistence of singly dispersed silver nanoparticles in natural freshwaters, synthetic seawater, and simulated estuarine waters. **Science of The Total Environment**, v. 409, n. 12, p. 2443–2450, 15 May 2011.

CIRIMINNA, R. *et al.* Citric acid: emerging applications of key biotechnology industrial product. **Chemistry Central Journal**, v. 11, n. 1, p. 1–9, 2017.

COJOCARU, E. *et al.* Electrospun nanofibrous membranes based on citric acid-functionalized chitosan containing rGO-TEPA with potential application in wound dressings. **Polymers**, v. 14, n. 2, 1 Jan. 2022.

CROISFELT, F. M. *et al.* Modified-release topical hydrogels: a ten-year review. **Journal of Materials Science**, v. 54, n. 16, p. 10963–10983, 30 Aug. 2019.

DE LIMA, G. F.; DE SOUZA, A. G.; ROSA, D. Nanocellulose as reinforcement in carboxymethylcellulose superabsorbent nanocomposite hydrogels. **Macromolecular Symposia**, v. 394, n. 1, 1 Dec. 2020.

DEL VALLE, L.; DIAZ, A.; PUIGGALI, J. Hydrogels for biomedical applications: cellulose, chitosan, and protein/peptide derivatives. **Gels**, v. 3, n. 3, p. 27, 2017.

DEMITRI, C. *et al.* Novel superabsorbent cellulose-based hydrogels crosslinked with citric acid. **Journal of Applied Polymer Science**, v. 110, n. 4, p. 2453–2460, 15 Nov. 2008.

DHAND, V. *et al.* Green synthesis of silver nanoparticles using Coffea arabica seed extract and its antibacterial activity. **Materials Science and Engineering: C**, v. 58, p. 36–43, 1 Jan. 2016.

DOMÍNGUEZ, A. V. *et al.* Antibacterial activity of colloidal silver against gram-negative and gram-positive bacteria. **Antibiotics**, v. 9, n. 1, 1 Jan. 2020.

DUFRESNE, A. **Nanocellulose: from nature to high performance tailored materials**. Berlin: De Gruyter, 2018. v. 2.

FU, L. H. *et al.* Multifunctional cellulose-based hydrogels for biomedical applications. **Journal of Materials Chemistry B**, v. 7, n. 10, p. 1541–1562, 2019.

GAO, Y. *et al.* Bioavailability and toxicity of silver nanoparticles: Determination based on toxicokinetic–toxicodynamic processes. **Water Research**, v. 204, 1 Oct. 2021.

GASPERINI, L.; MANO, J. F.; REIS, R. L. Natural polymers for the microencapsulation of cells. **Journal of the Royal Society Interface**, v. 11, n. 100, 6 Nov. 2014.

GHORPADE, V. S. *et al.* Citric acid crosslinked carboxymethylcellulose-polyvinyl alcohol hydrogel films for extended release of water soluble basic drugs. **Journal of Drug Delivery Science and Technology**, v. 52, p. 421–430, 1 Aug. 2019.

GULREZ, S.K. H.; AL-ASSAF, S.; PHILIPS, G. O. **Hydrogels: Methods of Preparation, Characterisation and Applications**. 1. ed. London: InTechOpen, 2011.

HARMON, R. S. *et al.* Laser-induced breakdown spectroscopy—an emerging analytical tool for mineral exploration. **Minerals 2019, Vol. 9, Page 718**, v. 9, n. 12, p. 718, 20 Nov. 2019.

JORGENSEN, J. H.; FERRARO, M. J. Antimicrobial susceptibility testing: A review of general principles and contemporary practices. **Clinical Infectious Diseases**, v. 49, n. 11, p. 1749–1755, Dec. 2009.

JUNG, J. H. *et al.* Metal nanoparticle generation using a small ceramic heater with a local heating area. **Journal of Aerosol Science**, v. 37, n. 12, p. 1662–1670, 1 Dec. 2006.

KABIR, S M F. *et al.* Cellulose-based hydrogel materials: chemistry, properties and their prospective applications. **Progress in Biomaterials**, v. 7, n. 3, p. 153–174, Sept. 2018.

KANIKIREDDY, V. *et al.* Carboxymethyl cellulose-based materials for infection control and wound healing: A review. **International Journal of Biological Macromolecules**, v. 164, p. 963–975, 2020.

KHATOON, U. T.; VELIDANDI, Aditya; NAGESWARA RAO, G.V.S. Sodium borohydride mediated synthesis of nano-sized silver particles: Their characterization, anti-microbial and cytotoxicity studies. **Materials Chemistry and Physics**, v. 294, p. 126997, 15 Jan. 2023.

KRAJCAROVÁ, L. *et al.* Mapping of the spatial distribution of silver nanoparticles in root tissues of Vicia faba by laser-induced breakdown spectroscopy (LIBS). **Talanta**, v. 173, p. 28–35, 1 oct. 2017. Accessed: 3 Jan. 2023.

KUJATH, P.; MICHELSEN, A. Wounds – from physiology to wound dressing. **Deutsches Aerzteblatt Online**, v. 105, n. 13, 2008.

KUMAR, H. *et al.* Development of silver nanoparticles-loaded CMC hydrogel using bamboo as a raw material for special medical applications. **Chemical Papers**, v. 73, n. 4, p. 953–964, 5 apr. 2019.

LEVARD, C. *et al.* Environmental transformations of silver nanoparticles: Impact on stability and toxicity. **Environmental Science and Technology**, v. 46, n. 13, p. 6900–6914, 3 July. 2012.

LIU, P. *et al.* Radiation crosslinking of CMC-Na at low dose and its application as substitute for hydrogel. **Radiation Physics and Chemistry**, v. 72, n. 5, p. 635–638, Apr. 2005.

LIU, T. *et al.* Green synthesis of silver nanoparticles with size distribution depending on reducing species in glycerol at ambient pH and temperatures. **ACS Omega**, v. 5, n. 26, p. 16246–16254, 7 July. 2020.

LUTY-BŁOCHO, M. *et al.* On the rate of interaction of sodium borohydride with platinum (Iv) chloride complexes in alkaline media. **Materials**, v. 14, n. 11, 1 June. 2021.

MAI, S.*et al.* Análise dos registros de produção de curativos realizados no Brasil, 2017 - 2019. **ESTIMA, Brazilian Journal of Enterostomal Therapy**, 30 Mar. 2021.

MALEŠ, L. *et al.* Efficiency of differently processed membranes based on cellulose as cationic dye adsorbents. **Nanomaterials**, v. 10, n. 4, 1 Apr. 2020.

MALI, K. K. *et al.* Citric acid crosslinked carboxymethyl cellulose-based composite hydrogel films for drug delivery. **Indian Journal of Pharmaceutical Sciences**, v. 80, n. 4, p. 657–667, 2018.

MANKAD, V.; KUMAR, R. K.; JHA, P. K. Investigation of blue-shifted plasmon resonance: An optical properties study of silver nanoparticles. **Nanoscience and Nanotechnology Letters**, v. 5, n. 8, p. 889–894, Aug. 2013.

MARX, D. E.; BARILLO, D. J. Silver in medicine: the basic science. **Burns**, v. 40, n. S1, p. S9–S18, 1 Dec. 2014.

MORES, S. *et al.* Citric acid bioproduction and downstream processing: Status, opportunities, and challenges. **Bioresource Technology**, v. 320, n 1. Nov. 2020, 2021.

NARAYANASWAMY, R.; TORCHILIN, V. P. Hydrogels and their applications in targeted drug delivery. **Molecules**, v. 24, n. 3, 2019.

NASUTION, H. *et al.* Hydrogel and effects of crosslinking agent on cellulose-based hydrogels: A Review. **Gels**, v. 8, n. 9, 2022.

NATIONAL INSTITUTE OF STANDARDS AND TECHNOLOGY. *Carboxymethyl cellulose, sodium salt*. Available at: <https://webbook.nist.gov>. Accessed: 7 Aug. 2022a.

NATIONAL INSTITUTE OF STANDARDS AND TECHNOLOGY. *Citric acid*. Available at: <https://webbook.nist.gov>. Accessed: 7 Aug. 2022b.

NOGUEIRA, B. L. *et al.* Os curativos a base de prata e sua eficácia em queimaduras: uma revisão integrativa / Silver-based dressings and their effectiveness in burns: an integrative review. **Brazilian Journal of Development**, v. 8, n. 2, p. 8535–8556, 2 Feb. 2022.

OKUR, M. E. *et al.* Recent trends on wound management: New therapeutic choices based on polymeric carriers. **Asian Journal of Pharmaceutical Sciences**, v. 15, n. 6, p. 661–684, 1 Nov. 2020.

OPREA, M.; VOICU, S. I.. Recent advances in composites based on cellulose derivatives for biomedical applications. **Carbohydrate Polymers**, v. 247, n. 1, 2020.

OTTONI, C. A. *et al.* Environmental impact of biogenic silver nanoparticles in soil and aquatic organisms. **Chemosphere**, v. 239, 1 Jan. 2020.

PARIKH, R. Y. *et al.* Extracellular synthesis of crystalline silver nanoparticles and molecular evidence of silver resistance from Morganella sp.: towards understanding biochemical synthesis mechanism. **Chembiochem: a European journal of chemical biology**, v. 9, n. 9, p. 1415–1422, 16 June. 2008.

PARK, E.J. *et al.* Silver nanoparticles induce cytotoxicity by a Trojan-horse type mechanism. **Toxicology in Vitro**, v. 24, n. 3, p. 872–878, 1 Apr. 2010.

PARVEEN, R.; TREMILIOSI-FILHO, G. A step ahead towards the green synthesis of monodisperse gold nanoparticles: The use of crude glycerol as a greener and low-cost reducing agent. **RSC Advances**, v. 6, n. 97, p. 95210–95219, 2016.

POLTE, J. *et al.* Formation mechanism of colloidal silver nanoparticles: analogies and differences to the growth of gold nanoparticles. **ACS Nano**, 2012.

PRIYADARSHI, R.; KUMAR, B.; RHIM, J. W. Green and facile synthesis of carboxymethylcellulose/ZnO nanocomposite hydrogels crosslinked with Zn2+ ions. **International Journal of Biological Macromolecules**, v. 162, p. 229–235, 2020.

QIU, Y. *et al.* **Developing Solid Oral Dosage Forms: Pharmaceutical Theory and Practice**. Amsterdam: Academic Press, 2009. v. 1, 1st ed.

RAHMAN, K. U. *et al.* Flexible bacterial cellulose-based BC-SiO2-TiO2-Ag membranes with self-cleaning, photocatalytic, antibacterial and UV-shielding properties as a potential multifunctional material for combating infections and environmental applications. **Journal of Environmental Chemical Engineering**, v. 9, n. 1, 1 Feb. 2021.

RIGAKU CORPORATION. Silver Oxide Difractogram, 2019.

SAGHAZADEH, S. *et al.* Drug delivery systems and materials for wound healing applications. **Advanced Drug Delivery Reviews**, v. 127, p. 138–166, 1 Mar. 2018.

SAHA, P.; KIM, Beom Soo. Plant extract and agricultural waste-mediated synthesis of silver nanoparticles and their biochemical activities. **Green Synthesis of Silver Nanomaterials**, p. 285–315, 1 Jan. 2022.

SAITO, T. *et al.* Cellulose nanofibers prepared by TEMPO-mediated oxidation of native cellulose. **Biomacromolecules**, v. 8, n. 8, p. 2485–2491, Aug. 2007.

SANNINO, A.; DEMITRI, C.; MADAGHIELE, M. Biodegradable cellulose-based hydrogels: Design and applications. **Materials**, v. 2, n. 2, p. 353–373, 2009.

SAPUTRA, A. H. *et al.* Synthesis and characterization of hydrogel from cellulose derivatives of water hyacinth (Eichhornia crassipes) through chemical cross-linking method by using citric acid. **Journal of Engineering Science and Technology**, v. 10, n. 1, p. 75–86, 2015.

SAPUTRA, A. H.; RUTH. Synthesis and swelling characterization of nata-de-coco-andwater-hyacinth-based hydrogel. **IOP Conference Series: Materials Science and Engineering**, v. 509, n. 1, 3 May 2019.

SARKAR, A.; KAPOOR, S.; MUKHERJEE, T. Synthesis and characterisation of silver nanoparticles in viscous solvents and its transfer into non-polar solvents. **Research on Chemical Intermediates**, v. 36, n. 4, p. 411–421, June. 2010.

SHEN, X. *et al.* Hydrogels based on cellulose and chitin: Fabrication, properties, and applications. **Green Chemistry**, v. 18, n. 1, p. 53–75, 16 Nov. 2015.

SILVA, L. P. *et al.* **Silver Nanoparticles as Antimicrobial Agents: Past, Present, and Future**. 1. ed. Amsterdam: Elsevier, 2017.

SWEIS, I. E.; CRESSEY, B. C. Potential role of the common food additive manufactured citric acid in eliciting significant inflammatory reactions contributing to serious disease states: A series of four case reports. **Toxicology Reports**, v. 5, n. 1, p. 808–812, 2018.

SYAFIUDDIN, A. *et al.* A review of silver nanoparticles: research trends, global consumption, synthesis, properties, and future challenges. **Journal of the Chinese Chemical Society**, v. 64, n. 7, p. 732–756, 1 July. 2017.

THAKKAR, K. N.; MHATRE, S. S.; PARIKH, R. Y. Biological synthesis of metallic nanoparticles. **Nanomedicine: Nanotechnology, Biology, and Medicine**, v. 6, n. 2, p. 257–262, Apr. 2010.

THÉRIEN-AUBIN, H. *et al.* Temperature-responsive nanofibrillar hydrogels for cell encapsulation. **Biomacromolecules**, v. 17, n. 10, p. 3244–3251, 2016.

VIGNESHWARAN, N. *et al.* Biomimetics of silver nanoparticles by white rot fungus, Phaenerochaete chrysosporium. **Colloids and Surfaces B: Biointerfaces**, v. 53, n. 1, p. 55–59, 1 nov. 2006.

WANG, B. *et al.* High-efficient production of citric acid by Aspergillus niger from high concentration of substrate based on the staged-addition glucoamylase strategy. **Bioprocess and Biosystems Engineering**, v. 40, n. 6, p. 891–899, 1 June. 2017.

WANG, L. *et al.* Use of synchrotron radiation-analytical techniques to reveal chemical origin of silver-nanoparticle cytotoxicity. **ACS nano**, v. 9, n. 6, p. 6532–6547, 23 June. 2015.

WICHTERLE, O; LÍM, D. Hydrophilic gels for biological use. **Nature**, v. 185, n. 4706, p. 117–118, 1960.

XIE, X.; LIU, Q. Development and physicochemical characterization of new resistant citrate starch from different corn starches. **Starch/Staerke**, v. 56, n. 8, p. 364–370, 2004.

YOKOYAMA, F *et al.* Morphology and structure of highly elastic poly(vinyl alcohol) hydrogel prepared by repeated freezing-and-melting. **Colloid and Polymer Science**, v. 264, n. 7, p. 595–601, 1986.

ZHOU, N.; SHI, H. Metal nanomaterials. **Nano-inspired Biosensors for Protein Assay with Clinical Applications**, p. 39–65, 1 Jan. 2019.

APENDIX – INHIBITION HALOS

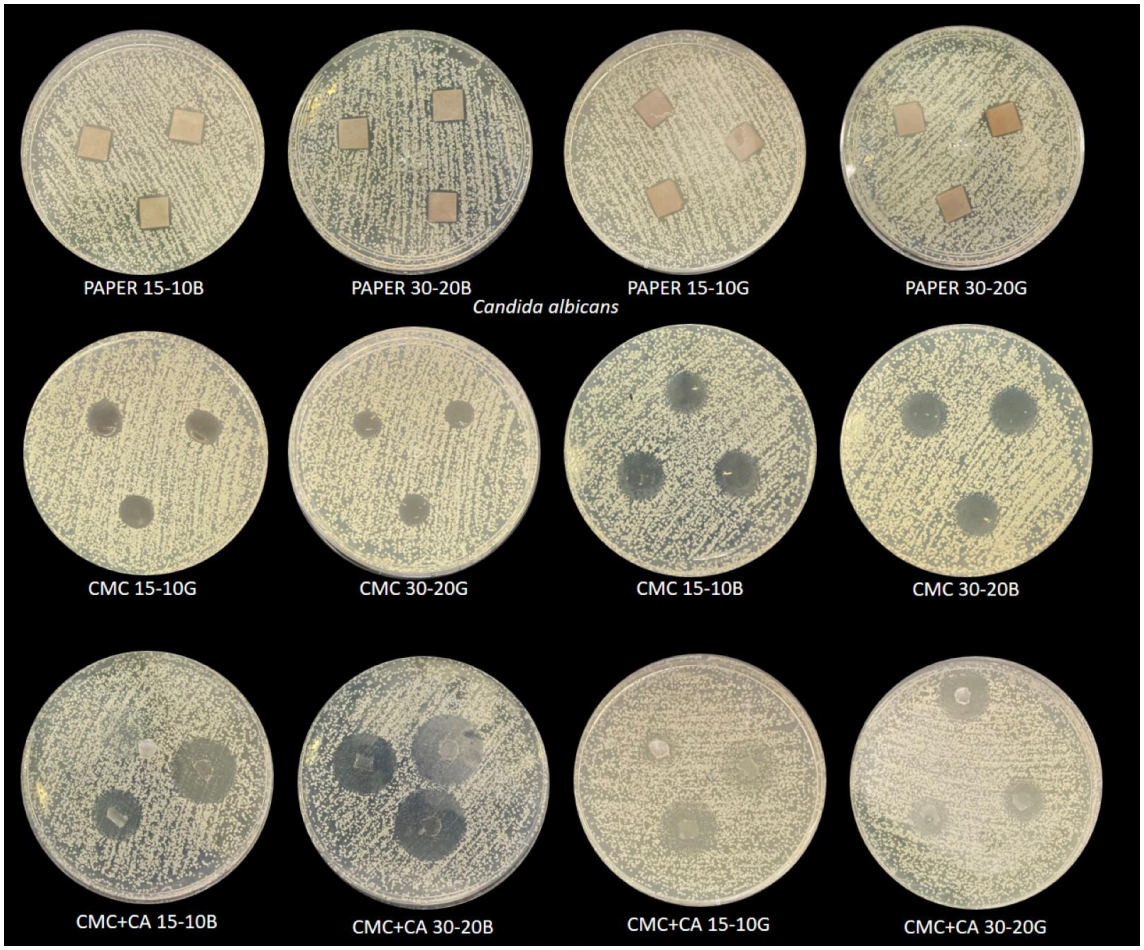

Appendix A1: Inhibition halos of the *C. albicans* exposed to different samples treated with silver.
Source: Author (2023).

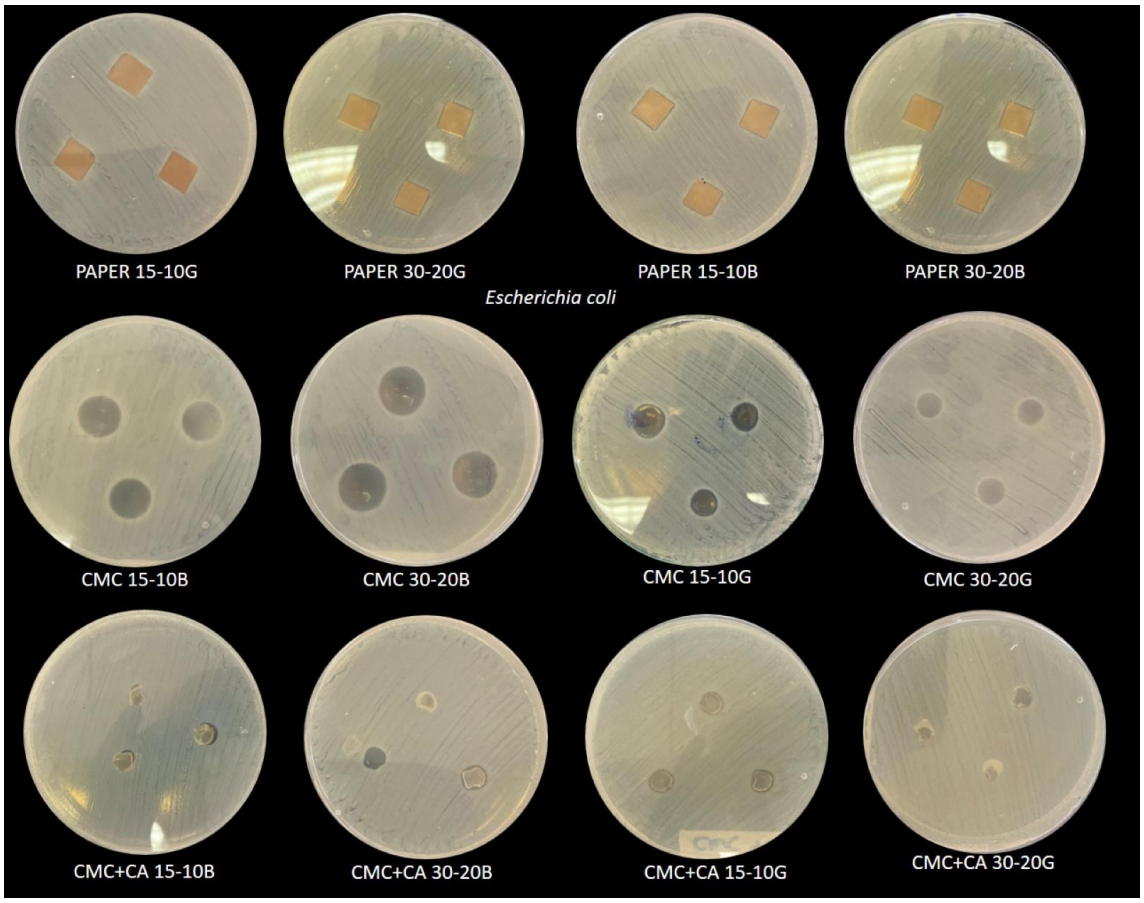

Appendix A2: Inhibition halos of the *E. coli* exposed to different samples treated with silver. Source: Author (2023).

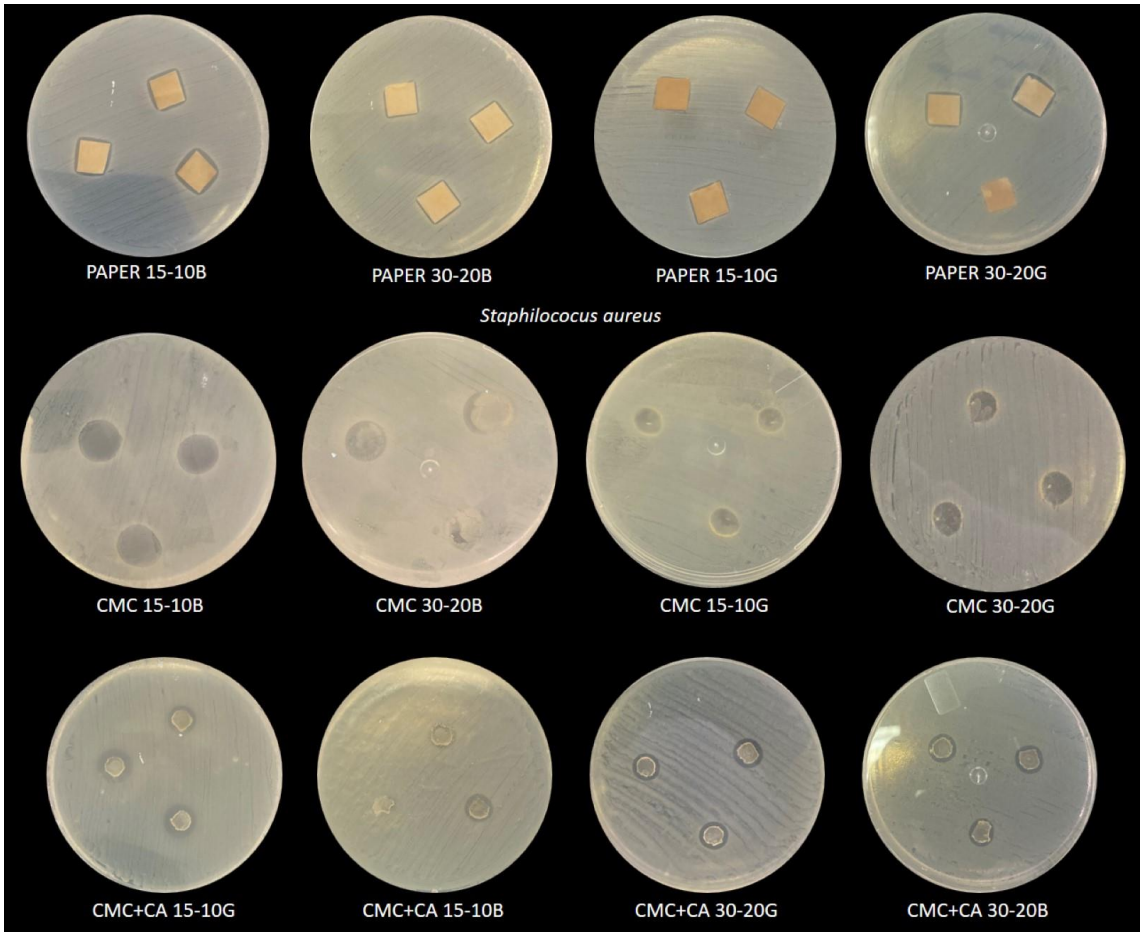

Appendix A3: Inhibition halos of the *S. aureus* exposed to different samples treated with silver. Source: Author (2023).